

Master Thesis

# Recommendation system for scientific tools and workflows

Anup Kumar

Examiners: Prof. Dr. Rolf Backofen

Prof. Dr. Wolfgang Hess

Adviser: Dr. Björn Grüning

University of Freiburg  
Department of Computer Science  
Bioinformatics Group Freiburg

July 9, 2018

**Thesis period**

08.01.2018 – 09.07.2018

**Examiners**

Prof. Dr. Rolf Backofen and Prof. Dr. Wolfgang Hess

**Adviser**

Dr. Björn Grüning

# Declaration

I hereby declare, that I am the sole author and composer of my thesis and that no other sources or learning aids, other than those listed, have been used. Furthermore, I declare that I have acknowledged the work of others by providing detailed references of said work.

I hereby also declare, that my Thesis has not been prepared for another examination or assignment, either wholly or excerpts thereof.

---

Place, Date

---

Signature

*Dedicated to my mom and dad*

# Acknowledgement

I would like to offer my sincere gratitude to all the people who encouraged and supported me to accomplish this work. I am grateful to my mentor Dr. Björn Grüning who entrusted me with the task of building a recommendation system for the Galaxy. He facilitated this work by providing me with all indispensable means. Being precise, his pragmatic suggestions concerning the Galaxy tools and workflows helped me discern them better and improve the overall quality of the work. His advice to create a visualiser for showing the similar tools worked wonders as it enabled me to find and rectify a few bugs which were tough to establish. For the next task, creating a separate visualiser for looking through the next predicted tools was conducive in all merits. I offer regards and thanks to Dr. Ulrike Wagner-Höher and Kai Höher (MSc.) for the German translation of the abstract. I offer thanks to Dr. Mehmet Tekman and Joachim Wolff for their expert feedback, insights and general advice. I appreciate and thank Helena Rasche for extracting the workflows. I thank Andrea Bagnacani for the intuitive discussions. At length, I wish to thank all other members, Dr. Anika Erxleben and Dr. Bérénice Batut, of the Freiburg Galaxy team for their continued support and help. I appreciate and thank Dr. Anika Erxleben, Dr. Björn Grüning and Tommoy Saikia for proofreading the thesis.

# Abstract

The thesis researches two concepts to develop a recommendation system for the Galaxy's scientific data-processing tools and workflows. The concepts incorporate finding similarities among tools and predicting next tools in workflows. They are dealt separately in the thesis. The first part explores a way to find similarities among tools. It implies which similar tools exist for each tool within a collection of tools. In addition, it quantifies the similarities among tools by assigning a similarity score for each pair of tools. A list of similar tools for a tool can give more options to the users for their data processing using the Galaxy. Similarities among tools are computed using approaches from natural language processing and optimisation. Over 1,000 tools are used for this task. Visualisers are created to see similar tools. The second part formulates a prediction system to display possible next tools in scientific workflows. These scientific workflows are complex and are created using more than 4,000 tools in the bioinformatics field. The knowledge of possible next tools can make it easier for the less experienced Galaxy users to create them. Moreover, it can curtail the amount of time taken to create a workflow. The unique paths (tool sequences) extracted from workflows are fed to the recurrent neural networks to learn the semantics of tool connections. The predictions are made by learning higher-order dependencies prevalent in these tool connections. More than 167,000 paths are used to learn the predictive model. The absolute classification precision of  $\approx 89\%$  and compatible classification precision of  $\approx 99\%$  are achieved. The absolute top-1 accuracy is  $\approx 91\%$ .

# Zusammenfassung

Die Arbeit erforscht zwei Konzepte, um ein Empfehlungssystem für Galaxy's wissenschaftliche Datenverarbeitungs-Werkzeuge/Tools und Workflows zu entwickeln. Die Konzepte werden in dieser Arbeit separat behandelt und beinhalten das Auffinden von Ähnlichkeiten bei Werkzeugen und die Vorhersage nachfolgender Werkzeuge in Workflows. Der erste Teil erforscht die Methode zum Auffinden von Ähnlichkeiten bei Tools innerhalb einer Gruppe von Tools. Darüber hinaus wird die Ähnlichkeit zwischen Tools paarweise durch die Verwendung eines Punktesystems quantifiziert. Eine Liste ähnlicher Tools für ein Tool kann den Benutzern mehr Optionen für die Datenverarbeitung mit dem Galaxy zur Verfügung stellen. Zur Berechnung der Ähnlichkeit von Tools wird dabei die natürliche Sprachverarbeitung und Optimierung berücksichtigt. Für diese Aufgabe wurden über 1.000 Tools verwendet. Visualisierer werden erstellt, um ähnliche Tools zu sehen. Der zweite Teil entwirft ein Vorhersage-System, welches die nächsten möglichen Tools bei Workflows darlegt. Diese wissenschaftlichen Workflows sind komplex und werden mit mehr als 4.000 Tools in der Bioinformatik erstellt. Die Kenntnis möglicher nächster Tools kann es wenig erfahrenen Galaxy-Benutzern leichter machen, Workflows zu erstellen. Außerdem kann die zur Schaffung eines Workflow benötigte Zeitdauer verkürzt werden. Die einzelnen, aus Workflows entnommenen Pfade (Tool-Sequenzen) werden in rückgekoppelte neuronale Netze eingebracht, um die Bedeutung von Tool-Verbindungen zu ermitteln. Die Vorhersagen wurden durch das Lernen vorherrschender Abhängigkeiten höherer Ordnung der Tool-Verbindungen gewonnen. Zur Erstellung des Vorhersage-Modells wurden über 167.000 Pfade verwendet. Die absolute Klassifikationsgenauigkeit von  $\approx 89\%$  und die kompatible Klassifikationsgenauigkeit von  $\approx 99\%$  werden erreicht. Die absolut Top-1-Genauigkeit beträgt  $\approx 91\%$ .

# Contents

<b>1</b>	<b>Find similar scientific tools</b>	<b>1</b>
<b>1</b>	<b>Introduction</b>	<b>2</b>
1.1	Galaxy . . . . .	2
1.2	Scientific tools . . . . .	3
1.3	Motivation . . . . .	4
<b>2</b>	<b>Approach</b>	<b>5</b>
2.1	Metadata of tools . . . . .	5
2.1.1	Attributes . . . . .	5
2.1.2	Useful metadata . . . . .	7
2.2	Dense vector for a document . . . . .	12
2.2.1	Latent semantic analysis . . . . .	12
2.2.2	Paragraph vectors . . . . .	15
2.3	Similarity measures . . . . .	18
2.3.1	Cosine similarity . . . . .	18
2.3.2	Jaccard index . . . . .	19
2.4	Optimisation . . . . .	19
2.4.1	Gradient descent . . . . .	20
2.4.2	Learning rate decay . . . . .	21
2.4.3	Weight update . . . . .	22
<b>3</b>	<b>Experiments and results</b>	<b>25</b>
3.1	Latent semantic analysis . . . . .	25
3.1.1	Full-rank document-token matrices . . . . .	26
3.1.2	5% of full-rank . . . . .	29
3.2	Paragraph vectors . . . . .	32
3.3	Comparison of two approaches . . . . .	35
<b>4</b>	<b>Conclusion</b>	<b>38</b>
4.1	Metadata of tools . . . . .	38
4.2	Approaches . . . . .	38
4.2.1	Latent semantic analysis . . . . .	38

4.2.2	Paragraph vectors . . . . .	39
4.3	Optimisation . . . . .	40
<b>5</b>	<b>Future work</b>	<b>41</b>
5.1	Get true similarity values . . . . .	41
5.2	Exclude low similarity scores . . . . .	41
5.3	Formulate different error functions . . . . .	41
5.4	Acquire more tools . . . . .	42
5.5	Learn tool similarity using workflows . . . . .	42
<b>II</b>	<b>Predict next tools in scientific workflows</b>	<b>43</b>
<b>6</b>	<b>Introduction</b>	<b>44</b>
6.1	Galaxy workflows . . . . .	44
6.1.1	Motivation . . . . .	45
<b>7</b>	<b>Related work</b>	<b>46</b>
<b>8</b>	<b>Approach</b>	<b>48</b>
8.1	Actual next tools . . . . .	48
8.2	Compatible tools . . . . .	50
8.3	Length of workflow paths . . . . .	50
8.4	Learning . . . . .	50
8.4.1	Workflow paths . . . . .	50
8.4.2	Bayesian network . . . . .	54
8.4.3	Recurrent neural network . . . . .	54
8.5	Network architecture . . . . .	58
8.5.1	Embedding layer . . . . .	58
8.5.2	Recurrent layer . . . . .	59
8.5.3	Output layer . . . . .	59
8.5.4	Activations . . . . .	59
8.5.5	Regularisation . . . . .	60
8.5.6	Optimiser . . . . .	61
8.5.7	Precision . . . . .	62
8.6	Prediction pattern . . . . .	62

<b>9 Experiments</b>	<b>64</b>
9.1 Decomposition of paths . . . . .	64
9.2 Dictionary of tools . . . . .	65
9.3 Padding with zeros . . . . .	65
9.4 Network configuration . . . . .	66
9.4.1 Mini-batch learning . . . . .	67
9.4.2 Dropout . . . . .	67
9.4.3 Optimiser . . . . .	67
9.4.4 Learning rate . . . . .	68
9.4.5 Activations . . . . .	68
9.4.6 Number of recurrent units . . . . .	68
9.4.7 Dimension of embedding layer . . . . .	68
<b>10 Results and analysis</b>	<b>69</b>
10.1 Notes on plots . . . . .	70
10.2 Performances of different approaches of path decomposition . . . . .	71
10.2.1 Decomposition of only test paths . . . . .	71
10.2.2 No decomposition of paths . . . . .	72
10.2.3 Decomposition of the train and test paths . . . . .	73
10.3 Performance evaluation on different parameters . . . . .	74
10.3.1 Optimiser . . . . .	75
10.3.2 Learning rate . . . . .	76
10.3.3 Activation . . . . .	77
10.3.4 Batch size . . . . .	78
10.3.5 Number of recurrent units . . . . .	79
10.3.6 Dropout . . . . .	81
10.3.7 Dimension of embedding layer . . . . .	82
10.3.8 Accuracy (top-1 and top-2) . . . . .	83
10.3.9 Precision with the length of paths . . . . .	85
10.3.10 Performance with a small number of workflows . . . . .	86
10.3.11 Neural network with dense layers . . . . .	87
<b>11 Conclusion</b>	<b>89</b>
11.1 Network configuration . . . . .	89
11.2 The amount of data . . . . .	90
11.3 Decomposition of paths . . . . .	90

11.4 Classification . . . . .	90
<b>12 Future work</b>	<b>91</b>
12.1 Train on longer and test on shorter paths . . . . .	91
12.2 Restore original distribution . . . . .	91
12.3 Use convolution . . . . .	91
12.4 Use other classifiers . . . . .	91
12.5 Decay prediction based on time . . . . .	92
<b>Bibliography</b>	<b>92</b>
<b>A Appendix</b>	<b>97</b>
A.1 Visualiser . . . . .	97
A.2 Code repository . . . . .	97
A.2.1 Find similar scientific tools . . . . .	97
A.2.2 Predict next tools in scientific workflows . . . . .	98

# List of Figures

1	Basic flow of dataset transformation . . . . .	2
2	Common features of two tools . . . . .	3
3	Similarity graph . . . . .	4
4	Sequence of steps to find similar tools . . . . .	6
5	Distribution of tokens . . . . .	8
6	Tool, document and tokens . . . . .	9
7	Singular value decomposition . . . . .	12
8	Singular values of document-token matrices . . . . .	14
9	Variation of the fraction of ranks of document-token matrices with the fraction of sum of singular values . . . . .	15
10	Distributed memory . . . . .	17
11	Distributed bag-of-words . . . . .	17
12	Decay of learning rate for gradient descent optimiser . . . . .	22
13	Difference between actual and approximated gradients . . . . .	24
14	Similarity matrices computed using full-rank document-token matrices	27
15	Distribution of weights learned for similarity matrices computed using full-rank document-token matrices . . . . .	28
16	Average of weighted similarities computed using uniform and optimal weights . . . . .	29
17	Similarity matrices computed using document-tokens matrices reduced to 5% of their full-ranks . . . . .	30
18	Distribution of weights learned for similarity matrices computed using document-token matrices reduced to 5% of their full-ranks . . . . .	31
19	Average of weighted similarities computed using uniform and optimal weights . . . . .	32
20	Similarity matrices using paragraph vectors approach . . . . .	33

21	Distribution of weights for similarity matrices computed using paragraph vectors approach . . . . .	34
22	Average of weighted similarities computed using optimal and uniform weights . . . . .	35
23	A workflow . . . . .	44
24	Multiple next tools . . . . .	45
25	Sequence of steps to predict tools for workflows . . . . .	49
26	Distribution of the number of compatible tools . . . . .	51
27	Distribution of sizes of workflow paths . . . . .	52
28	No path decomposition . . . . .	52
29	Path decomposition . . . . .	53
30	Higher-order dependency . . . . .	55
31	Recurrent neural network . . . . .	56
32	Gated recurrent unit . . . . .	57
33	Scores for the predicted tools . . . . .	63
34	Vectors of a path and its next tools . . . . .	66
35	Performance of the decomposition of only test paths . . . . .	72
36	Performance of no decomposition of paths . . . . .	73
37	Performance of the decomposition of all paths . . . . .	74
38	Performance of different optimisers . . . . .	76
39	Performance of multiple learning rates . . . . .	77
40	Performance of multiple activation functions . . . . .	78
41	Performance of different batch sizes . . . . .	79
42	Performance of multiple values of memory units . . . . .	80
43	Performance of multiple values of dropout . . . . .	82
44	Performance of different dimensions of the embedding layer . . . . .	83
45	Absolute and compatible top-1 and top-2 accuracies . . . . .	84
46	Variation of precision with the length of paths . . . . .	85
47	Performance with a small number of workflows . . . . .	86
48	Performance of a neural network with dense layers . . . . .	88

# List of Tables

1	A sparse document-token matrix . . . . .	11
2	Similar tools (top-2) for <i>hisat</i> computed using full-rank document-token matrices . . . . .	36
3	Similar tools (top-2) for <i>hisat</i> computed using document-token matrices reduced to 5% of full-rank . . . . .	36
4	Similar tools (top-2) for <i>hisat</i> computed using paragraph vectors approach . . . . .	37
5	Decomposition of a workflow . . . . .	49

## **Part I.**

**Find similar scientific tools**

# 1. Introduction

## 1.1. Galaxy

Galaxy is an open-source biological data processing and research platform [1]. It supports numerous types of data formats like *fasta*, *fastq*, *gff*, *vcf* and many more<sup>1</sup> and they are extensively used for data processing. It offers scientific tools and workflows to transform these datasets (figure 1). Each tool has an exclusive way to process datasets. An example of data processing is to convert a sequence of nucleotides<sup>2</sup> into its reverse-complement counterpart.

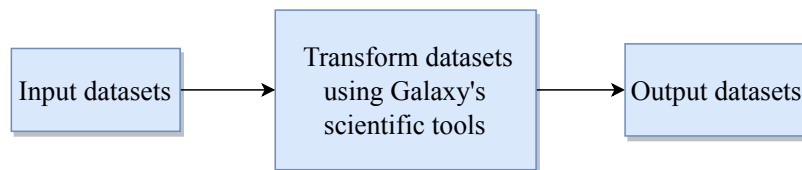


**Figure 1.: Dataset transformation:** The image shows a general flow of data transformation using the Galaxy's scientific tools.

Tools are classified into multiple categories based on their functions and types. For example, the tools which manipulate text, like replacing texts and selecting lines of a dataset, are grouped together under *text manipulation*. Similarly, there are various tool categories like *imaging*, *convert formats*, *genome annotation* and many others<sup>3</sup>. These tools are the building blocks of a workflow. A workflow is a data processing pipeline where a set of tools are connected one after another. The connected tools in a workflow should be compatible with each other. It means that the output file types of one tool should be present in the input file types of the next tool. An example of a workflow is *variantcalling-freebayes*. It is used for the detection of variants (specifically single and multiple nucleotide polymorphisms and insertions and deletions) following a bayesian approach.

<sup>1</sup><https://galaxyproject.org/learn/datatypes>

<sup>2</sup>[https://usegalaxy.eu/?tool\\_id=MAF\\_Reverse\\_Complement\\_1&version=1.0.1](https://usegalaxy.eu/?tool_id=MAF_Reverse_Complement_1&version=1.0.1)

<sup>3</sup><https://toolshed.g2.bx.psu.edu/repository>

## 1.2. Scientific tools

A tool entails a specific function. It consumes a dataset, brings about some transformation and produces an output dataset which is fed to other tools. For example, the tool *trimmomatic* trims a *fastq* file and produces a *fastqsanger* file which is used as an input file for a different tool like *fastqc*. A tool has multiple attributes which include its input and output file types, name, description, help text and many more<sup>4</sup>. These attributes constitute the metadata of tools. The metadata shows that some tools have similar functions while some share similarities in their input and output file types. For example, the tool *hicexplorer\_hicpca*<sup>5</sup> has an output type named *bigwig*. A tool which also has *bigwig* as its input and/or output type, there is some similarity between these tools as they do a transformation on a similar file type. Similar tools can also be found by analysing other attributes like name and description.

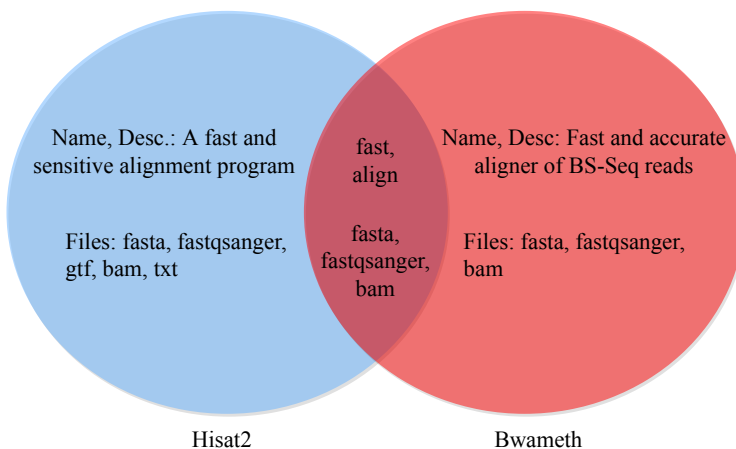


**Figure 2.: Common features of two tools:** The venn diagram shows common features of two tools - *hisat2* and *bwameth*. Few attributes like name, description and file types (input and output) are used to extract common features. Based on the common features, shown in the middle of the venn diagram, similarity between them can be assessed.

Figure 2 shows two tools - *hisat2* and *bwameth*. Their respective metadata is collected from their input and output file types and name and description attributes. Both of them have common file types (*fasta*, *fastqsanger*, *bam*). Moreover, they share a similar function of aligning. By extrapolating this way of finding similar features

<sup>4</sup><https://docs.galaxyproject.org/en/master/dev/schema.html>

<sup>5</sup>[https://usegalaxy.eu/?tool\\_id=toolshed.g2.bx.psu.edu/repos/bgruening/hicexplorer\\_hicpca/hicexplorer\\_hicpca/2.1.0&version=2.1.0](https://usegalaxy.eu/?tool_id=toolshed.g2.bx.psu.edu/repos/bgruening/hicexplorer_hicpca/hicexplorer_hicpca/2.1.0&version=2.1.0)

among tools, a set of similar tools for each tool can be created.

### 1.3. Motivation

The Galaxy has thousands of tools with a diverse set of functions. New tools keep getting added to the existing set of tools. It is hard to have knowledge of so many existing tools for the Galaxy users. In addition, it is important to make them aware of the presence of the newly added tools. They may be similar to some of the existing tools. Devising a method to compute similarities among tools should solve these issues.

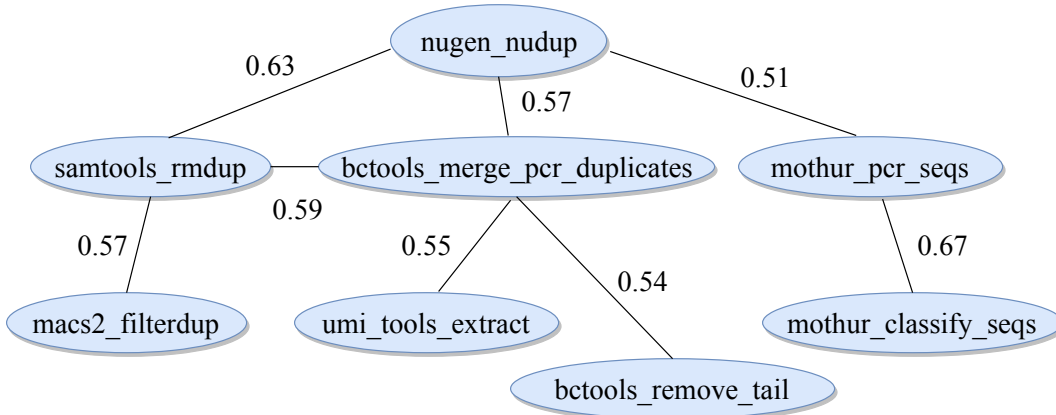


**Figure 3.: Similarity graph of tools:** In the graph, a node is represented by a tool and an edge shows a similarity score for a pair of tools. The higher the similarity score, the more similar a pair of tools is.

To elaborate more, a tool *nugen\_nudup*<sup>6</sup> (figure 3) is taken. It finds and removes *pcr* duplicates. A few similar tools are collected. Tools like *samtools\_rmdup* and *bctools\_merge\_pcr\_duplicates* also have a similar function. Each tool has a set of similar tools and together they make a graph of related tools. This similarity graph shows *connectedness* among tools and can help a user to find multiple ways to process data by replacing a tool with a similar tool. Figure 3 shows a small example of the similarity graph. In the next part of the thesis in which tools are predicted in workflows, these similar tools can be shown for each predicted tool. A combined set of similar and predicted tools should give more options to the users for their data processing using the Galaxy. Collectively, they make a tool recommendation system.

---

<sup>6</sup>[https://toolshed.g2.bx.psu.edu/repository?repository\\_id=4f614394b93677e3](https://toolshed.g2.bx.psu.edu/repository?repository_id=4f614394b93677e3)

## 2. Approach

This section gives a comprehensive description of an approach to compute similarities among tools. The approach involves a sequence of steps (figure 4). The Galaxy’s codebase and tool repositories are at *github*. The metadata of tools is extracted from the *github*’s tool repositories. It is cleaned to get a set of words for each tool which uniquely identifies it. This set is used to create a fixed-length vector for each tool (in table 1, each row is a vector). The words from all the tools are merged to create a collection. Its size gives the size of the vector. Each word from the collection has a position in the vector. In the vector for a tool, the positions of the respective words (words from the tool’s set) contain the frequencies of their occurrence. The positions of those words not present in the set for a tool are equal to zero. These vectors are used to compute similarity scores for each pair of tools using similarity measures. The similarity scores of each tool with all the other tools create a similarity matrix. A similarity matrix is computed for each attribute. These similarity matrices are combined by optimisation to get a weighted average similarity matrix. All steps to compute similarities among tools are explained in further sections.

### 2.1. Metadata of tools

One of the Galaxy’s tool repositories is *Galaxy tools maintained by iuc*<sup>1</sup>. A tool is defined in an *extensible markup language (xml)* file which can be parsed efficiently to gather the metadata from multiple attributes. The *xml* file of a tool starts with a *tool* tag.

#### 2.1.1. Attributes

A tool has multiple attributes which include input and output file types, help text, name, description, citations and many more<sup>2</sup>. But, not all of these attributes are

---

<sup>1</sup><https://github.com/galaxyproject/tools-iuc>

<sup>2</sup><https://docs.galaxyproject.org/en/master/dev/schema.html>

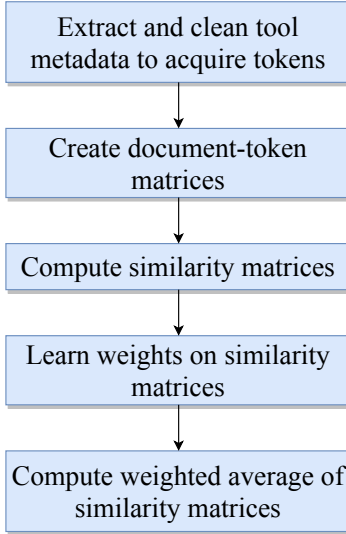


**Figure 4.: Sequence of steps to find similar tools:** The flowchart shows a series of steps to establish similarities among tools using the approaches from natural language processing to compute similarity matrices and optimisation to compute a weighted average of the similarity matrices.

significant in identifying a tool. Therefore, only the following attributes are considered to collect the metadata of tools:

- Input file types
- Output file types
- Name
- Description
- Help text

Moreover, the input and output file types are combined by taking a union set to create one attribute as together they contain information about file types of a tool. A similar combination is done for the name and description attributes as well. These combined attributes give a complete metadata of a tool's file types (input and output) and its functionality (name and description). Further, help text attribute is also included in the metadata. This attribute contains more information compared to the previous two combined attributes. Apart from being larger in size, it is noisy too. It gives a detailed information about the functions of a tool and the format of its input

data<sup>3</sup>. Much of the information collected by this attribute is not important to clearly distinguish a tool. Therefore, only the first few lines of text from this attribute are considered which illustrate the core functions of tools. The rest of the information is discarded.

### 2.1.2. Useful metadata

#### Duplicates and stop-words removal

The metadata of tools collected from multiple attributes is raw. It contains lots of noisy and duplicate items which do not add any value. These items should be removed from the metadata to retain items which are unique and useful. For example, the tool *bamleftalign* has *bam* and *fasta* as input files and *bam* as an output file. While combining these file types to make a set of file types for a tool, the duplicates are discarded. Hence, *bam* and *fasta* together make a set of file types for the tool. This set does not maintain any order of the file types. The attributes like name, description and help text contain sentences (complete or partially complete) in the English language. Therefore, to process these, strategies from natural language processing<sup>4</sup> are needed. A sentence contains many words and can have many different parts of speech. The parts of speech include a subject, object, preposition, interjection, verb, adjective, adverb, article and many more<sup>5</sup>. Only those words are retained from the sentences which categorise a tool uniquely. For example, the tool *tophat* has "*tophat for illumina find splice junctions using rna-seq data*" as its combined name and description attribute. The words like *for*, *using* and *data* cannot distinguish the tool as they can be present in the description of many other tools. These words are called stop-words<sup>6</sup> and are discarded. In addition, numbers are also removed. All the remaining words are converted to lower case.

#### Stemming

After removing the duplicates and stop-words, the metadata becomes clean and contains words which can identify tools uniquely. Different forms of a word are used in sentences due to the rules of grammar. For example, a word *regress* has

---

<sup>3</sup>[https://planemo.readthedocs.io/en/latest/standards/docs/best\\_practices/tool\\_xml.html#help-tag](https://planemo.readthedocs.io/en/latest/standards/docs/best_practices/tool_xml.html#help-tag)

<sup>4</sup><https://www.ncbi.nlm.nih.gov/pmc/articles/PMC3168328>

<sup>5</sup><https://web.stanford.edu/~jurafsky/slp3/10.pdf>

<sup>6</sup><https://www.ranks.nl/stopwords>

multiple forms like *regresses*, *regression* and *regressed*. All these forms share the same root and point towards the same concept. Therefore, it is beneficial to converge all different forms of a word to one basic form. This process is called stemming<sup>7</sup>. The *nltk*<sup>8</sup> package is used for stemming. It reduces the size of metadata and keeps the meaning of a word same across its multiple forms. After stemming, the words are called tokens. Figure 5 shows a distribution of tokens in the metadata for all three attributes of tools. These tokens are used for computing similarities among tools. The help text attribute contains more tokens than input and output file types and name and description attributes.

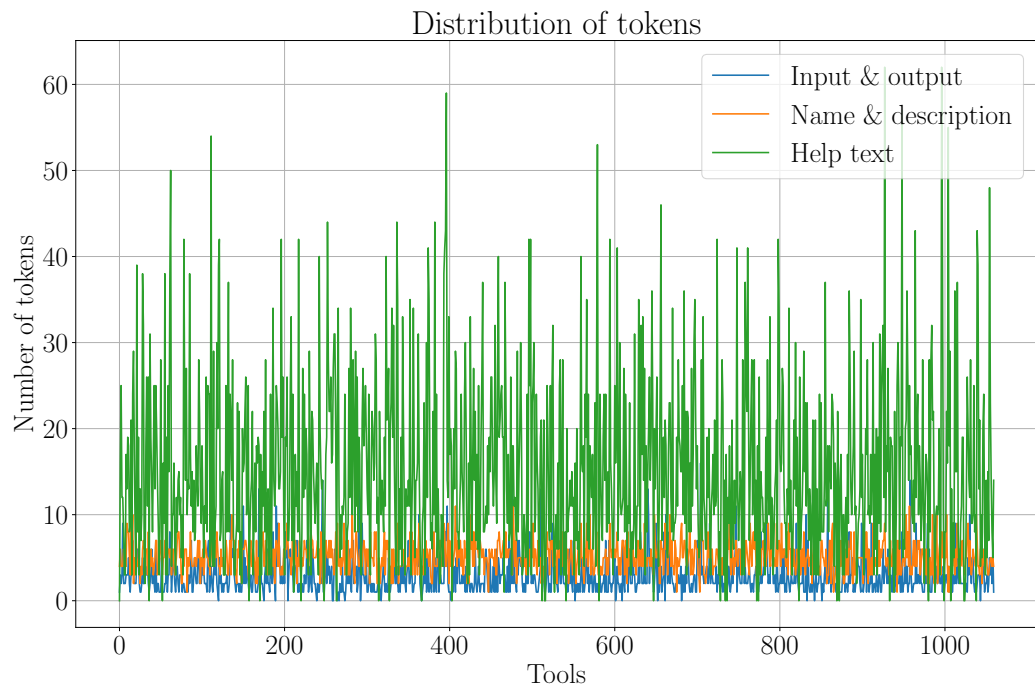


**Figure 5.: Distribution of tokens:** The plot shows a distribution of the number of tokens for input and output file types, name and description and help text attributes of tools. The number of tokens for help text attribute is higher than for input and output and name and description attributes.

---

<sup>7</sup><https://nlp.stanford.edu/IR-book/html/htmledition/stemming-and-lemmatization-1.html>

<sup>8</sup><http://www.nltk.org>

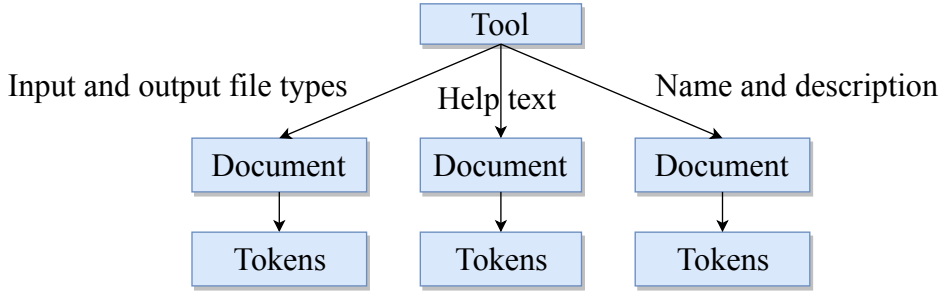


**Figure 6.: Relationship between a tool, its documents and their tokens:**

The image shows that a tool has three documents corresponding to each attribute and each document contains tokens. The documents are equal to the number of tools for each attribute. The number of tokens in each document varies.

### Relevance factors for tokens

After stemming the words from metadata, meaningful sets of tokens are collected for input and output file types, name and description and help text for each tool. These sets are called documents (figure 6). The tokens present in these documents do not carry equal importance. Some tokens are more relevant to a document, but some are not. An importance factor is computed for each token in a document. These factors are arranged in a big, sparse document-token matrix. Each attribute has its own document-token matrix. In these matrices, each row represents a document and each column represents a token. To compute these importance factors, the *bestmatch25* (*bm25*) [2] algorithm is used. The variables used in implementing this algorithm are as follows:

- Token frequency<sup>9</sup> ( $tf$ )
- Document frequency ( $df$ ) and inverted document frequency ( $idf$ )
- Average document length ( $|D|_{avg}$ )
- Number of documents ( $N$ )
- Size of a document ( $|D|$ )

Token frequency ( $tf$ ) gives the count of a token's occurrence in a document. If a token *regress* appears twice in a document, its  $tf$  is 2. It is a weight given to the token. Inverted document frequency ( $idf$ ) for a token is defined as:

---

<sup>9</sup><https://nlp.stanford.edu/IR-book/pdf/06vect.pdf>

$$idf = \log \frac{N}{df} \quad (1)$$

where  $df$  is the count of documents in which the token is present and  $N$  is the total number of documents. If a document is randomly sampled from a set of documents, the probability of the token to be present in this document is  $p_i = \frac{df}{N}$ . From information theory [3], the information contained by this event is computed by  $-\log p_i$ .  $Idf$  is higher when a token appears only in a few documents. It means that the token is a good candidate for representing those documents. A token which appears in many documents is not a good representative of those documents.  $|D|_{avg}$  is the average number of tokens computed over all documents.  $|D|$  is the number of tokens for a document. The  $bm25$  score of a token is calculated using the following equations:

$$\alpha = (1 - b) + \frac{b \cdot |D|}{|D|_{avg}} \quad (2)$$

$$tf^* = tf \cdot \frac{k + 1}{k \cdot \alpha + tf} \quad (3)$$

$$bm25_{score} = tf^* \cdot idf \quad (4)$$

where  $k$  and  $b$  are the hyperparameters of the  $bm25$  algorithm and their ideal values should be found according to the data.  $k$  is always a positive number. When  $k$  is zero, the  $bm25$  score for a token is defined only by its  $idf$  ( $tf^* = 1$ ). When  $k$  is much larger than  $tf$  ( $k \gg tf$ ), the  $bm25$  score is computed using the raw term frequency ( $tf^* \approx tf$ ). The parameter  $b$  is a real number between zero and one ( $0 \leq b \leq 1$ ). When it is zero, the document length is not normalised. It means that the fraction  $\frac{|D|}{|D|_{avg}}$  is not accounted for computing the  $bm25$  score. When  $b$  is one, this fraction is completely accounted for. In this case, when  $|D| \gg |D|_{avg}$  for any document, its tokens would get a lower  $bm25$  score. For this work, the standard values of  $k$  and  $b$  (1.75 and 0.75, respectively) are used. Using equation 4, the  $bm25$  score is computed for each token in all the documents. Table 1 shows the  $bm25$  scores for four documents (rows) along with five tokens (columns). Following this approach, the document-token matrices are computed for all three attributes of tools. For input and output file types, the matrix will have only two values - one if a token is present for a document and zero if not. For other attributes, the  $bm25$  scores are

positive real numbers.

Document/Token	Regress	Linear	Gap	Mapper	Perform
LinearRegression	5.22	4.1	0.0	0.0	3.84
LogisticRegression	3.54	0.0	0.0	0.0	2.61
Tophat2	0.0	0.0	1.2	1.47	0.0
Hisat	0.0	0.0	0.0	0.0	0.0

**Table 1.: A sparse document-token matrix:** The table shows a matrix of documents arranged along the rows and tokens along the columns. Each value in the matrix is a *bm25* score assigned to a token. The matrix is sparse because the total number of tokens (for all the documents) is larger than the number of tokens present for each document.

The document-token matrices are sparse. Each entry in these matrices is a *bm25* score for each token. This representation is important to know which tokens are better representatives, but which are not for a document. A token is important for a document if the *bm25* score is high. However, it does not give any information about its relation to other tokens. The information about the co-occurrence of tokens in a document defines a concept hidden in that document. A concept in a document is formed by using the relation among a few tokens. To illustrate this idea, an example of three words, *relabel list identifiers*, is considered. These three words mean little and point to different things if each word is considered separately. But, together they point towards a concept. The *bm25* model lacks the ability to find the correlation among tokens. To learn hidden concepts within documents and correlation among tokens, two approaches are explored:

- *Latent semantic analysis*<sup>10</sup>
- *Paragraph vectors*

Using these approaches, a multi-dimensional dense vector is learned for each document.

---

<sup>10</sup><http://lsa.colorado.edu/papers/dp1.LSAintro.pdf>

## 2.2. Dense vector for a document

### 2.2.1. Latent semantic analysis

A concept is a relationship among few tokens. *Latent semantic analysis* is a mathematical way to learn these hidden concepts in documents. It is achieved by computing a low-rank representation of a document-token matrix [4, 5, 6]. *Singular value decomposition (svd)* is used to achieve it. This decomposition follows the equation:

$$X_{n \times m} = U_{n \times n} \cdot S_{n \times m} \cdot V_{m \times m}^T \quad (5)$$

where  $n$  is the number of documents and  $m$  is the number of tokens.  $S$  is a diagonal matrix containing singular values in descending order and has the same shape as the document-token matrix  $X$ . The singular values are real numbers. It contains the weights of concepts present in the document-token matrix  $X$ . The matrices  $U$  and  $V$  are orthogonal matrices and satisfy:

$$U^T \cdot U = I_{n \times n} \quad (6)$$

$$V^T \cdot V = I_{m \times m} \quad (7)$$

where  $I$  is an identity matrix. Mathematically, the singular values<sup>11</sup> from matrix  $S$  are the square roots of the eigenvalues of  $X^T \cdot X$  or  $X \cdot X^T$ . The eigenvectors of  $X \cdot X^T$  are the columns of matrix  $U$  and the eigenvectors of  $X^T \cdot X$  are the columns of matrix  $V$ .

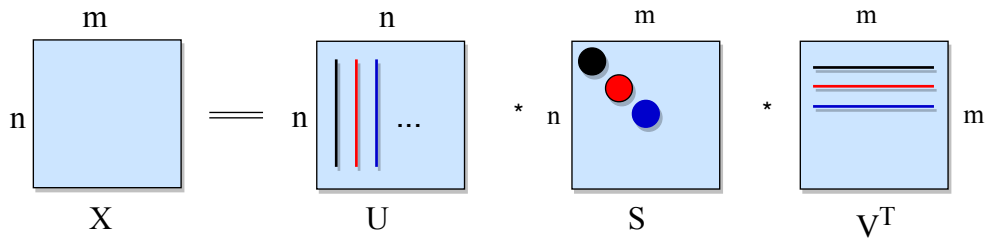


**Figure 7.: Singular value decomposition:** The image shows how a matrix is decomposed using the *singular value decomposition (svd)*. The matrix  $X$  is factorised into three matrices,  $U$ ,  $S$  and  $V$ , using equation 5. These factor matrices ( $U$ ,  $S$  and  $V$ ) are used for the low-rank estimation of the matrix  $X$ .

---

<sup>11</sup>[http://web.mit.edu/be.400/www/SVD/Singular\\_Value\\_Decomposition.htm](http://web.mit.edu/be.400/www/SVD/Singular_Value_Decomposition.htm)

Figure 7 explains how the *svd* of a matrix is computed (inspired from a lecture<sup>12</sup>). Matrix  $U$  contains information about how the tokens, arranged along the columns, are mapped to concepts. Matrix  $V$  stores information about how concepts are mapped to documents which are arranged along the rows.

### Low-rank approximation

A document-token matrix suffers from sparsity and shows no relation among tokens. A low-rank approximation of this matrix discards the features with small singular values (the last entries of the matrix  $S$  along the diagonal in equation 5) to deal with issues of sparsity and correlation among tokens. The features with large singular values (the top entries of the matrix  $S$  along the diagonal in equation 5) are retained. A low-rank approximation,  $X_k$  ( $k < m$ ), is computed using equation 8. The resulting matrix is dense [7]. The size of the reconstructed matrix  $X$  remains the same but its rank reduces to  $k$ .

$$X_{n \times m} = U_k \cdot S_k \cdot V_k^T \quad (8)$$

where  $U_k$  is the first  $k$  columns of  $U$ ,  $V_k$  is the first  $k$  rows of  $V$  and  $S_k$  is the first  $k$  singular values in  $S$ .  $X_k$  is called as the rank- $k$  approximation of full-rank matrix  $X$ . Figure 9 shows how the fraction of the sum of singular values changes with the fraction of the ranks of document-token matrices. If the ranks of matrices are reduced to 70% of corresponding full-ranks,  $\approx 90\%$  of the sum of singular values can be captured. The reduction to half of the full-ranks achieves  $\approx 80\%$  of the sum of singular values. This variation is shown for the document-token matrix of input and output file types attribute in figures 8 and 9 but its rank is not reduced for the analysis.

The ranks of the document-token matrices for name and description and help text attributes are reduced 5% of their corresponding full-ranks. It gives dense, low-rank approximations of these document-token matrices. In these matrices, the dense vector representations for the documents are shown along the rows and the tokens are arranged along the columns. The similarity (correlation or distance) is computed using similarity measures for each pair of document vectors. There are many similarity measures which can be used like *euclidean distance*, *cosine similarity*, *manhattan distance* or *jaccard index*. In this work, *cosine similarity* is used for name

---

<sup>12</sup><http://theory.stanford.edu/~tim/s15/l19.pdf>

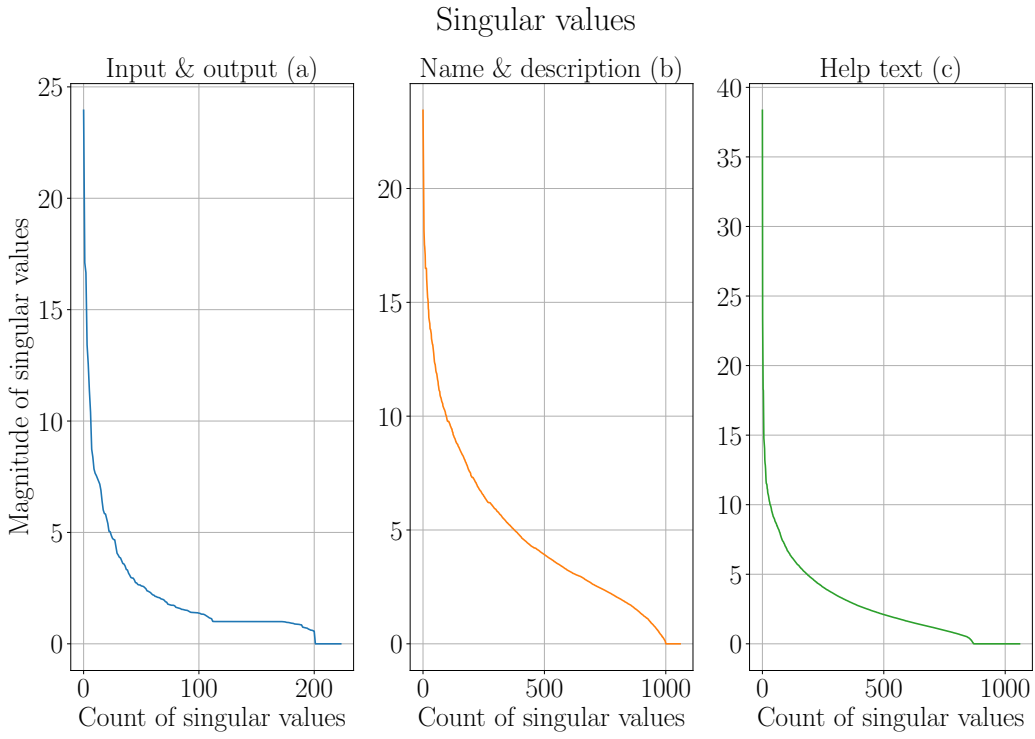


**Figure 8.: Singular values of document-token matrices:** The plot shows singular values computed using singular value decomposition (equation 5) for the document-token matrices of three attributes (input and output file types (a), name and description (b) and help text (c)). The diagonal matrix  $S$  contains the singular values sorted in a descending order. The x-axis shows the count of singular values and the y-axis shows the corresponding magnitude. The singular values are real numbers. In (a), (b) and (c), very few singular values have a large magnitude.

and description and help text attributes and *jaccard index* for input and output file types attribute to compute the similarity between each pair of document vectors. A real number between zero and one is assigned as the similarity score for a pair of documents. The higher the score, the higher is the similarity between a pair of documents. Computing this similarity for all the documents of an attribute gives a similarity matrix  $SM_{n \times n}$  where  $n$  is the number of documents. It is a symmetric matrix (also called correlation matrix). Three such matrices are computed, each corresponding to one attribute (input and output file types, name and description and help text) (figures 14, 17 and 20).

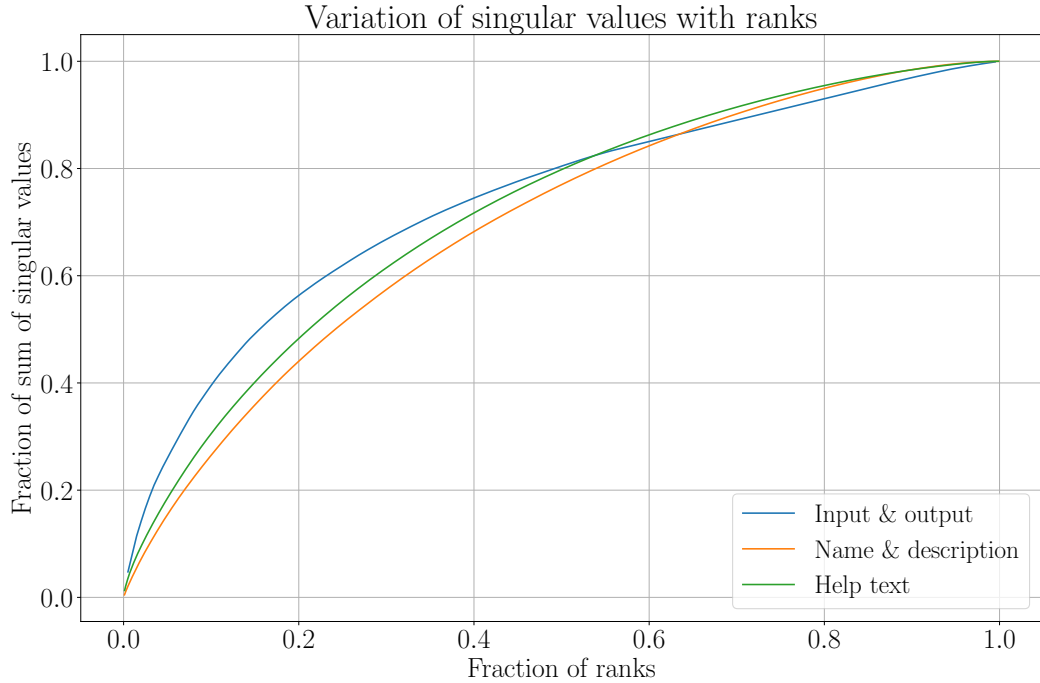


**Figure 9.: Variation of the fraction of ranks of document-token matrices with the fraction of sum of singular values:** This plot shows the variation of the ranks of the document-token matrices with the sum of their singular values. The ranks and sum of the singular values of these matrices vary. Therefore, they are converted to respective percentages for each matrix to merge them into one plot. For example, 0.2 on x-axis means 20% of the full-rank of a matrix. In equation  $rank_{fraction} = \frac{k}{N}$ ,  $k$  is the reduced rank and  $N$  is the full-rank of a matrix. Similarly, the y-axis shows the fraction of the sum of all singular values for each matrix. In equation  $sum_{fraction} = \frac{\sum_{i=1}^k s_i}{\sum_{i=1}^K s_i}$ ,  $K$  is the number of all singular values and  $s_i$  is the  $i^{th}$  singular value. The value  $k$  defines the number of top singular values considered for a document-token matrix when it is reduced to rank  $k$ . This plot shows that the rank reduction of a document-token matrix is directly proportional to the reduction of the sum of its singular values.

### 2.2.2. Paragraph vectors

Using *latent semantic analysis*, dense vectors are learned to represent each document. One limitation of this approach is to assess the quantity by which to lower the ranks of the document-token matrices in order to achieve the right document vectors. This

factor can be different for different document-token matrices. There are ways to find an optimal rank by optimisation using *frobenius norm* (as a loss function). But, it is not simple [8]. The weighted similarity scores are dominated by the similarity scores of input and output file types attribute. The similarity scores from the other attributes remain under-represented (section 4.1). Due to these drawbacks, the tools which have similar functions do not get pushed up on the ranking ladder (more similar tools should be at the top of the ranking ladder). To avoid these limitations, an approach known as *doc2vec* (document to vector) [9] is explored. It learns dense, fixed-size vectors for documents using a neural network. They are unique because they capture semantics present in the documents. The documents which share a similar context are represented by similar vectors. When *cosine similarity* is computed between a pair of vectors sharing similar context, a higher similarity score is observed. Moreover, it allows documents to have variable lengths.

## Approach

*Paragraph vectors* approach learns vector representations for documents and their words. The words which are used in a similar context have similar vectors. For example, tokens like *data* and *dataset* are generally used in similar context. Therefore, they are represented by the vectors which are similar. The vector representations of words in a document are learnt by maximising the following function:

$$\frac{1}{T} \cdot \sum_{t=k}^{T-k} \log p(w_t | w_{t-k}, \dots, w_{t+k}) \quad (9)$$

where  $T$  is the total number of words ( $w_i$ ) in a document and  $k$  is the window size. A window defines a context. A few words, which make a context, are taken and using them, each word is predicted [9]. The probability  $p$  is computed using a *softmax classifier*<sup>13</sup> and *backpropagation*<sup>14</sup> is used to compute the gradient. The *stochastic gradient descent* is used as an optimiser. Dense vectors are learned for each word and each document and they are called word and paragraph vectors, respectively. The word and paragraph vectors are averaged or concatenated to make a classifier which predicts the next words for a context. There are two ways to choose a context:

- Distributed memory: In this approach, a fixed length window of words are

---

<sup>13</sup><http://cs231n.github.io/linear-classify/#softmax>

<sup>14</sup><http://colah.github.io/posts/2015-08-Backprop>

chosen and the word and paragraph vectors<sup>15</sup> are used to predict words for this context. The word vectors are shared across all the paragraphs (documents) and a paragraph vector is unique to each paragraph. Figure 10 explains this approach.

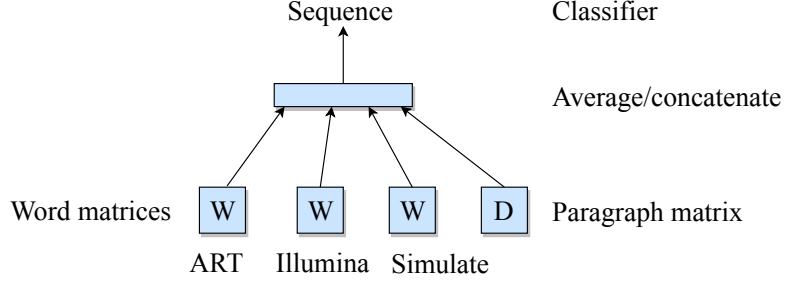


**Figure 10.: Distributed memory:** The image shows a mechanism for learning word and paragraph (document) vectors.  $W$  is a word matrix where each word is represented by a vector.  $D$  is a paragraph matrix where each paragraph (document) is represented by a vector. The word vectors are shared across all paragraphs (documents), but not the paragraph vectors. Three words *art*, *illumina* and *simulate* represent a context. The averaged or concatenated words and paragraph vectors make a classifier which is used to predict the word *sequence*.

- Distributed bag-of-words: In this approach, words are randomly chosen from a paragraph. A word is chosen randomly from this set of words and predicted using paragraph vectors. No order is followed in choosing words. Figure 11 explains this approach.

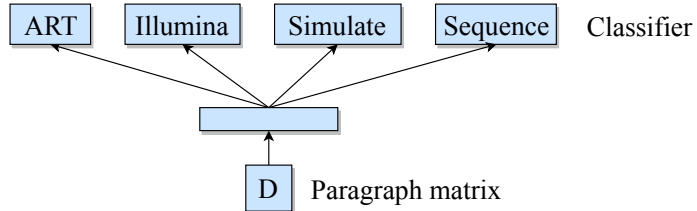


**Figure 11.: Distributed bag-of-words:** The image shows how paragraph vectors are learned by predicting a random word chosen from a randomly selected set of words.  $D$  is a paragraph matrix where each paragraph (document) is represented by a vector. In this approach, the order of the words does not matter.

---

<sup>15</sup>A paragraph and a document have the same meaning.

Figures 10 and 11 are inspired by the original work, distributed representations of sentences and document<sup>16</sup>. The second approach of learning paragraph vectors (distributed bag-of-words) is simple and is used to learn document (paragraph) vectors for name and description and help text attributes. Only paragraph vectors are learned in this approach and the number of parameters is also less than the distributed memory approach. These reasons make it computationally less expensive [9]. The number of parameters is  $\approx N \times z$  where  $N$  is the number of documents (paragraphs) and  $z$  is the dimensionality of each vector.

## 2.3. Similarity measures

Using *latent semantic analysis* and *paragraph vectors* approaches, document vectors are learned. A similarity measure is applied to get a similarity score for a pair of document vectors. This score quantifies the amount of similarity between a pair of documents. In this work, two similarity measures, *cosine similarity* and *jaccard index*, are used. They return a real number between zero and one as a similarity score.

### 2.3.1. Cosine similarity

It calculates the value of cosine angle between a pair of document vectors. Two vectors,  $x$  and  $y$ , are taken:

$$x \cdot y = |x| \times |y| \times \cos \theta \quad (10)$$

$$\cos \theta = \frac{x \cdot y}{|x| \times |y|} = \frac{x \cdot y}{\sqrt{x \cdot x} \times \sqrt{y \cdot y}} \quad (11)$$

where  $(\cdot)$  is the dot product. If  $(x \cdot x)$  or  $(y \cdot y)$  is zero,  $\cos \theta$  is set to zero. If the documents are dissimilar, then it is zero and if they are completely similar, it is one. For all other cases, it stays between zero and one. This score is understood as the probability of similarity between a pair of documents<sup>17</sup>.

---

<sup>16</sup><https://arxiv.org/abs/1405.4053>

<sup>17</sup><https://nlp.stanford.edu/IR-book/html/htmledition/dot-products-1.html>

### 2.3.2. Jaccard index

*Jaccard index* is a measure of similarity between two sets of entities and is given by the equation:

$$j = \frac{A \cap B}{A \cup B} \quad (12)$$

where  $A$  and  $B$  are two sets. The operation  $\cap$  gives the number of entities present in both the sets and operation  $\cup$  gives the number of unique entities combining both the sets [10]. This measure is used to compute similarity between two documents based on their file types. For example, the tool *linear\_regression* has *tabular* and *pdf* as its file types. Another tool *lda\_analysis* has *tabular* and *txt* as its file types. *Jaccard index* ( $j$ ) for the pair of tools is:

$$j = \frac{\text{length}[(\text{tabular}, \text{pdf}) \cap (\text{tabular}, \text{txt})]}{\text{length}[(\text{tabular}, \text{pdf}) \cup (\text{tabular}, \text{txt})]} = \frac{1}{3} = 0.33 \quad (13)$$

## 2.4. Optimisation

The similarity matrices are computed by applying similarity measures for each pair of document vectors. These matrices have the same dimensions ( $N \times N$ ,  $N$  is the number of documents (tools)). The scores in the similarity matrices are independent of each other. To combine these matrices, a simple idea would be to take an average of the corresponding rows from three similarity matrices. By doing this, the combined similarity scores of one document with all other documents are achieved. Iterating this process for all documents gives an average similarity matrix. The diagonal entries of this matrix are one and all the other entries are real numbers between zero and one. A better way to compute the combination of similarity matrices is to learn weights on the corresponding rows of three similarity matrices. These weights, real numbers between zero and one, are used to compute the weighted average of similarity matrices (equation 14). For the corresponding rows in similarity matrices, the weights sum up to one. Instead of using the fixed weights (of  $1/3 = 0.33$  ( $3$  is the number of similarity matrices)), an optimisation technique (section 2.4.1) is employed to compute them. A weighted similarity of a tool<sup>18</sup> with all other tools is computed as:

---

<sup>18</sup>A tool has three documents and each document has a similarity matrix of size  $N \times N$  where  $N$  is the number of tools.

$$SM^k = w_{io}^k \cdot SM_{io}^k + w_{nd}^k \cdot SM_{nd}^k + w_{ht}^k \cdot SM_{ht}^k \quad (14)$$

where each weight ( $w$ ) is a positive, real number and they satisfy  $w_{io}^k + w_{nd}^k + w_{ht}^k = 1$ .  $SM_{io}^k$ ,  $SM_{nd}^k$  and  $SM_{ht}^k$  are similarity scores (matrix rows) of the input and output file types, name and description and help text attributes, respectively for the  $k^{th}$  document. The similarity scores,  $SM^k$ , has a dimensionality of  $1 \times N$  where  $N$  is the number of tools. The gradient descent optimiser is used to learn the weights by minimising an error function. The ideal similarity values are set based on similarity measures and are used to define an error function. The maximum similarity between a pair of documents can be one (*cosine distance* and *jaccard index* can be at most one).

$$SM_{ideal} = [1.0, 1.0, \dots, 1.0]_{1 \times N} \quad (15)$$

where  $SM_{ideal}$  is ideal similarity scores of a document against all other documents and  $N$  is the number of documents. Using the ideal and computed similarity scores, mean squared error is computed (equations 16-18) for all three attributes. The attribute which measures lower error should get a higher weight and the attribute which measures higher error should get a lower weight.

#### 2.4.1. Gradient descent

Gradient descent is a popular algorithm for optimising a function with respect to its parameters. The equations 16-23 learn weights for the  $k^{th}$  tool by minimising mean squared error functions which are given as:

$$Error_{io}(w_{io}^k) = \frac{1}{N} \times \sum_{j=1}^N [(w_{io}^k \times SM_{io}^k - SM_{ideal})^2]_j \quad (16)$$

$$Error_{nd}(w_{nd}^k) = \frac{1}{N} \times \sum_{j=1}^N [(w_{nd}^k \times SM_{nd}^k - SM_{ideal})^2]_j \quad (17)$$

$$Error_{ht}(w_{ht}^k) = \frac{1}{N} \times \sum_{j=1}^N [(w_{ht}^k \times SM_{ht}^k - SM_{ideal})^2]_j \quad (18)$$

$$Error(w^k) = Error_{io}(w_{io}^k) + Error_{nd}(w_{nd}^k) + Error_{ht}(w_{ht}^k) \quad (19)$$

$$\arg \min_{w^k} Error(w^k) \quad (20)$$

$$w_{io}^k + w_{nd}^k + w_{ht}^k = 1 \quad (21)$$

In equations 16-19, the subscripts *io*, *nd* and *ht* refer to input and output file types, name and description and help text, respectively. Each weight term in equation 21 is a real number between zero and one and the equation is satisfied for each tool. To minimise the equation 20, the gradient of the error function with respect to weights is calculated (equation 22). The gradient specifies the rate of change of error with respect to weights. The equation to compute gradient for any attribute is given as:

$$Gradient(w^k) = \frac{\partial Error}{\partial w^k} = \frac{2}{N} \times ((w^k \times SM^k - SM_{ideal}) \cdot SM^k) \quad (22)$$

where *Gradient* is a three-dimensional vector ( $Gradient_{io}$ ,  $Gradient_{nd}$ ,  $Gradient_{ht}$ ) and the symbol  $(\cdot)$  refers to dot product of two vectors.  $SM^k$  is a vector of similarity scores for each attribute. Using the gradient, weights are updated for each attribute using the following equation:

$$w^k = w^k - \eta \cdot Gradient(w^k) \quad (23)$$

where  $\eta$  is learning rate.

#### 2.4.2. Learning rate decay

Finding a good learning rate is an important part of gradient descent optimisation. If it is high, it poses a risk of optimiser divergence. On the other hand, if it is small, the optimiser can take a long time to converge. Both of these situations are undesirable and should be avoided by starting off with a small learning rate and gradually decrease it over iterations. The decay is important because as learning saturates, only small steps towards the minimum of the error function are needed to converge. This technique is called time-based decay [11]. Figure 12 shows the decay of learning rate over iterations computed using the following equation:

$$lr^{t+1} = \frac{lr^t}{(1 + (decay * iteration))} \quad (24)$$

where  $lr^{t+1}$  and  $lr^t$  are learning rates for  $t + 1$  and  $t$  iterations, respectively and  $decay$  controls how steep or flat the learning rate curve is. *Iteration* is an iteration number. A high value of decay can make the learning rate drop quickly while a low value can make the learning rate drop slowly.

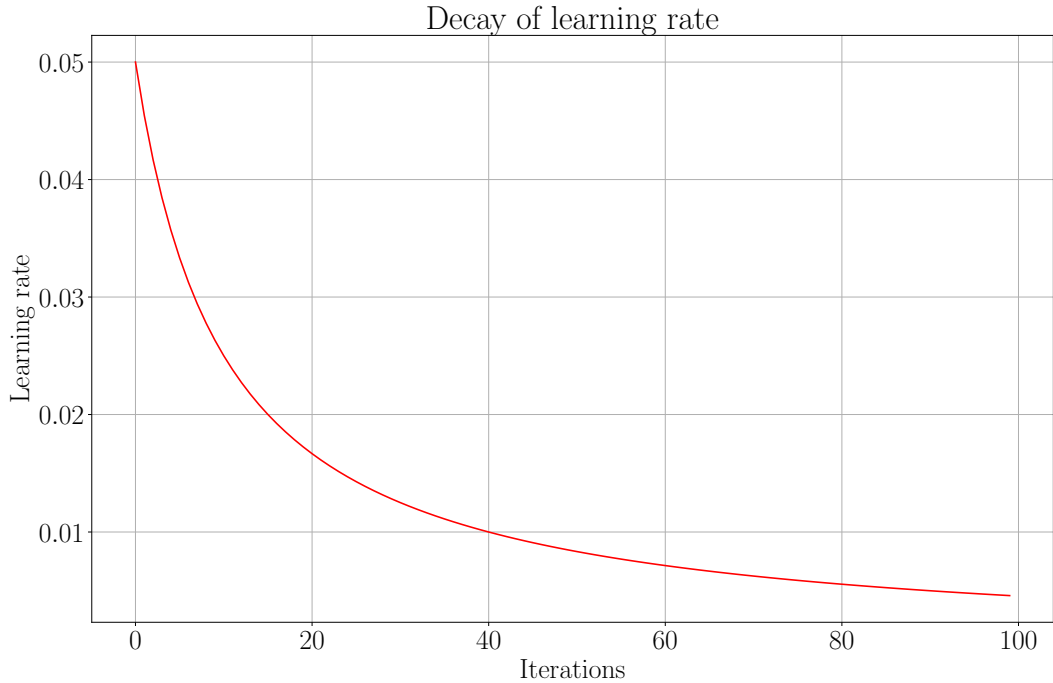


**Figure 12.: Decay of learning rate for gradient descent optimiser:** The plot shows how the learning rate for gradient descent changes with the iterations. It starts with a small value and decreases gradually over time. It is essential to have the learning rates which neither drops too quickly nor too slowly. Both of these ways can lead to the divergence or slow convergence of the optimiser respectively.

### 2.4.3. Weight update

#### Momentum

To reach the minimum point of an error function (equation 20), an optimiser should go down continuously without being blocked at saddle points<sup>19</sup>. At these points, the derivative of a function is zero. Adding a momentum term to weights avoids

---

<sup>19</sup><https://arxiv.org/abs/1703.00887>

these saddle points and an optimiser converges to the lowest point quickly. It gives a necessary push to keep going down the error function by adding a fraction of the previous update to the current update [11, 12]. The weight is updated for each iteration using:

$$update_{t+1} = \gamma \cdot update_t - \eta \cdot Gradient(w_t) \quad (25)$$

$$w_{t+1} = w_t + update_{t+1} \quad (26)$$

where  $update_{t+1}$  is the update for changing weights for the current iteration ( $t+1$ ).  $update_t$  is the previous update. Eta ( $\eta$ ) is a learning rate and  $Gradient$  is with respect to weight  $w_t$ . Gamma ( $\gamma$ ) specifies the fraction of previous update to be used.

### Nesterov's accelerated gradient

The inclusion of momentum is useful to get necessary advance towards finding the minimum of the error function. However, the speed of going down the slope of an error function should become less if there is a possibility of change in gradient direction. In this situation, the speeding up can be avoided by estimating the forthcoming gradient (gradient for the next step) and then correcting it [13]. The weight is updated for each iteration using:

$$update_{t+1} = \gamma \cdot update_t - \eta \cdot Gradient(w_t + \gamma \cdot update_t) \quad (27)$$

$$w_{t+1} = w_t + update_{t+1} \quad (28)$$

The meanings of terms in equation 28 remain the same as in the previous equations 25 and 26.

### Gradient verification

To verify that the gradient computed using partial derivative is correct, an approximated gradient (linear approximation) is computed using equation 29. The difference between these two variants should be close to zero.

$$Gradient(w) = \frac{\partial Error}{\partial w} \approx \frac{Error(w + \epsilon) - Error(w - \epsilon)}{2 \cdot \epsilon} \quad (29)$$

where  $\epsilon$  is a small number ( $\approx 10^{-4}$ ). Figure 13 shows the difference of the actual (using partial derivative) and approximated gradients for all three attributes.

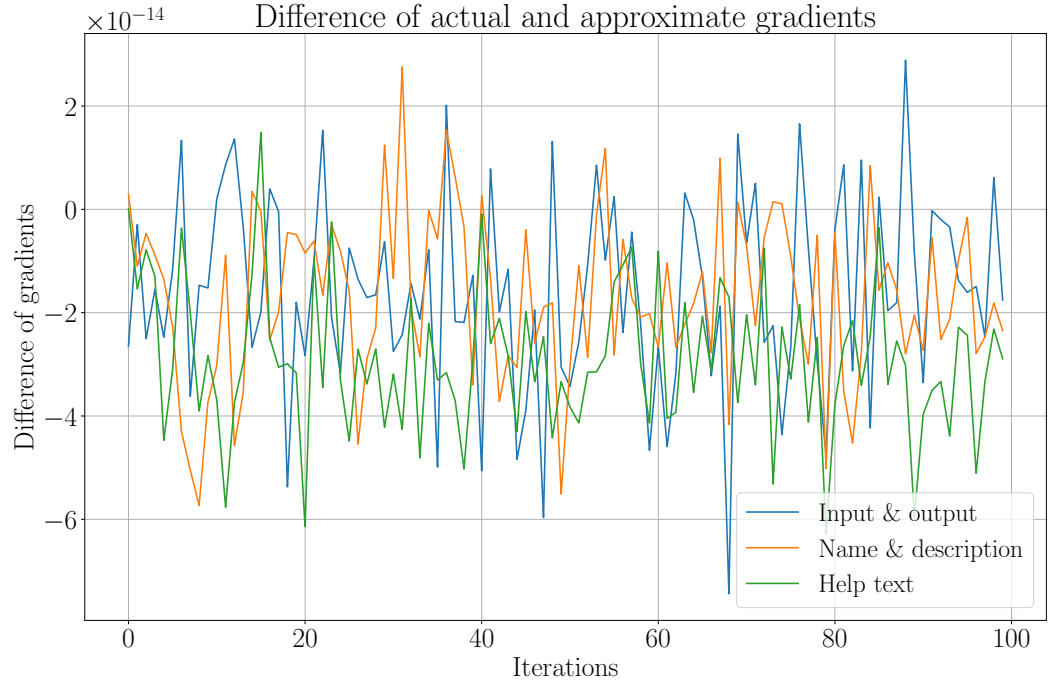


**Figure 13.: Difference between actual and approximated gradients:** The plot shows the difference between the actual and approximated gradients. They are computed for three attributes and averaged for all tools over 100 iterations of optimisation. The difference of gradients is consistent ( $\approx 10^{-14}$ ) which means that the actual and approximated gradients are same. It also proves that the gradients computed using partial derivative are correct.

# 3. Experiments and results

Over 1,050 scientific tools are used for computing similarities among them. Three different attributes, input and output file types, name and description and help text, are used for compiling metadata of tools. The help text attribute is noisy and contains text parts which are not useful for finding similarities among tools. Therefore, only the first four lines of text are used from this attribute. *Jaccard index* is used as a similarity measure for input and output file types attribute and *cosine similarity* is used for name and description and help text attributes. *Gradient descent* is used to optimise the combination of similarity scores computed from three attributes by learning weights for the similarity scores. *Mean squared error* is used as an error function for the optimiser. A true similarity value between a pair of tools is set to one. The optimiser executes for 100 iterations to stabilise the error drop. *Nesterov's accelerated gradient* is used to ensure a steady drop in error. A time-based decay strategy is implemented to decay the learning rate after each iteration. The initial value of learning rate is set to 0.05 and its drop is kept steady.

## 3.1. Latent semantic analysis

Document-token and the corresponding similarity matrices are sparse. Using *latent semantic analysis*, dense vectors are learned for each document by reducing the ranks of document-token matrices. It allowed the corresponding similarity matrices to become dense too. Due to this, larger weights are learned for similarity matrices. The rank reduction is not applied to the document-token matrix of input and output file types. It is not beneficial to find any correlation among file types. *Singular value decomposition (svd)* for reducing the ranks of document-token matrices is used from its implementation at *numpy's linear algebra package*<sup>1</sup>.

---

<sup>1</sup><https://docs.scipy.org/doc/numpy-1.14.0/reference/generated/numpy.linalg.svd.html>

### 3.1.1. Full-rank document-token matrices

Figure 14 shows the similarity matrices computed using full-rank document-token matrices for input and output (figure 14a), name and description (figure 14b) and help text (figure 14c) attributes. These similarity matrices and weights (from figure 15) are combined to get a weighted average similarity matrix (figure 14d). The weights for input and output file types are larger than that of the other two attributes (figure 15). It is because the similarity matrix of input and output file types (figure 14a) is denser than for name and description (figure 14b) and help text (figure 14c). Figure 16 shows the average of weighted similarities computed using weights learned by the optimiser (optimal weights) and uniform weights ( $\frac{1}{3}$ , where 3 is the number of attributes). A row-wise average is computed from the weighted similarity matrix (14d) to get an average of weighted similarities with optimal weights. The similarity matrices from figures 14a, 14b and 14c are combined using uniform weights and then, a row-wise average is computed to get an average of weighted similarities using uniform weights. The similarity values in figure 16 are small ( $\approx 0.02 - 0.14$ ).

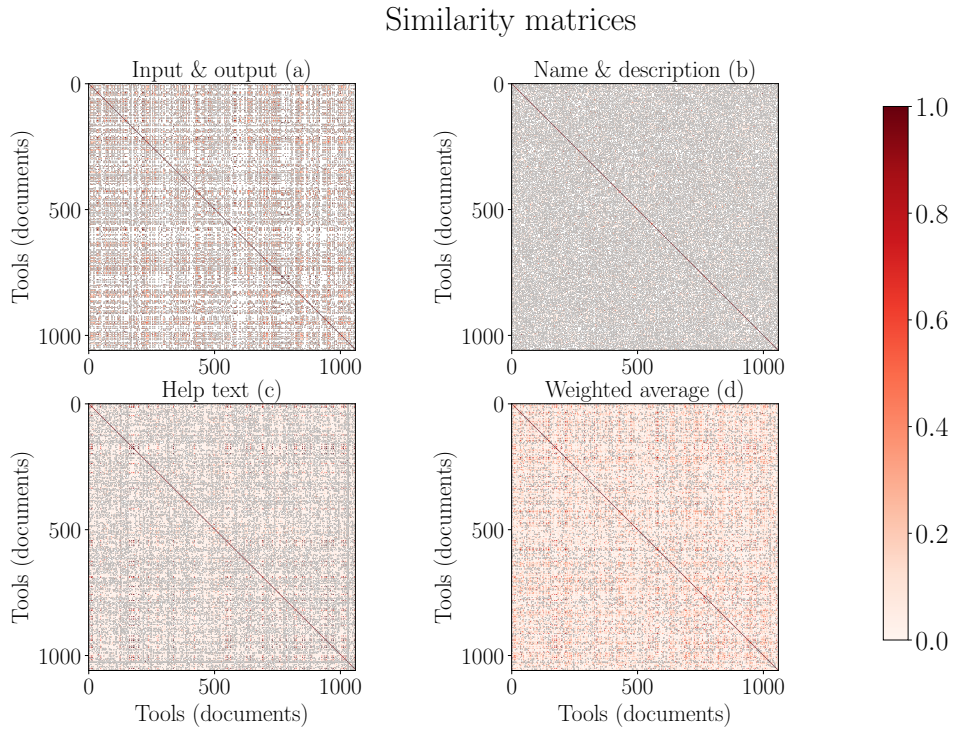


**Figure 14.: Similarity matrices computed using full-rank document-token matrices:** The heatmaps show the similarity matrices for input and output file types (a), name and description (b) and help text (c) attributes. The subplot (d) shows a weighted average of the similarity matrices computed in (a), (b) and (c). The weights used in computing (d) are shown in figure 15. The corresponding document-token matrices have their full-ranks. The similarity matrix in (a) is denser than the similarity matrices in (b) and (c). The similarity matrices in (b) and (c) are sparse.

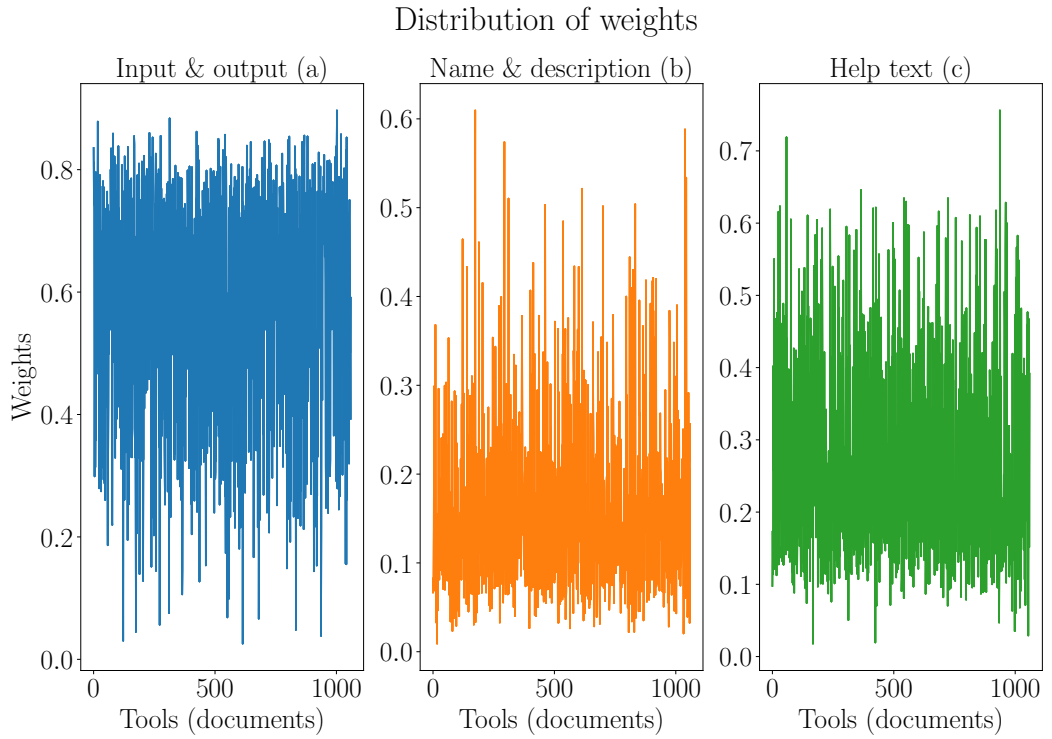


**Figure 15.: Distribution of weights learned for similarity matrices computed using full-rank document-token matrices:** The plot shows the distribution of weights learned for the similarity matrices in 14a, 14b and 14c by the optimiser for different attributes. The corresponding document-token matrices have their full-ranks. The weights for (a) are larger than for (b) and (c) because the corresponding similarity matrix (14a) is denser than the similarity matrices in (14b) and (14c).

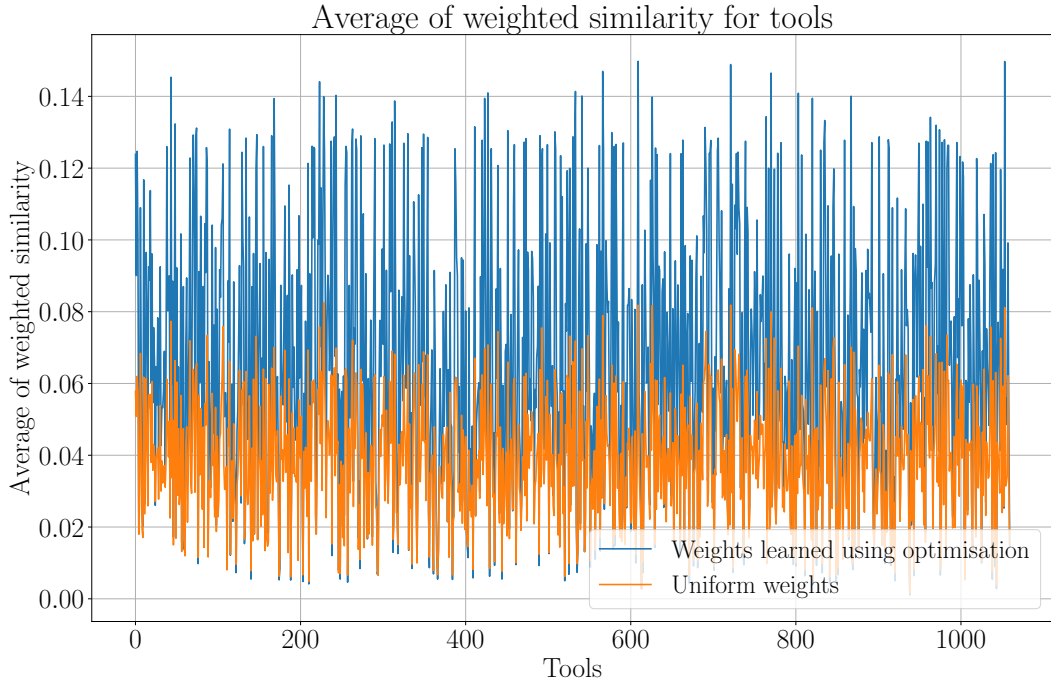


**Figure 16.: Average of weighted similarities computed using uniform and optimal weights:** The plot shows the average of weighted similarities computed using the uniform and optimal weights (learned by the optimiser). The corresponding document-token matrices have their full-ranks. The similarity values are low for the uniform as well as optimal weights. For the optimal weights, they are larger than for the uniform weights.

### 3.1.2. 5% of full-rank

The ranks of the document-token matrices for name and description and help text attributes are reduced to 5% of their corresponding full-ranks. By choosing this low value, only the top  $\approx 20\%$  of the sum of singular values is considered (figure 9). Figure 17 shows that the similarity matrices of name and description and help text become denser compared to figure 14. The weights learned for name and description (18b) and help text (18c) are also larger than for input and output file types (18a). An average of the weighted similarities is computed (figure 19) following the same approach explained in section 3.1.1. The similarity values in figure 19 increase ( $\approx 0.05 - 0.22$ ) compared to figure 16.

### Similarity matrices

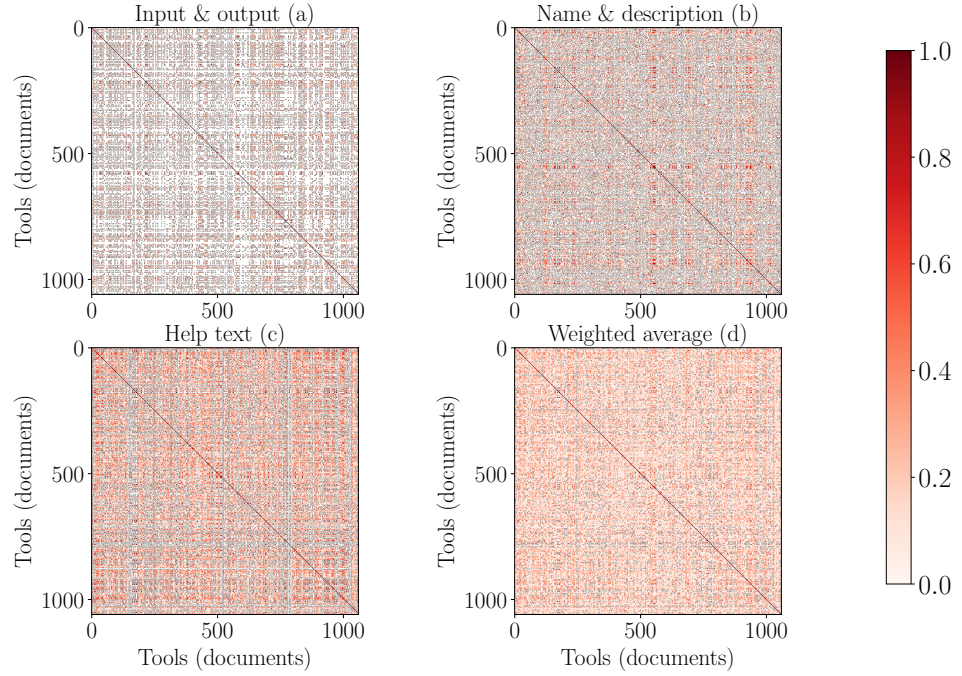


**Figure 17.: Similarity matrices computed using document-tokens matrices reduced to 5% of their full-ranks:** The heatmaps show the similarity matrices for input and output file types (a), name and description (b) and help text (c) attributes. The subplot (d) shows the weighted average of similarity matrices computed in (a), (b) and (c). The corresponding document-token matrices are reduced to 5% of their full-ranks. The weights used in computing (d) are shown in figure 18. The similarity matrices in (17b) and (17c) become denser than in (14b) and (14c), respectively.

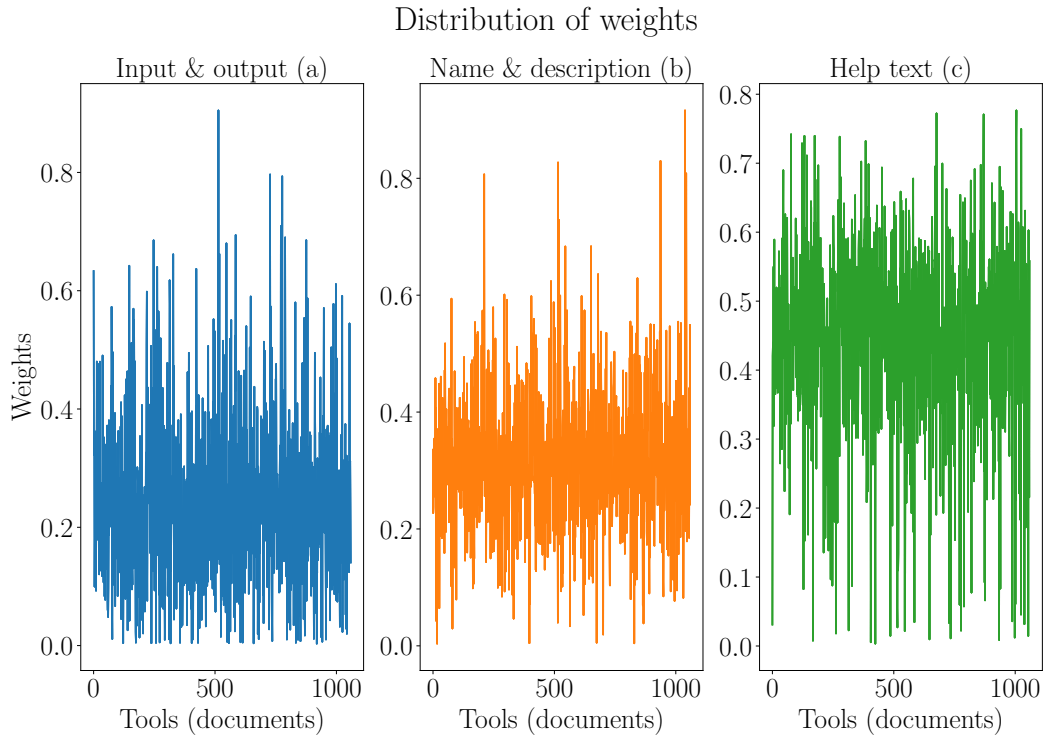


**Figure 18.: Distribution of weights learned for similarity matrices computed using document-token matrices reduced to 5% of their full-ranks:** The plot shows the distribution of weights learned for the similarity matrices (17a, 17b and 17c) by the optimiser. The corresponding document-token matrices are reduced to 5% of their full-ranks. The weights for (b) and (c) are larger than for (a).

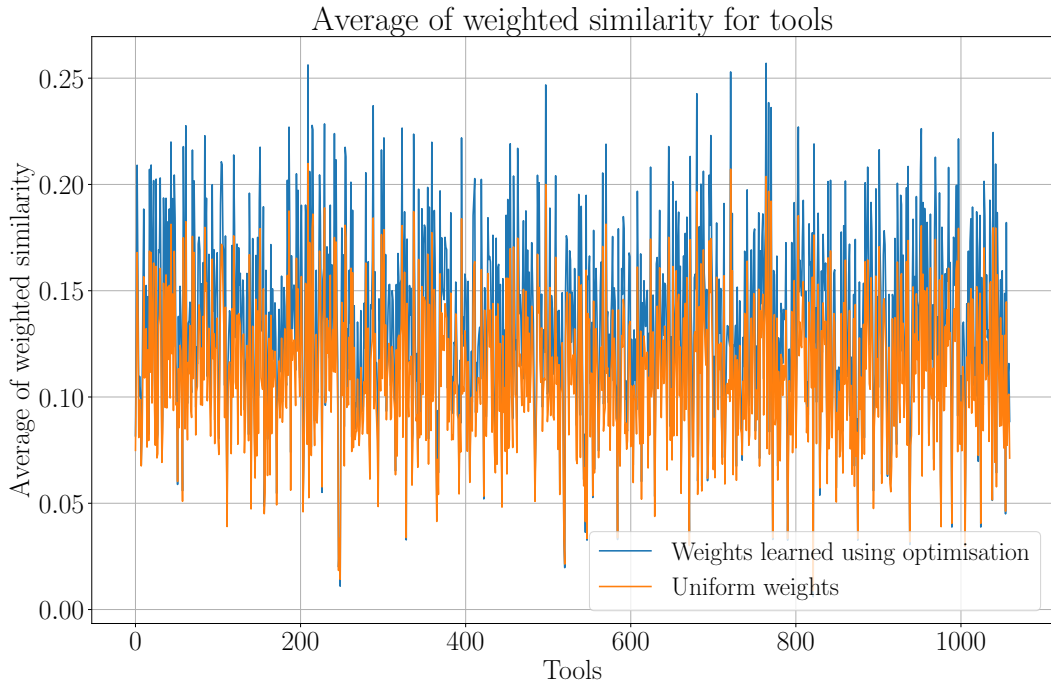


**Figure 19.: Average of weighted similarities computed using uniform and optimal weights:** The plot shows the averages of weighted similarities computed using uniform and optimal (learned by the optimiser) weights. The corresponding document-token matrices are reduced to 5% of their full-ranks. The similarity values increase compared to figure 16 for the uniform as well as optimal weights.

### 3.2. Paragraph vectors

*Paragraph vectors* approach is used to learn a fixed-length, multi-dimensional vector for each document of name and description and help text attributes. When the number of tokens for a document is lower, a lower number of dimensions is used for computing dense vectors. Figure 5 shows that the number of tokens is higher for help text than for name and description. Therefore, the dimension is set to 100 and 200 for name and description and help text, respectively. The window size for sampling text is 5 and 15 for name and description and help text, respectively. The neural network is iterated over 10 epochs and each epoch has 800 iterations. In each epoch, all documents are used for training. A python implementation of this approach, *gensim*<sup>2</sup>,

---

<sup>2</sup><https://radimrehurek.com/gensim/models/doc2vec.html>

is used to learn these vectors. Out of the two approaches (*distributed memory* and *distributed bag-of-words*) to learn dense vectors, *distributed bag-of-words* approach is applied to learn these vectors. It does not compute word vectors which makes it computationally less expensive. Using document-token matrices, the similarity matrices are computed (figure 20) by applying similarity measures. The similarity matrices for name and description and help text are denser compared to figures 14 and 17. The weights learned for name and description (21b) and help text (21c) attributes are larger compared to input and output file types (21a) attribute. Figure 22 shows that the averages of weighted similarities are larger than those of the *latent semantic analysis* approaches (figures 16 and 19). The average of weighted similarity increases to  $\approx 0.30$  using optimal weights. For uniform weights too, the average increases to  $\approx 0.25$  (figure 22).

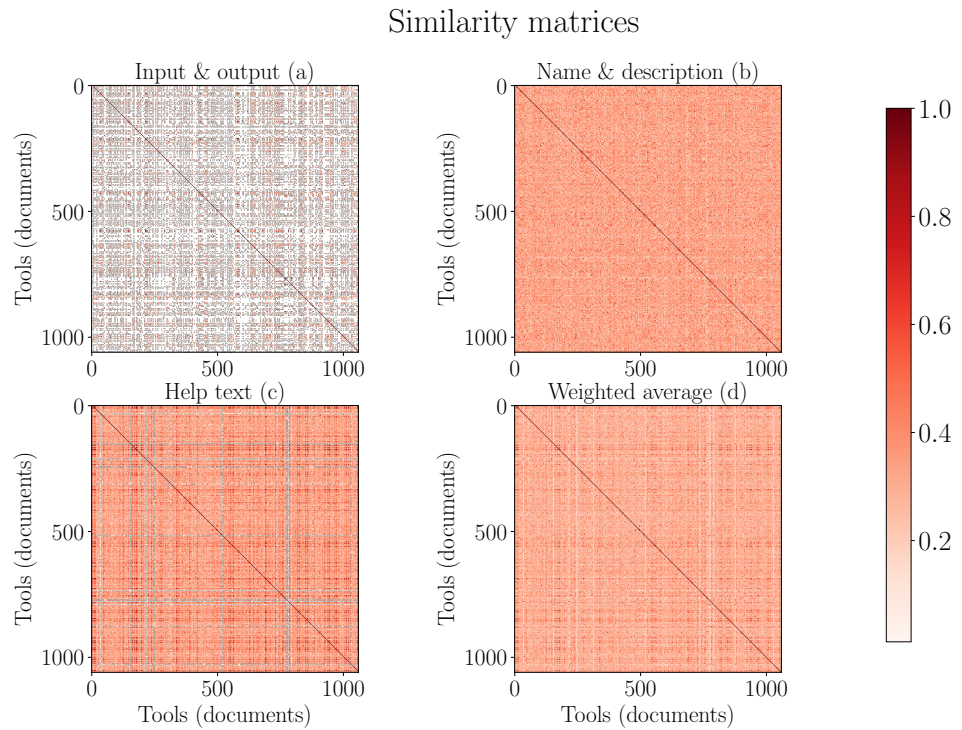


**Figure 20.: Similarity matrices using paragraph vectors approach:** The heatmaps show the similarity matrices for input and output (a), name and description (b) and help text (c) attributes. The subplot (d) shows a similarity matrix which is the weighted average computed using (a), (b) and (c). The weights used in computing the weighted average similarity matrix in (d) are shown in figure 21. The similarity matrices in (b) and (c) are denser than the similarity matrix in (a).

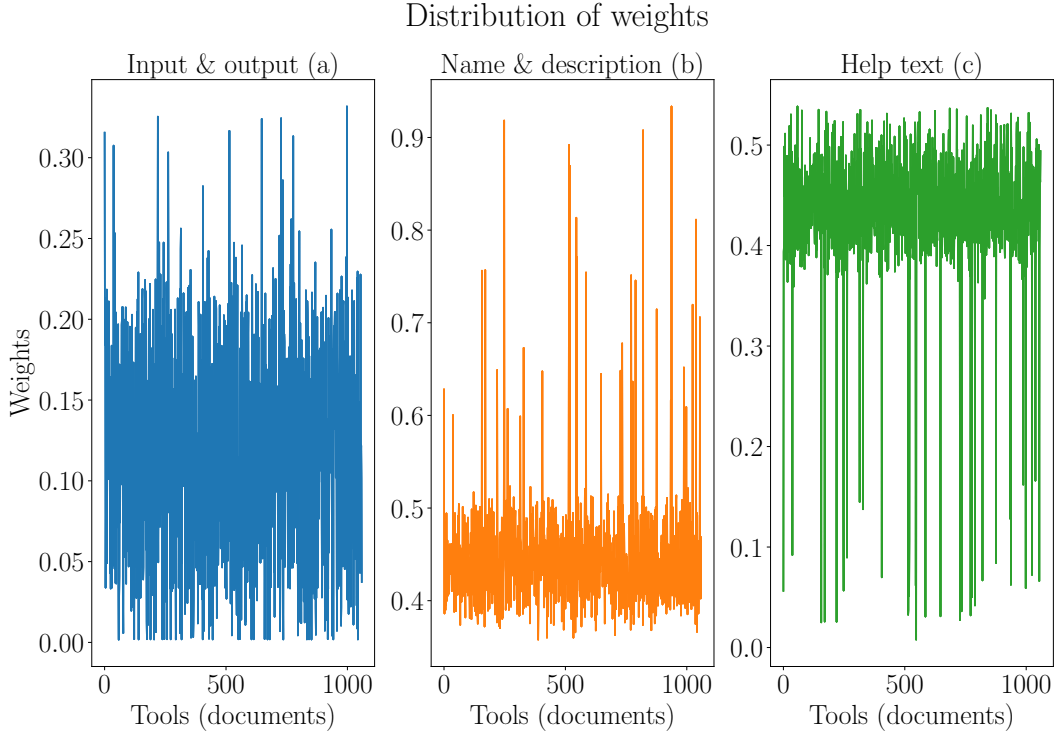


**Figure 21.: Distribution of weights for similarity matrices computed using paragraph vectors approach:** The plot shows the distribution of weights learned for the similarity matrices (20a, 20b and 20c) by the optimiser. The document vectors are learned by the *paragraph vectors* approach for name and description and help text attributes. The weights for (b) and (c) are larger than for (a) because the corresponding similarity matrices in (20b) and (20c) are denser than the similarity matrix in (20a).

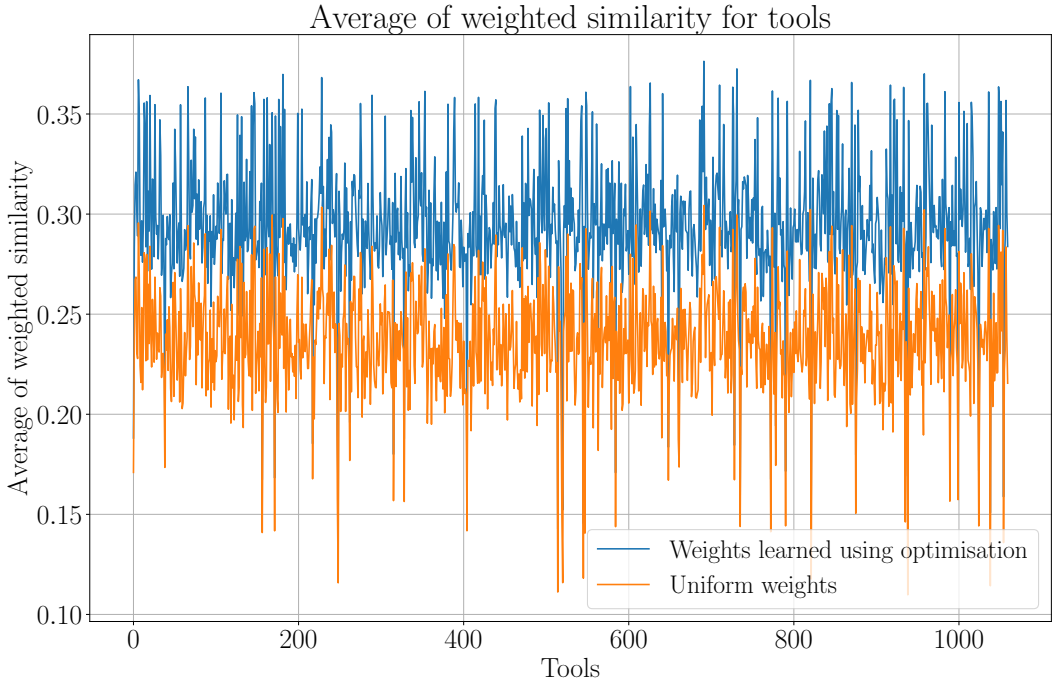


**Figure 22.: Average of weighted similarities computed using uniform and optimal weights:** The plot shows a comparison of the averages of weighted similarities computed using optimal (learned by the optimiser) and uniform weights. The document vectors are learned by the *paragraph vectors* approach for name and description and help text attributes. The similarity values increase compared to figures 16 and 19 for the uniform as well as optimal weights.

### 3.3. Comparison of two approaches

A comparison is made among the similar tools computed by two approaches (*latent semantic analysis* and *paragraph vectors*) used in this work. All similar tools for *hisat* are sorted in the descending order of their similarity scores and only the top two similar tools are selected for making a comparison. Top-2 similar tools for *hisat* are computed, once with its full-rank document-token matrices (table 2) and again with the document-token matrices reduced to 5% of their full-ranks (table 3). Moreover, two similar tools for *hisat* are computed (table 4) using *paragraph vectors* approach for comparison. Using tables 2, 3 and 4, the similar tools for *hisat* are compared with their respective similarity scores for different attributes. The description below each table gives the values of the optimal weights (learned by the optimiser). For

example, the weighted similarity in the first row of table 2 is calculated using the following equation:

$$0.38 \cdot 0.77 + 0.10 \cdot 0.07 + 0.13 \cdot 1.0 = 0.42 \quad (30)$$

Similar tools	Input & output	Name & desc.	Help text	Wt. similarity
Hisat2	0.38	0.07	1	0.42
Srma_wrapper	0.5	0.12	0.01	0.4

**Table 2.: Similar tools (top-2) for *hisat* computed using full-rank document-token matrices:** The table shows top-2 similar tools selected for *hisat*. Full-rank document-token matrices are used for computing similarity matrices. The weights learned by the optimiser are 0.77 (input and output file types), 0.10 (name and description) and 0.13 (help text). *Wt. similarity* is weighted similarity. The similarity scores for name and description is low.

Similar tools	Input & output	Name & desc.	Help text	Wt. similarity
Hisat2	0.38	1	1	0.83
Srma_wrapper	0.5	1	0.64	0.69

**Table 3.: Similar tools (top-2) for *hisat* computed using document-token matrices reduced to 5% of full-rank:** The table shows top-2 similar tools selected for *hisat*. Document-token matrices of name and description and help text attributes are reduced to 5% of their full-ranks. The weights learned by the optimiser are 0.27 (input and output file types), 0.23 (name and description) and 0.5 (help text). *Wt. similarity* is weighted similarity. The similarity scores for name and description is high.

In table 2, for name and description column, the similarity scores are too less (0.07 and 0.12 for *hisat2* and *srma\_wrapper*, respectively). In table 3, the similarity scores for name and description are not correct because they get 1.0 as similarity scores despite their descriptions are not exactly same. These incorrect interpretations can lead to wrong similarity assessment. As the low-rank estimation of the document-token matrix of input and output file types attribute is not done, its score remains the same in tables 2 and 3 (first columns).

Similar tools	Input & output	Name & desc.	Help txt.	Wt. similarity
Hisat2	0.38	0.46	1	0.67
Tophat	0.25	0.73	0.54	0.58

**Table 4.: Similar tools (top-2) for *hisat* computed using paragraph vectors approach:** The table shows top-2 similar tools selected for *hisat*. The weights learned by the optimiser are 0.14 (input and output file types), 0.44 (name and description) and 0.42 (help text). *Wt. similarity* is weighted similarity.

*Hisat2* has the same score for input and output column in all the tables 2, 3 and 4. In table 4, the similarity scores seem to be reasonable, neither too high and nor too low. The similar tool ranked second (*tophat*) in table 4 is more relevant than those from tables 2 and 3. From tables 2, 3 and 4, it is concluded that the *paragraph vectors* approach works better than the *latent semantic analysis* approach. A complete list of similar tools computed using all different approaches can be seen using the links of visualisers mentioned in the appendix.

# 4. Conclusion

## 4.1. Metadata of tools

The help text attribute was noisy containing a lot of words which were generic and provided little information to identify the tools. On the other hand, it was necessary for the analysis as it supplied more metadata. Therefore, it needed more filtering than other attributes. Only the first four lines of text were taken for the analysis from help text. The metadata from input and output file types and name and description was helpful. The extraction of metadata from the *github*'s multiple repositories was slow<sup>1</sup>. Therefore, the metadata from the *xml* files was read into a tabular file and it was used as the data source for this analysis.

## 4.2. Approaches

### 4.2.1. Latent semantic analysis

*Latent semantic analysis* approach relied on the rank reduction of document-token matrices. It removed unimportant dimensions and worked better than using the full-rank documents-token matrices. However, due to the lack of knowledge of the exact amount of rank reduction, the loss of important dimensions was also risked. During optimisation, more importance was given to input and output file types which were many times undesirable. The similarity scores learned for different attributes were sometimes under-represented or over-represented as explained in section 3.3. Due to these limitations, this approach should not be used for computing similarities among tools. It may lead to wrong similarity assessment. However, this approach was simple and took less time ( $\approx 350$  seconds) to complete. The low-rank estimations of the sparse document-token matrices were easily computed using *singular value decomposition*. The results can be visualised using the links

---

<sup>1</sup>The extraction of  $\approx 1,050$  tools took  $\approx 30$  minutes.

mentioned in the appendix (section A.1). Though this approach did not compute similar tools correctly, it provided insights to look for approaches which can learn better document vectors.

### 4.2.2. Paragraph vectors

The *paragraph vectors* worked in a more robust way than the *latent semantic analysis* approach to find similarities among tools. The vectors learned for the name and description and help text attributes were similar for similar documents. Due to these vectors, relevant similarity scores were computed among tools. The weighted similarity scores were more dominated by the similarity scores from the name and description and help text attributes because larger weights were learned for these attributes. Though this approach performs better than the previous approach, few dissimilar tools appear in the list of top-20 similar tools for a tool (these results can be seen in the visualiser<sup>2</sup>). It happens because the similarity assessment is dependent on the plain text in name and description and help text attributes. Sometimes they are not descriptive (for the name and description attribute) or even absent (for the help text attribute). Due to these issues, the amount of text for the neural network is less to learn vectors which can differentiate among documents in a good way. Despite this limitation, this approach leads to a good starting point to visualise similar tools. The tools at the top of the list of similar tools for many tools are relevant. The computation of similar tools was slow as it took  $\approx 1,000$  seconds to finish. Most of the time was spent to learn the document vectors.

### Significance to the recommendation system

The second part of the thesis deals with the prediction of tools for workflows. To build a recommendation system, alongside the predicted tools for any workflow, their respective similar tools (for example, top-2 or top-3 similar tools) computed using *paragraph vectors* approach can be shown. This would give more options to the users for their data processing using the Galaxy as they can replace a tool by choosing a tool from the combined set of the predicted and similar tools. Moreover, this tool recommendation system can make users aware of the newly added tools if they are similar to the existing ones.

---

<sup>2</sup>[https://rawgit.com/anuprulez/similar\\_galaxy\\_tools/doc2vec/viz/similarity\\_viz.html](https://rawgit.com/anuprulez/similar_galaxy_tools/doc2vec/viz/similarity_viz.html)

### 4.3. Optimisation

Learning weights on similarity scores worked in a stable way. The *gradient descent* optimiser was used with *mean squared error* as the loss function. *Mean squared error* was used because the hypothesis similarity scores distribution needed to be as close as possible to the true distribution (based on the similarity measures). The risk of getting stuck at saddle points or local minima was reduced by using momentum with an accelerated gradient to update the weights (parameters of the error function). The gradient computed using partial derivative was verified with the approximated gradient (linear approximation) by computing a difference between them.

# 5. Future work

## 5.1. Get true similarity values

To quantify improvements in the ranking of similar tools for a tool computed by different approaches, true similarity scores should be set for each pair of tools. For example, a dictionary of 10 similar tools can be created for each tool. Then, the computed similar tools can be verified against this true set of similar tools. Otherwise, it is required to have a visualiser to look through the similar tools. It would ensure whether the approaches actually work in finding similar tools. At the same time, it is not an easy task to create these logical categories and define similarity scores within these categories.

## 5.2. Exclude low similarity scores

The similarity matrices were dense. The low scores from similarity matrices can be excluded to retain only high scores. One way is to find the median of similarity scores for a tool. The similarity scores lower than the median can be set to zero. Then, the optimisation would use only important scores to compute and minimise the error.

## 5.3. Formulate different error functions

*Mean squared error* was used as a loss function for the optimiser. Other error measures like *cross-entropy* can be used. With a new error function, it is necessary to redefine the true similarity value which would depend on the similarity measures. Using *cross-entropy* error function with the same similarity measures (*cosine similarity* and *jaccard index*), one term in the error function would always be zero as the true similarity between a pair of tools would be 1.0. Different similarity measures like

*euclidean distance* can be used. For this, the true similarity value between a pair of tools should be 0.

## 5.4. Acquire more tools

The number of tools for performing the analysis can be increased. It would provide more data and consequently, more context to learn better semantics in text documents.

## 5.5. Learn tool similarity using workflows

It can be assumed that the tools which are similar are used for similar kind of data processing. This concept can be used to assess similarities among tools. The *distributed memory* approach learns vectors for words in a document. The document can be replaced by paths extracted from workflows and tools can be replaced by words. Then, dense vectors for tools (figure 34e) can be learned. The tools which are used in a similar context would learn similar vectors.

## **Part II.**

**Predict next tools in scientific  
workflows**

# 6. Introduction

## 6.1. Galaxy workflows

A Galaxy workflow is a sequence of scientific tools to process biological data. The tools are connected one after another forming a data processing pipeline. This pipeline allows multiple transformations of datasets in one operation<sup>1</sup>. Adjacent tools are connected through compatible file types which means that the output file type of one tool is consumed by its next tool. A workflow is a directed acyclic graph as shown in figure 23. It can have multiple paths between its input and output tools and these paths can have one or more tools in common. Each path has a direction commencing from an input tool and ending at an output tool. In figure 23, the tools like *get flanks*, *awk* and *intersect* are common in both the paths.

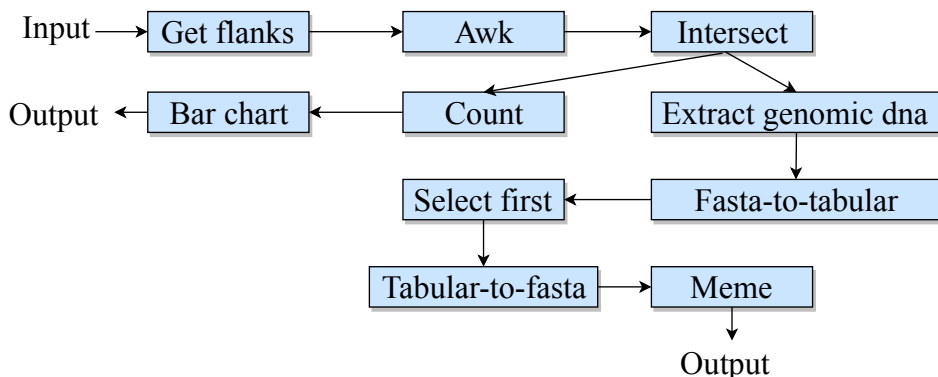


**Figure 23.: A workflow:** The image shows a workflow with two paths. It takes input data, processes it through multiple steps involving many tools and gives two outputs.

To create a workflow, a tool is chosen from the list of tools and is connected to the previous one. At each step, a tool can connect to one or more tools which are compatible with the previous one. The decision to select a tool may depend on

---

<sup>1</sup><https://galaxyproject.org/learn/advanced-workflow>

several factors like the kind of input data or data-processing required to attain the desired output. A workflow can also be created using datasets from the Galaxy history<sup>2</sup>.

### 6.1.1. Motivation

To create a workflow, having multiple paths where each path can have many tools, is a complex task. A user needs to have knowledge of the tools and their parameters like input and output types that should come next. There are multiple similar tools for each tool as explained in the first part of the thesis. A preference should be learned for these tools so that the most probable tools can be predicted while creating a workflow. These tools must be compatible with the previous tool because no two tools with incompatible file types can connect to each other on the canvas of Galaxy workflow editor. This knowledge can be gained only through experience. The prediction of tools with compatible file types should also avoid the wastage of the user's time when a workflow is created consisting of tools which may not give the desired results. A user who is new to the Galaxy platform and is not aware of the existing tools, creating a workflow can be a laborious and time-consuming effort. A recommendation system to predict tools for workflows can solve these issues.

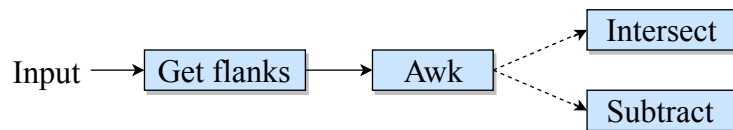


**Figure 24.: Multiple next tools:** The image shows a part of a workflow where one tool can be connected to multiple tools.

In figure 24, the tool *awk* can be connected to two tools, *intersect* and *subtract*. To impart the knowledge of follow-up tools and assist a user at each step of creating a workflow, a predictive system to recommend tools is proposed. It should recommend the most probable set of tools when a tool is used making it easier to create a workflow. A reduction in the amount of time taken to create workflows is also expected because the need to search for the next tools in the list of tools is avoided. The recommended tools should also make the creation of workflows less susceptible to errors as it recommends only those tools which have compatible file types. This should avoid the wastage of compute time.

---

<sup>2</sup><https://galaxyproject.org/tutorials/histories>

## 7. Related work

A workflow is a directed acyclic graph in which tools are connected sequentially. While creating the workflow, the next tools should be predicted by taking into account all the previous connected tools. To make such a prediction system, it is important to explore some work from the machine learning field which analyses similar data. Interestingly, learning from sequential data is a popular task in many fields like natural language processing [14, 15], clinical data analysis [16] and speech processing [17, 18].

In the natural language processing field, deep learning models are used to learn sequences of words. It aims to categorise a corpus based on its sentiments and learn part-of-speech tagging and a dense vector for each word. The categorisation of sentiments involves learning core contexts present in the sentences (sequences of words). The part-of-speech tagging divides a sentence into multiple parts-of-speech like an adjective, adverb, object, subject and conjunction. It also depends on finding the contexts hidden in the long sequences of words. An accuracy of  $\approx 85\%$  is achieved using the recurrent neural network (*gated recurrent unit*) for sentiment analysis and for part-of-speech tagging, the accuracy goes up to  $\approx 93\%$  [14].

For clinical data too, learning long sequences of data proves to be beneficial [16]. In this work, the health states of patients recorded at different time points are analysed by accessing their electronic health records. The future health states of patients are predicted using the sequences of their health states in the past. The *long-short term memory (lstm)*, a kind of recurrent neural network, is used to classify the sequences of health states. An accuracy of  $\approx 85\%$  is achieved by applying the necessary regularisation techniques like dropout and weight normalisation.

The research presented in [17, 18] use the recurrent neural network to model music and speech signals. The performances of the traditional recurrent, *long-short term memory (lstm)* and gated recurrent units (*gru*) are analysed. After the analysis, it is concluded that the traditional recurrent units do not learn semantics present in sequences, but the *lstm* and *gru* do. In this study, the sequences of 20 continuous

samples (20 steps in time-series of speech) are learned and the next 10 continuous samples (next 10 time steps) are predicted. It is also found out that the *gru* performs better than the *lstm* in terms of accuracy and running time. For musedata<sup>1</sup>, a collection of piano classical music, the performances (average of the negative log-likelihood) noted on the test set are - *gru*: 5.99, *lstm*: 6.23 and traditional recurrent units: 6.23. Six different types of musical and speech data are tested and four out of these six types, the *gru* works better than the other two units.

The studies mentioned above benefit from the state-of-the-art sequential learning techniques like the *lstm* and *gru* recurrent neural network. Building a recommendation system to predict tools for the Galaxy's scientific workflows is motivated by these successful studies.

---

<sup>1</sup>[www.musedata.org](http://www.musedata.org)

# 8. Approach

The prediction of a set of tools at each step of designing a workflow is proposed in this work. A learning algorithm is needed which can learn tool connections in a path and predict its next tools. This learning algorithm is called a classifier. There are two coveted features of this classifier:

- It should grasp the semantics of tool connections in workflow paths and use them to predict tools (with a high accuracy of  $\geq 90\%$ ).
- Running/training time should be reasonable.

The classifier's accuracy to predict tools and running time are noted for doing a comparison. The Galaxy stores thousands of workflows and they are extracted from its database (section 9). But, they cannot be used in their existing form by any classifier. They need to be preprocessed which is necessary to make them usable for analysis by the classifier. Figure 25 highlights the sequence of steps to preprocess them. First, paths are extracted from workflows and the duplicates are removed. More information about the number of paths and tools used to create them is given in section 9.

These paths are required by the classifier to understand the dependencies among tools. They are processed by using three different approaches (section 8.4.1) to create shorter paths. The paths are divided into training and test paths. The classifier consumes training paths to learn their characteristics along with their next tools. The robustness of learning is verified on test paths.

## 8.1. Actual next tools

Figure 23 shows that a workflow can have more than one path and these paths can share a few tools. Moreover, a path can connect to more than one tool. A classifier needs data in the form of a path and its next tools (a tool or a set of different tools).

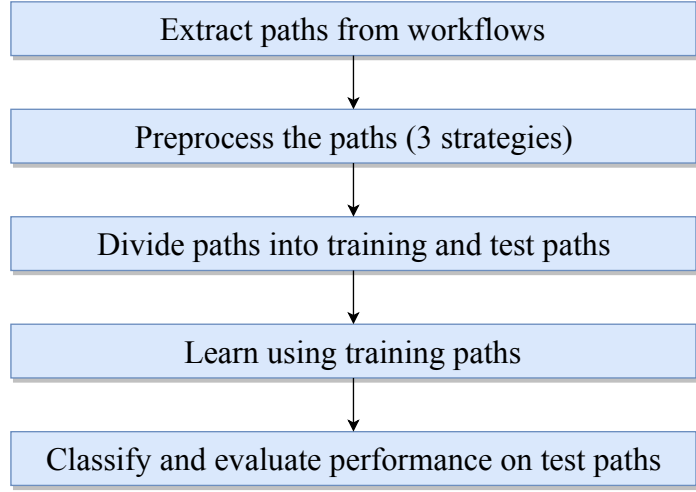


**Figure 25.: Sequence of steps to predict tools for workflows:** The flowchart shows a sequence of steps to predict tools for workflows. Workflows are decomposed into paths. Further, these paths of varying lengths are decomposed to have shorter paths by following three different strategies explained in section 8.4.1. A classifier learns tool connections from training paths. The learning is evaluated on test paths.

Path	Tool(s)
Get flanks	Awk
Get flanks > Awk	Intersect
Get flanks > Awk > Intersect	Count, Extract genomic dna
Get flanks > Awk > Intersect > Count	Bar chart

**Table 5.: Decomposition of a workflow:** This table shows a few paths and their respective next tools extracted from a workflow shown in figure 23. The next tools of a path are the actual next tools present in the workflow.

A workflow is decomposed into paths. Using the technique, shown in table 5, these paths are further decomposed into shorter paths and their respective next tools. This idea is considered because of the necessity of getting predictions in the same way. It means that when the tool *get flanks* is selected, a classifier should suggest *awk* as a possible next tool. Again, the tool *awk* is selected and the sequence becomes *get flanks > awk*. Given this sequence, the classifier should predict the tool *intersect*. To this sequence, when the tool *intersect* is added, the classifier should predict two tools, *count* and *extract genomic dna* (figure 23). Following this approach of decomposition of paths, shorter paths and their respective next tools are created. The tools that

are assigned to a path are its actual next tools.

## 8.2. Compatible tools

All pairs of connected tools are extracted from workflows. A pair of tools are connected because of their compatible input and output file types. Using the set of pairs of tools, a list of compatible tools<sup>1</sup> is collected for each tool. In a path, *get flanks > awk > intersect > count > bar chart*, the tool *intersect* connects to the tool *count*. It means that these two tools have compatible file types. There are multiple other tools which can connect to *intersect* like *join, cut, subtract* and many others. These form a set of compatible tools for *intersect* and can be predicted for the paths ending in the tool *intersect*. When a classifier predicts tools for a path and if the last tool of this sequence is compatible with the predicted tools, then the predictions are correct and should be accounted for. These tools are not fed to the classifier for learning. They are used only to verify whether the prediction of tools includes these compatible tools. Figure 26 shows a distribution of the number of compatible tools for each tool.

## 8.3. Length of workflow paths

The length (number of tools) of paths in workflows varies. Figure 27 shows a distribution of the number of tools present in each path. Most of the paths have less than 20 tools while a few have over 20 tools. It is important to find whether the prediction of tools by a classifier varies with the length of workflow paths (figure 46).

## 8.4. Learning

### 8.4.1. Workflow paths

A path enforces a directed flow of information through multiple tools connected in a series (from left to right). The paths are preprocessed in such a way so that they can retain their semantics and can be understood by any classifier. The different ways (no decomposition, decomposition of only test paths and decomposition of all paths)

---

<sup>1</sup>A compatible tool and a compatible next tool have the same meaning.

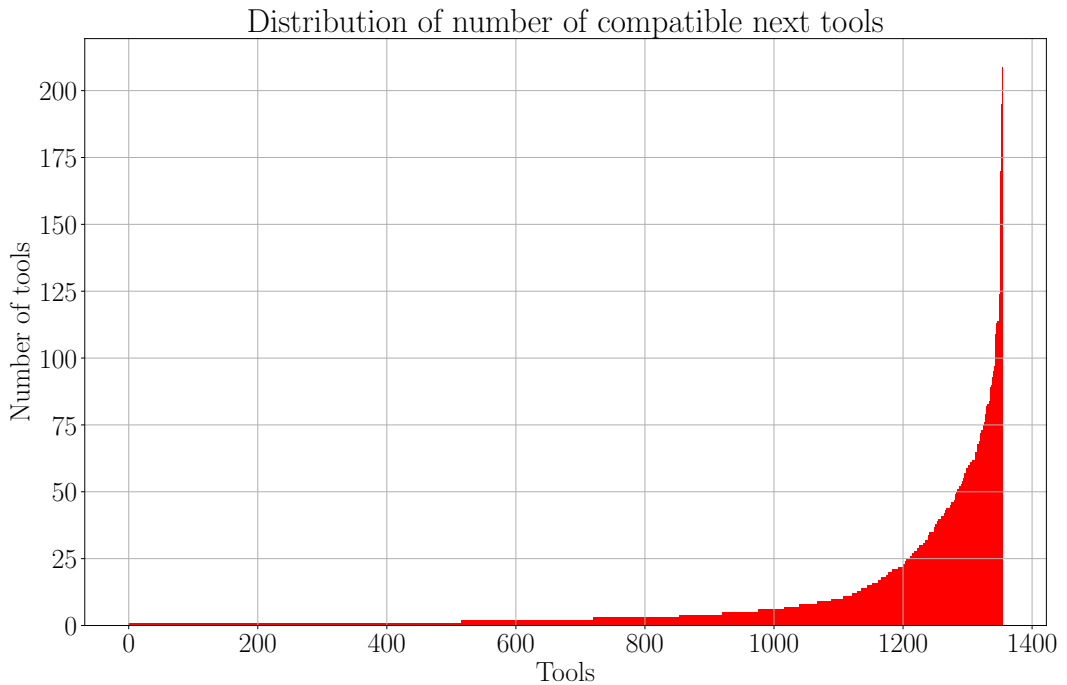


**Figure 26.: Distribution of the number of compatible tools:** The bar plot shows a distribution of the number of compatible tools for each tool. The x-axis shows tools which have at least one compatible tool. The tools which come only at the end in all the workflows are not shown in this plot. The y-axis shows the number of compatible tools. Most of the tools have less number of compatible tools.

of decomposing these paths into tool sequences<sup>2</sup> are discussed. The decomposed tool sequences are further divided into training and test paths. The classifier uses training paths to learn features. The amount of learning is evaluated on test paths. It is ensured that the intersection set of training and test paths is empty. Otherwise, the evaluation of the learned model would be biased [19, 20, 21]. Different methods of the decomposition of paths are discussed in the following sections:

### No decomposition

The workflow paths are used as they are. The last tool of each path is taken as its next tool. A dictionary is created in which these paths are keys and their next tools are values. This dictionary is shuffled and divided into training and test paths. It

---

<sup>2</sup>A path and a tool sequence refer to the same entity, a chain of tools, in the thesis. They are used interchangeably.

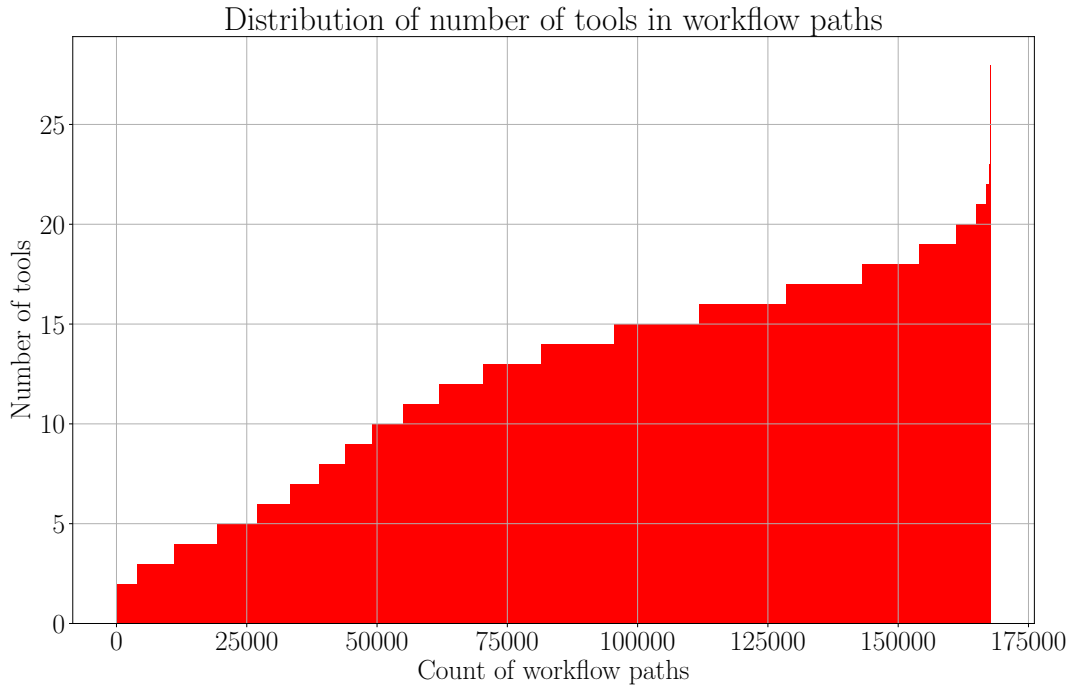


**Figure 27.: Distribution of sizes of workflow paths:** The plot shows a distribution of the sizes of workflow paths. A workflow path consists of multiple tools. This distribution shows how many tools are there for each path. About 167,000 paths are extracted from the Galaxy workflows and most of them have less than 20 tools. The mean length of these paths is 12.33. The maximum and minimum lengths are 28 and 2, respectively.

enforces that no path is present in both the sets of paths. A classifier needs to learn tool connections in these paths and their respective next tools. The learned model is evaluated using the test paths. Figure 28 explains this idea.

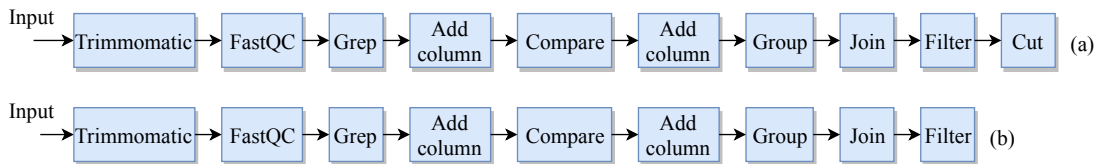


**Figure 28.: No path decomposition:** The image shows a workflow path. For a path of length  $n$  (a), a shorter path of length  $n - 1$  (b) is taken out and the last tool is assigned as its next tool. For example, the tool *cut* is a next tool of the previous path (b).

## Decomposition of test paths

The training paths are used as they are to train a classifier. But, the test paths are decomposed keeping the first tool fixed in each path. Figure 29 shows this decomposition. For a path of length  $n$ ,  $n - 1$  unique paths are created and the last tool of each path becomes its next tool. A path should contain at least two tools (the second tool is the next tool of the first). This decomposition increases the size of test paths. Moreover, it creates a problem of duplication in training and test paths. A test path is decomposed into shorter paths. It can happen that one or more of these shorter paths are present in the training paths. The evaluation would be biased in this case. To avoid this situation, the duplicates are removed from the training and test paths before they are fed to the classifier.

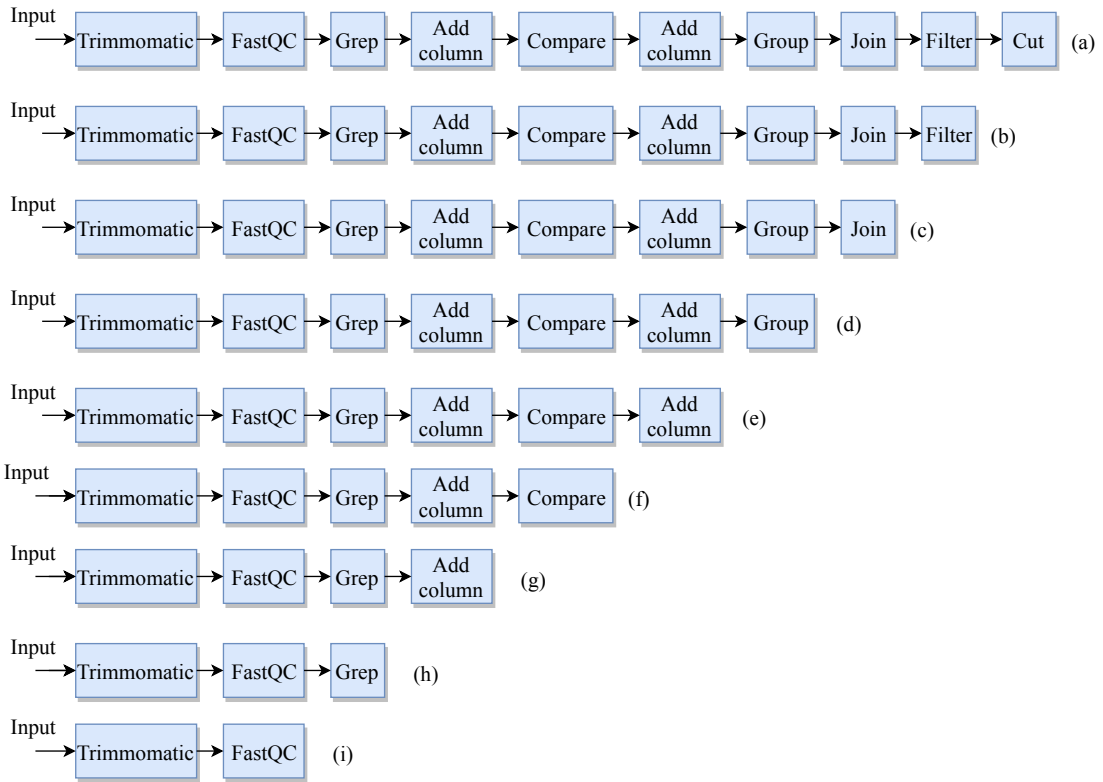


**Figure 29.: Path decomposition:** The image shows how a path is decomposed into smaller tool sequences keeping the first tool fixed. For each path, the last tool is dependent on all its previous tools (higher-order dependency).

### **Decomposition of test and train sets**

The decomposition of paths keeping the first tool fixed enlarges the complete set of paths. With an enlarged set of paths, a classifier should get features (tool connections) repeated multiple times which can be beneficial for learning [22]. All paths are decomposed following the strategy explained in figure 29 to obtain a mixture of shorter and longer paths. A dictionary is created where each key represents a path and its value is a set of next tools. This dictionary is shuffled and divided into training and test paths.

#### **8.4.2. Bayesian network**

A workflow possesses the structure of a directed acyclic graph. The bayesian network is one of the approaches to model this graph. From the bayesian network, it is inferred that if the parents of a node are given (in a directed graph), then this node is conditionally independent of all the other nodes which are not its descendants (the set of nodes it cannot reach through directed edges) [23, 24]. It means that each node in this graph is dependent only on its parents. The structure of workflows can be explained by the bayesian network. Using this approach, the missing values (of nodes) can be predicted. Here, the missing values would be the next tools. But, there are a few limitations of this approach which are worth considering. It involves computing joint probabilities of nodes in a graph and also the conditional probabilities among them. When the number of nodes increases, it will become hard to keep the computational cost low. Making predictions by learning a probabilistic network is a hard problem [25, 26, 27]. Due to these reasons, the bayesian network is not used in this work for predicting tools in workflows.

#### **8.4.3. Recurrent neural network**

A workflow may have multiple paths. These paths are extracted from workflows and the duplicates are removed. They are assumed to be independent of each other which keeps the analysis simple and powerful. In a path, each tool is dependent on all its parents (previous tools in the path). This relation is called higher-order dependency [28]. It is important to learn these higher-order dependencies in order to be able to predict tools for a path. Figure 30 shows these dependencies for a path. Tool *sort* is not only dependent on *text reformatting* tool but on tools *datamash* and *concatenate datasets* too.

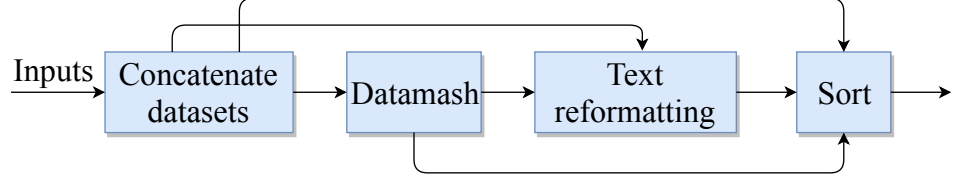


**Figure 30.: Higher-order dependency:** The image shows a path where four tools are arranged in a sequential manner. Each tool depends not only on its immediate parent tool, but all previous tools in the path.

A classifier should model these dependencies for variable length paths. The recurrent neural network is a natural choice for the classifier which can learn these dependencies in workflow paths [29]. To model these dependencies, the network keeps a hidden state at each step of processing paths. It combines information from the previous steps and the current step. It is computed as:

$$h_t = \phi(h_{t-1}, x_t) \quad (31)$$

where  $h_t$  is the hidden state at step (or time)  $t$ ,  $h_{t-1}$  and  $x_t$  are the hidden state at the previous step ( $t - 1$ ) and input at  $t$ , respectively and  $\phi$  is a nonlinear function.

More formally, the equation 31 is written as:

$$h_t = g(W_{input} \times x_t + U_{recurrent} \times h_{t-1}) \quad (32)$$

where  $W_{input}$  and  $U_{recurrent}$  are the weight matrices for the input and recurrent units, respectively. The hidden state keeps information about the previous steps. At each step,  $x_t$  is an input.  $g()$  is a bounded, nonlinear function like *sigmoid* (equation 40). The joint probability of all these input variables ( $x_i$ ) is given by:

$$p(x_1, x_2, \dots, x_T) = p(x_1) \cdot p(x_2|x_1) \cdot p(x_3|x_1, x_2) \cdot \dots \cdot p(x_T|x_1, x_2, \dots, x_{T-1}) \quad (33)$$

where  $x_t$  is the input at step  $t$ ,  $p(\cdot)$  is a probability distribution and  $T$  is the length of a path. From equation 33, the input at step  $t$  is reliant on the previous steps in a sequence. To predict next step (or next tool in a path), the last conditional probability ( $p(x_T|x_1, x_2, \dots, x_{T-1})$ ) should be captured using the hidden state ( $h_t$ ) [17, 30].

In equation 32, there are two matrices, one each for the inputs and recurrent units,

respectively. Learning higher-order dependencies depends on the gradients of errors with respect to the parameters (recurrent and input weight matrices). The gradient at a step is the product of gradients from all previous steps. If the gradients from previous steps are small which inherently means that the recurrent units are not capturing higher-order dependencies, then their product can quickly slip towards zero and disappear (the product of small numbers would be small). In another scenario when gradients from previous steps are large, the product can easily explode to become a large number. Both these situations are collectively known as vanishing and exploding gradients problem respectively [31]. The traditional recurrent units are prone to show this behaviour. To avoid these situations, which can hamper learning, two variants of recurrent units are proposed:

- *Long-short term memory units (lstm)* [32]
- *Gated recurrent units (gru)* [30]

In this work, *gru* is explored which is proposed recently and is simpler than the *lstm* and contains fewer parameters. The performance of these two variants is comparable [17]. Figure 31 shows a recurrent neural network with two hidden layers.

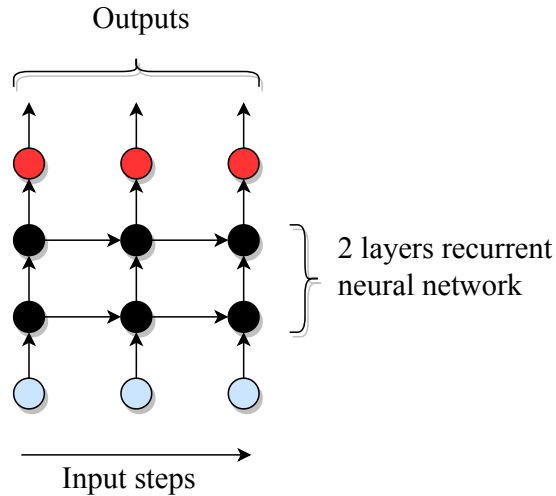


**Figure 31.: Recurrent neural network:** The image shows the stacked recurrent units layers and how they pass information from the input layer to the output. The output of the first recurrent layer is used as an input to the next recurrent layer. The blue circles denote the input steps (for example, consecutive tools in a path), the black ones form the two recurrent layers and the red circles form the output layer [33].

## Gated recurrent units

The *gru* has gates which control the flow of information from earlier to later steps in a multi-step input sequence. Figure 32 shows the reset and update gates. The reset gate  $r$  checks how much information from previous steps should be carried to the next step. If it is 0, then all information from previous steps is discarded. If it is 1, all information is taken to the next step. The update gate controls how much of the unit's own activation would be used to compute the current activation.

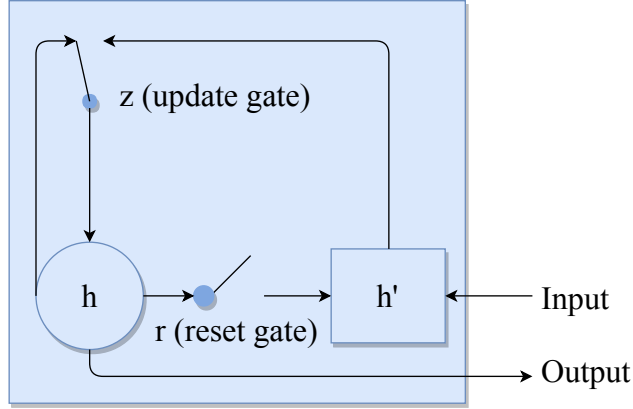


**Figure 32.: Gated recurrent unit:** The image shows a *gru* with two gates,  $r$  as a reset gate and  $z$  as an update gate. The activation of the *gru* is  $h$  and the proposed activation is  $h'$  [17].

$$h_t = (1 - z_t) \times h_{t-1} + z_t \times h'_t \quad (34)$$

where  $h_t$  and  $h_{t-1}$  are the current and previous step activations, respectively,  $z_t$  is the value of the update gate and  $h'_t$  is the current proposed activation. The update gate is calculated using the following equation:

$$z_t = \sigma(W_z \times x_t + U_z \times h_{t-1}) \quad (35)$$

where  $\sigma(\cdot)$  is the *sigmoid* function and  $W_z$  and  $U_z$  are the input and recurrent weight matrices, respectively. The current proposed activation (in equation 34) is computed using:

$$h'_t = \tanh(W \times x_t + U \times (r_t \odot h_{t-1})) \quad (36)$$

where  $h'_t$  is the current proposed activation and  $W$  and  $U$  are the input and recurrent weights matrices, respectively. The  $r_t$  is the value of the reset gate and

$h_{t-1}$  is the previous step activation. The symbol  $\odot$  is an element-wise multiplication between  $r_t$  and  $h_{t-1}$ . *Tanh* is an activation function and is given as:

$$f(y) = \frac{e^y - e^{-y}}{e^y + e^{-y}} \quad (37)$$

The reset gate is given as:

$$r_t = \sigma(W_r \times x_t + U_r \times h_{t-1}) \quad (38)$$

where  $r_t$  is the reset gate which controls the amount of information from the previous activation should be used at step  $t$ .  $W_r$  and  $U_r$  are the input and recurrent weights matrices, respectively. The  $x_t$  is the current input at step  $t$  and  $h_{t-1}$  is the previous step activation. An important point to note here is that an output does not only depend on current input but on previous inputs too (equation 34). A memory of previous inputs is maintained. It enables the gated recurrent units to extract latent features present in long sequences that lead to a specific output.

## 8.5. Network architecture

The recurrent neural network is used to classify paths and predict next tools. It consists of several layers. The first layer consumes paths and the last layer gives predictions. The hidden recurrent layers do all the computations required to do the classification of paths. While classifying, the paths are mapped to their respective next tools. Figure 33 shows how it predicts scores for tools of being next tools of a path.

### 8.5.1. Embedding layer

The first layer is an embedding layer. It learns a dense, fixed-length vector for each tool (figure 34e). An index (an integer) is assigned to each tool and it is converted to an embedding vector. It represents features associated with the tool. It means that an embedding vector for a tool encodes the context in which the tool is being used. The tools which are used in a similar context, their embedding vectors are similar.

### 8.5.2. Recurrent layer

Two hidden recurrent layers containing *gated recurrent units* are used. These layers are responsible for doing the computations given in equations 34-38. The hidden layers are stacked one upon another and they contain an equal number of *gated recurrent units*. Deeper features in paths are learned by stacking the recurrent layers. The hidden states of units in the first layer become inputs to the units of next hidden recurrent layer. Figure 31 shows the recurrent layers.

### 8.5.3. Output layer

The predictions are computed from the output (last) layer of the recurrent neural network. It is a dense layer having the same dimensionality as the number of tools. Each dimension holds a real number between zero and one which is a score assigned to a tool of being the next tool for any path.

### 8.5.4. Activations

An activation is a function which transforms the input of a neuron (a node in a neural network) to an output. It can either be linear or nonlinear. There are multiple activation functions like *softmax*, *sigmoid*, *tanh*, *relu*, *linear* and many more<sup>3</sup>. It is chosen based on the kind of output required for its further evaluation. The output of a neuron is given by:

$$y^j = \phi\left(\sum_{i=1}^N w_i \times x_i + b\right)^j \quad (39)$$

where  $y$  is an output of neuron  $j$ ,  $w_i$  is the weight of the  $i^{th}$  input connection to the neuron  $j$ ,  $x_i$  is an input and  $b$  is bias for neuron  $j$ .  $\phi$  is an activation function.  $N$  is the number of input connections to neuron  $j$ . *Sigmoid* function (equation 40) is used as an output activation (activation of the output layer) because the predicted tools are independent of each other and it learns the prediction for each tool separately.

$$f(x) = \frac{1}{1 + e^{-x}} \quad (40)$$

*Softmax* activation can replace it, but it normalises the exponents of output values which is undesired. *Sigmoid* assigns a real number between zero and one to each

---

<sup>3</sup><https://keras.io/activations>

tool at the output layer. Another activation is exponential linear unit (*elu*). It is used as an activation for the recurrent layers. In equation 36, *tanh* is replaced by *elu* activation. It is given by:

$$f(x) = \begin{cases} x, & \text{if } x > 0 \\ \alpha \times (e^x - 1), & \text{if } x \leq 0, \alpha > 0 \end{cases}$$

It has a special feature of being negative when an input is negative. This feature allows mean activation (output) to get closer to zero compared to other activation functions like *relu* which is always positive. As mean activations get closer to zero, the approximated and actual gradients get closer to each other. Due to this, learning becomes faster and an increased drop in error is achieved [34].

### 8.5.5. Regularisation

Overfitting is a common phenomenon in the field of machine learning. It occurs when a classifier starts memorising training data without learning its general features. It leads to an increased learning on the training data but no learning on unseen/test data. The error on the training data decreases but the error on the test data either stops decreasing or sometimes increases. The classifier stops generalising and would predict new data with an increased uncertainty. A variant of a neural network is used in this work for classification. It is prone to overfitting as it tends to derive a complex model from the training data. If the size of the training data is small, it starts overfitting. To generate a model which learns general features, it is important to apply measures to remove or reduce overfitting. Regularisation is a technique to overcome this common problem. There are many techniques to regularise a neural network like dropping out random units (dropout) and decaying weights to stop them from becoming large. In this work, dropout is used as a regularisation method to tackle overfitting [35].

#### Dropout

Dropout removes connections momentarily from a neural network and thereby changing the network structure during each weight update. It randomly sets the output of some connections to zero and due to this, the network behaves in a novel manner. It becomes less powerful and stops picking bias from training data. A real number between zero and one is specified as dropout which is the fraction of units

(memory units) to be dropped. It is applied to the input, output and recurrent connections of the recurrent neural network. The embedding layer also has a dropout layer for its output. The amount of dropout is a hyperparameter and a suitable value should be found out for which the drop in the training and validation losses remains stable and close to each other [36, 37]. Moreover, the amount of dropout depends on the complexity of a neural network and the amount of data.

### 8.5.6. Optimiser

An optimiser is used to minimise the error computed by an error function. *Rmsprop* is used as an optimiser for the recurrent neural network in this work. It follows an adaptive strategy for learning rate [38]. It adapts the learning rate according to gradients. It keeps a track of the previous gradients (gradients in the previous iterations) and updates learning rate by dividing with an average of the square of the previous gradients. The weight update is given by the following equations:

$$MeanSquare(w, t) = 0.9 \times MeanSquare(w, t - 1) + 0.1 \times (\frac{\partial E}{\partial w}(t))^2 \quad (41)$$

$$w_{t+1} = w_t - \frac{\eta}{\sqrt{MeanSquare(w, t) + \epsilon}} \times \frac{\partial E}{\partial w}(t) \quad (42)$$

where  $MeanSquare(w, t)$  is the mean of squared gradients until time  $t$ ,  $\frac{\partial E}{\partial w}$  is a partial derivative (gradient) of the error function with respect to parameter  $w$  at time  $t$  and  $\eta$  is learning rate.  $\epsilon$  is a small number (for example,  $10^{-5}$ ) and is added to avoid division by zero.

#### Learning rate

Learning rate is an important parameter for an optimiser which determines the amount of update at each time step. If the learning rate is high, there is a risk of an optimiser divergence. Instead of going to the minimum of error surface, which is the expected behaviour, the optimiser keeps oscillating on the error surface and bypass the minimum. On the other hand, if it is low, the optimiser may never reach or take a large amount of time to reach the minimum as learning steps become too small. Due to these reasons, setting a good learning rate is a key to guarantee convergence in a reasonable amount of time.

## Loss function

*Binary cross-entropy*<sup>4</sup> is used as a loss function for the optimiser *rmsprop*. It is well-suited for multilabel classification. It is a kind of classification of data with multiple outputs. For this work, there can be multiple next tools for a path. Therefore, multilabel classification is needed for this work. The loss function is given by:

$$loss_{mean} = -\frac{1}{N} \left( \sum_{i=1}^N y_i \times \log(p_i) + (1 - y_i) \times \log(1 - p_i) \right) \quad (43)$$

where  $N$  is the dimension of output layer (total number of predicted tools),  $y$  is actual next tool vector for a path and contains either zero or one,  $p$  is predicted next tool vector for the same path. The predicted next tool vector  $p$  contains real numbers between zero and one. The mean loss is a small number when actual next tool and predicted tool vectors are comparable. In equation 43, the sum is always negative or zero making the mean loss to be always positive or zero.

### 8.5.7. Precision

Precision is computed for each path at the end of each training epoch. All the predicted tools are matched either with actual next or compatible tools for a path and the fraction of the correctly predicted tools are computed. It is averaged over all paths to get an average precision for each training epoch. Two types of precision are computed, absolute and compatible. They are explained in section 10.1.

## 8.6. Prediction pattern

The recurrent neural network is designed to generate a probabilistic prediction of tools for each path. There are  $n$  unique tools which are used to create workflows. It assigns a score to each tool of being the next tool of a path. The dimensionality of the output is  $n$ . Figure 33 shows these scores. The position of each score is assigned to a tool.

---

<sup>4</sup>[https://github.com/keras-team/keras/blob/master/keras/backend/tensorflow\\_backend.py](https://github.com/keras-team/keras/blob/master/keras/backend/tensorflow_backend.py)

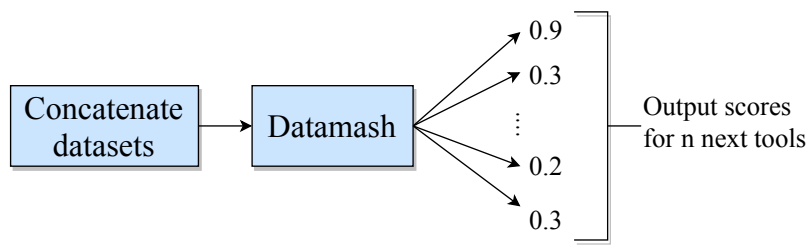


**Figure 33.: Scores for the predicted tools:** The image shows how the scores are assigned by the recurrent neural network to a set of  $n$  tools. The scores vary between zero and one. Each score contains an importance of each tool to become the next tool of a path. In the example, there are two tools in the path and the predicted scores of tools are given. The predicted scores are sorted in descending order and a few top (for example, top-1 or top-2) tools are selected.

# 9. Experiments

Workflows are collected from the Galaxy main<sup>1</sup> and Europe servers<sup>2</sup>. There are  $\approx 900,000$  paths in these workflows. Out of all these paths,  $\approx 167,000$  paths are unique. The duplicates are removed. About 1,800 tools are used to create these workflows. The recurrent neural network (*gru*) is trained on training paths (80% of all paths) and evaluated on test paths (20% of all paths). A small part of the training paths (20%) is reserved as validation paths. It is used to find the correct values of multiple parameters of the recurrent neural network. The loss is computed on these validation paths too. *BwForCluster*<sup>3</sup> provides the computing resources for preprocessing the workflows and training and evaluating the recurrent neural network.

## 9.1. Decomposition of paths

The paths are decomposed by following the approaches explained in section 8.4.1. The performance is measured separately for each approach. In the first approach, no path is decomposed and the recurrent neural network is trained and tested on actual paths. In the second approach, only test paths are decomposed as described in figure 29 and the recurrent neural network is trained on actual paths. In the last approach, both the training and test paths are decomposed as described in figure 29. The recurrent neural network is trained using a mixture of shorter and longer paths. The configuration of the recurrent neural network is kept the same for all the three approaches.

---

<sup>1</sup><https://usegalaxy.org>

<sup>2</sup><https://usegalaxy.eu>

<sup>3</sup>[https://www.bwhpc-c5.de/wiki/index.php/Main\\_Page](https://www.bwhpc-c5.de/wiki/index.php/Main_Page)

## 9.2. Dictionary of tools

Tool names present in paths cannot be used by any classifier. They need to be converted into numbers. To do that, a dictionary is created where each tool name is assigned to an integer. The tool names are replaced by their respective indices from the dictionary and each path becomes a sequence of integers (figure 34c). In addition, a reverse dictionary is also created to replace any index by its tool name.

## 9.3. Padding with zeros

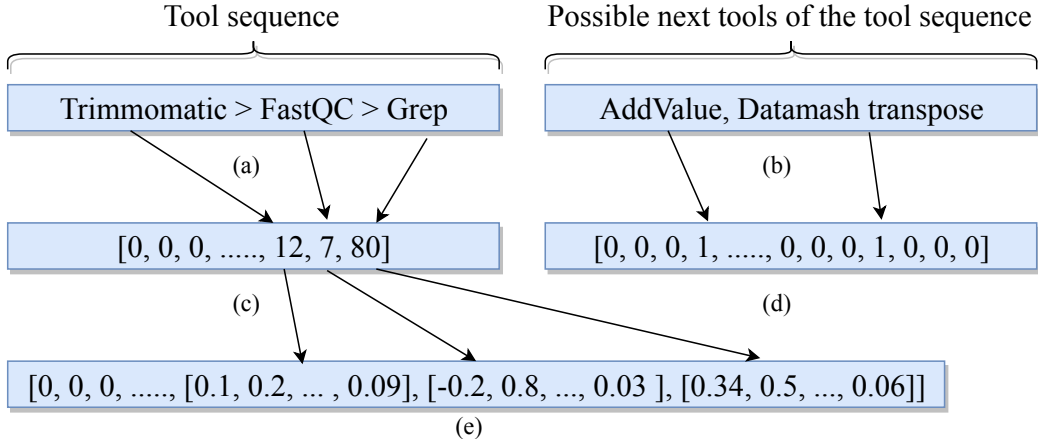
Some of the paths in the training, test and validation sets are short while some are long. But, the recurrent neural network can take only a fixed-size input. To deal with this issue, the maximum length of a path (number of tools) is set to 25 to captures all paths. Figure 27 shows that the number of tools in each path is less than 25. For shorter paths, a padding of zeros is added in the beginning to ensure that all the paths have the same length. Moreover, it is undesirable that the recurrent neural network learns any feature from these padded zeros. To avoid this, a flag is set (in the implementation of the embedding layer) to mask<sup>4</sup> these streams of zeros. Due to this, the recurrent neural network considers only the useful indices ( $> 0$ ) in a path. As zero is chosen for padding, it does not represent any tool in the dictionary.

Figure 34 shows the transformation of a path and its possible next tools into their vectors as shown in figures 34d and 34e, respectively. They are used by the recurrent neural network for training and evaluation. Figure 34a shows a path with three tools arranged in an order as it would appear in any workflow. Figure 34b shows next tools for the path. Section 9.2 explains that each tool is represented by an integer and is shown in figure 34c. The length of the vector in 34c is 25. The padding of zeros is also shown followed by the corresponding indices of tools (figure 34c). In each vector, the padding of zeros precedes the sequence of tool indices. Each index is further transformed into a fixed-length vector (embedding) as shown in figure 34e. The length of this embedding vector remains the same for all tools and is defined by the size of the embedding layer (512). 512 dimensional vector is learned for each tool's index and arranged as shown in figure 34e. The order of tools is maintained as present in an original path as shown in figure 34a. Figure 34d shows the arrangement of the next tools vector. A vector of zeros with a size equal to the

---

<sup>4</sup><https://keras.io/layers/embeddings>

number of tools is taken. The corresponding indices of next tools are set to one in this vector. For example, *addvalue* tool has an index 4 in the dictionary. Therefore, the fourth position of the next tool vector is set to one (figure 34d). This is repeated for all next tools for a path. Figure 34d contains two positions which are set to one representing the next tools for the path shown in figure 34a.



**Figure 34.: Vectors of a path and its next tool:** The image shows the vectors for a path (tool sequence) and its next tools in order to make them available for the recurrent neural network. Figures 34a and 34b show a path with three tools and its next tools, respectively. Figure 34c shows the arrangement of padding of zeros along with the indices of tools in a fixed-length vector (25). Figure 34d shows the arrangement of the next tools vector. In figure 34e, each index belonging to a tool is transformed into a fixed-length embedding vector.

## 9.4. Network configuration

The *gated recurrent unit*, a variant of the recurrent neural network, is used as the classifier. It has several layers and many hyperparameters. An embedding layer is used as an input layer which learns a fixed-size vector (512) for each index belonging to a tool. The number of unique tools in all the workflows is 1,800. As the number of tools increases, it is important to increase the size of the embedding layer. Dropout is applied to the output of this layer in order to reduce overfitting. Two hidden recurrent layers with *gated recurrent units* are used to model paths. Each layer has a fixed number of memory units. The number of memory units specifies the dimension of the hidden state (equation 34). Dropout is applied to the inputs,

outputs and recurrent connections for each hidden recurrent layer. The amount of dropout remains the same everywhere in the recurrent neural network. The last layer is a dense layer and has a size equal to the number of tools. This is because, for each path, the recurrent neural network generates scores for all tools to be the next tool of a path. The tools having higher scores at the output layer possess a higher probability of being the next tools for the path. The learning saturates and training and validation losses do not decrease anymore after 40 epochs. It means no more learning is possible and training should be stopped. The learned model saved for the last epoch is used to compute the predicted tools for test paths.

#### 9.4.1. Mini-batch learning

In mini-batch learning, a small set of paths from training paths is chosen to update the weights. Multiple candidate values (batch size) like 64, 128, 256 and 512 are chosen to see the effect on the loss and precision while keeping all other parameters fixed. Its value is set to 512 for the baseline recurrent neural network (section 10). It is allowed to learn on training paths over multiple epochs. An epoch consists of multiple iterations and in each epoch, all the training paths are used. In each iteration, 512 paths are used to approximate the weight update. If there are 2560 ( $512 \times 5$ ) training paths, then 5 iterations will make one epoch with 512 as the batch size. The recurrent neural network is sensitive to this number because a small number can add a lot of noise to the weight update [39].

#### 9.4.2. Dropout

The values like 0.0 (no dropout), 0.1, 0.2, 0.3 and 0.4 are used for dropout while keeping all other parameters fixed. The loss on validation paths is a key indicator of overfitting.

#### 9.4.3. Optimiser

A few optimisers like *stochastic gradient descent (sgd)*, *adam*, *rmsprop* and *adagrad* are used to find which one provides a stable learning and enables the recurrent neural network to achieve the best precision. All other parameters are kept fixed. They all minimise the cross-entropy loss. The default configurations of these optimisers are

used as set by the *keras* library<sup>5</sup>.

#### 9.4.4. Learning rate

Different learning rates are used to find a stable learning pattern by the recurrent neural network. Their values are 0.0001, 0.005, 0.001 and 0.01. A small learning rate tends to slow down the convergence of the optimiser while a high rate can diverge it. It is important to avoid both the situations to ensure a stable learning. All other parameters are kept fixed.

#### 9.4.5. Activations

There are multiple choices of activation functions like *tanh*, *sigmoid*, *relu* and *elu*. *Tanh* is the default activation<sup>6</sup> while *elu* is one of the recently proposed activations [34]. All other parameters are kept fixed.

#### 9.4.6. Number of recurrent units

The hidden recurrent layers need memory units (dimensionality of hidden state) to learn the mapping of paths to their respective next tools. Several sizes like 64, 128, 256 and 512 are chosen to find which one expresses the hidden states to ensure better learning. All other parameters are kept fixed.

#### 9.4.7. Dimension of embedding layer

This dimension specifies the length of the dense vectors learned for each tool. Various sizes like 64, 128, 256, 512 and 1024 are used to see the effect on the precision and loss. All other parameters are kept fixed.

---

<sup>5</sup><https://github.com/keras-team/keras/blob/master/keras/optimizers.py#L209>

<sup>6</sup><https://keras.io/layers/recurrent/#gru>

# 10. Results and analysis

In this section, the performance of the recurrent neural network is visualised and discussed for three different approaches of decomposition of paths (section 8.4.1). Different values of various parameters like the optimiser, learning rate, activation, batch size, number of memory units, dropout, embedding dimension and length of paths are used. The performances of different values for each parameter are compared. Top-1 and top-2 accuracies are computed and compared. A slightly different neural network with only dense layers is used too to find whether it performs better than the recurrent neural network. The values of the parameters used by the recurrent neural network are as follows:

- Number of training epochs is 40
- Batch size is 512
- Dropout is 0.2
- Number of memory units is 512
- Dimension of embedding layer is 512
- Maximum length of paths is 25
- Training paths are 80% and test paths are 20% of the complete set of paths
- Validation set is 20% of training paths
- Optimiser is *rmsprop*
- Output activation of recurrent layer is *elu*
- Output activation of dense layer is *sigmoid*
- Loss function is *binary cross-entropy*

These parameters remain the same for all three approaches and define a baseline configuration of the recurrent neural network. By experimenting with different values of these parameters, the possibilities to improve performance are explored.

## 10.1. Notes on plots

For the plots in figures 35-44 and 47-48, there are few common points to note:

- The x-axis shows the number of training epochs for all the subplots (a-d). For the subplots (a) and (b), the y-axis shows the precision and for the subplots (c) and (d), the y-axis shows the cross-entropy loss.
- The subplot (a) shows the absolute precision. If a path has five actual next tools, top five tools are extracted from the predicted tools by the recurrent neural network. If out of the five predicted tools, only four of them match the actual next tools, then the absolute precision for this path is  $\frac{4}{5}$ . An average precision is computed over the test paths.
- The subplot (b) shows the compatible precision. Some false positives (wrongly predicted tools) may also be present in the set of predicted tools for a path. These false positives are matched with the compatible set of tools belonging to the last tool of the path. If some or all of the false positives are present in this compatible set, then they add up to the absolute precision to give compatible precision. For example, in the last point, there is one false positive out of the five predicted tools. This false positive is checked in the compatible set of the last tool of the path. If it is present, then compatible precision becomes 1.0. If not, it stays equal to the absolute precision ( $\frac{4}{5}$ ). The compatible precision is at least as good as the absolute precision.
- The subplot (c) shows the cross-entropy loss on training paths. It is computed by the recurrent neural network as shown in equation 43.
- The subplot (d) shows the cross-entropy loss on validation paths. The last 20% of the training paths are validation paths. This loss is computed by the recurrent neural network after training on the first 80% of training paths.

## 10.2. Performances of different approaches of path decomposition

### 10.2.1. Decomposition of only test paths

In this approach, the test paths are decomposed keeping the first tool fixed as explained in figure 29. The training paths are kept as such. The results are shown in figure 35. The idea is to make the recurrent neural network learn tools connections using longer paths and predict next tools for shorter and longer paths. But, as the result suggests, the learning does not happen as desired. Absolute precision ( $\approx 22\%$ ) is worse than the compatible precision ( $\approx 43\%$ ) achieved at the end of training as shown in figures 35a and 35b. However, the cross-entropy loss for training and validation paths drops in a steady manner and saturates as shown in figures 35c and 35d. The learning happens, but only for training paths and not for test paths. The overall training and evaluation time was  $\approx 28$  hours. Each epoch took  $\approx 20$  minutes for training. The number of training paths was  $\approx 96,000$  while the number of test paths was  $\approx 62,000$ . But, only half of the test paths ( $\approx 31,000$ ) were used for evaluation.

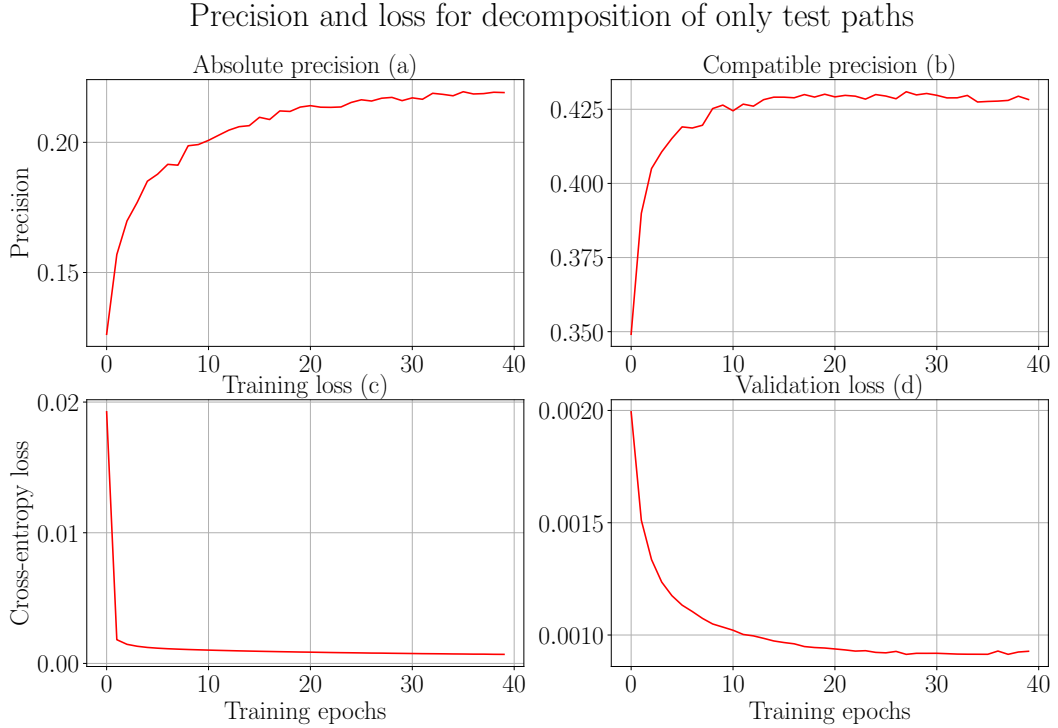


**Figure 35.: Performance of the decomposition of only test paths:** The plot shows classification performance of an approach where only test paths are decomposed keeping the first tool fixed. The training paths are kept as such. The idea is to train a recurrent neural network on longer paths and test on shorter and longer paths. The subplots (a) and (b) show the absolute and compatible precision, respectively. The subplots (c) and (d) show the training and validation losses, respectively.

### 10.2.2. No decomposition of paths

In this approach, paths as used as such for both, the training and test paths. The recurrent neural network is made to learn and evaluate on longer paths. The last tool in each path is used as its next tool. The results in figure 36 are encouraging. Subplot 36a reaches a precision of  $\approx 89\%$  at the end of training. The compatible precision is  $\approx 98\%$  and is much better than the previous approach. The validation loss (figure 36d) drop is steady and comparable to the training loss (figure 36c). The overall training and evaluation time was  $\approx 22$  hours. Each epoch took  $\approx 20$  minutes for training which is the same as the previous approach because the number of training paths remains almost the same. Overall, it took less time compared to the previous approach because of the smaller size of test paths. The number of training

paths was  $\approx 90,000$  while the number of test paths was  $\approx 22,000$ .

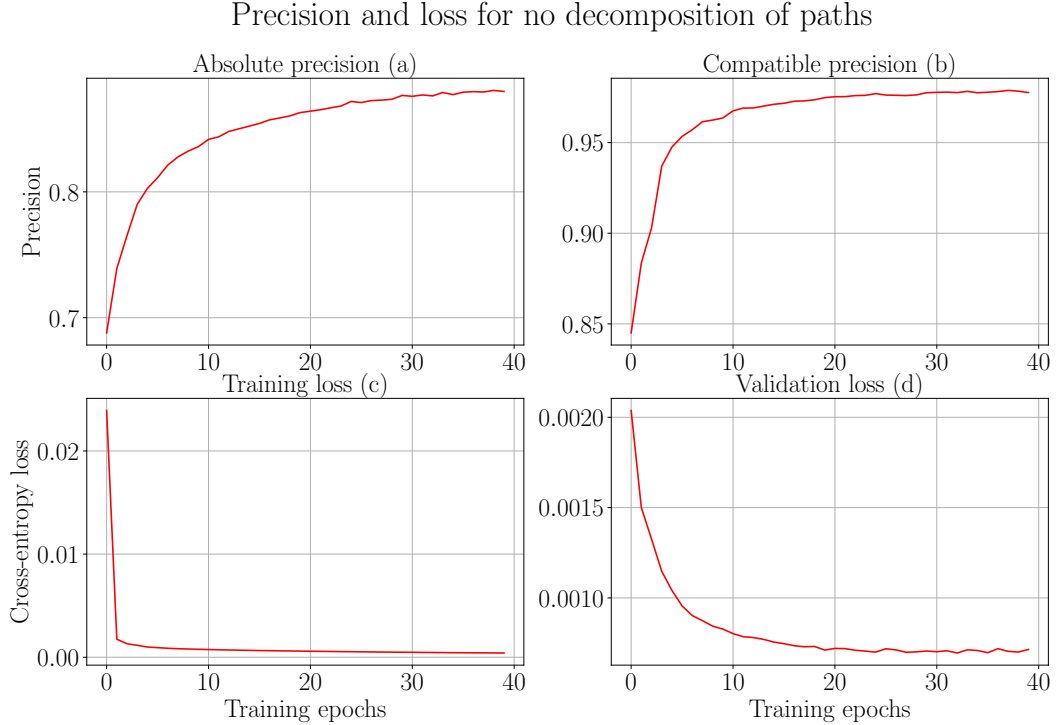


**Figure 36.: Performance of no decomposition of paths:** The plot shows classification performance of an approach where no paths are decomposed. The idea is to train and test the recurrent neural network on longer paths. The subplots (a) and (b) show the absolute and compatible precision, respectively. The subplots (c) and (d) show the training and validation losses, respectively.

### 10.2.3. Decomposition of the train and test paths

All paths are decomposed keeping the first tool fixed. The idea here is to make the recurrent neural network learn and predict on shorter as well as on longer paths. The results are shown in figure 37. Absolute precision is  $\approx 89\%$  while compatible precision is  $\approx 99\%$ . The results are comparable to the previous approach. To create a workflow, a tool is chosen and its next tools are predicted. Again, one more tool is added to the previous tool and using these two connected tools, the next tools are predicted and so on. Therefore, this approach is more practical than the previous approach. The paths are decomposed to have many shorter paths. Due to this, the size of the training paths increases which means that more training time is required. The training along with the evaluation of test paths finished in  $\approx 48$  hours. The

training for each epoch took  $\approx 45$  minutes. The number of training paths was  $\approx 168,000$  while the number of test paths was  $\approx 42,000$ .

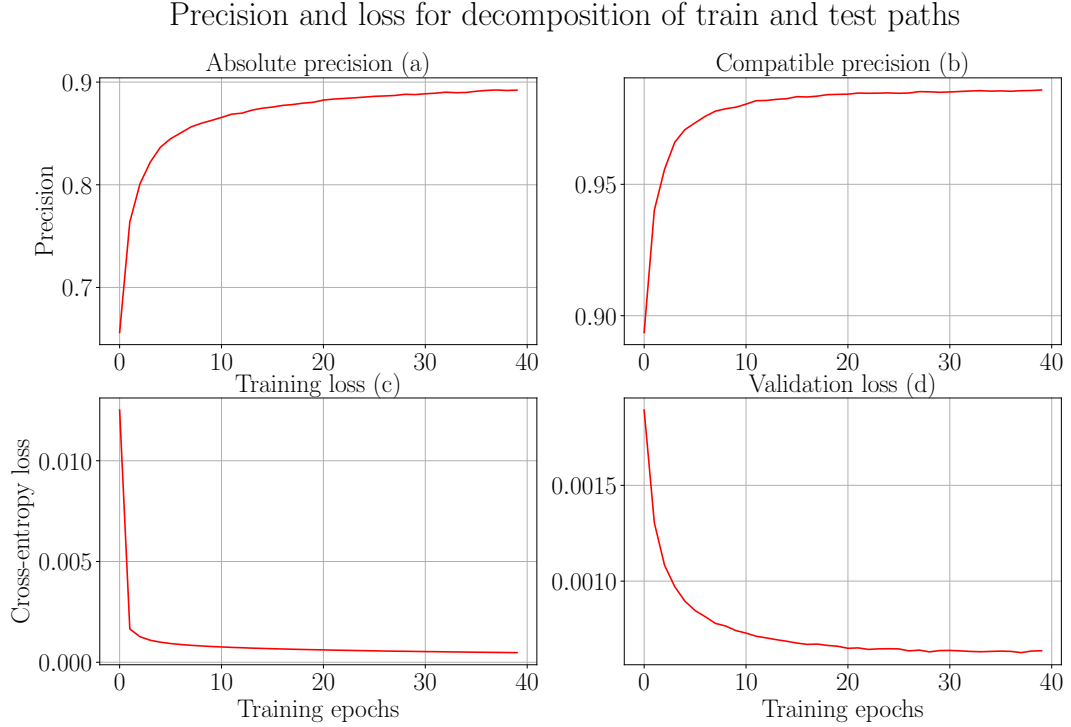


**Figure 37.: Performance of the decomposition of all paths:** The plot shows classification performance for an approach where all the paths are decomposed keeping the first tool fixed. The idea is to make the recurrent neural network learn and predict on shorter as well as longer paths. The subplots (a) and (b) show the absolute and compatible precision, respectively. The subplots (c) and (d) show the training and validation losses, respectively.

### 10.3. Performance evaluation on different parameters

The recurrent neural network has many parameters and they need to be tuned to the amount of data and to each other so that it learns and predicts in a reliable way. Their right combination is needed to attain a reasonable accuracy and to avoid too much (overfitting) and too less learning (underfitting). These parameters include optimiser, learning rate, activation, batch size, number of recurrent (memory) units, dropout and dimension of the embedding layer. There are a few more metrics on

which the evaluation is done. These include top-k accuracy and length of paths. A deep network with only dense layers is also used as a classifier to compare its classification performance with that of the recurrent neural network.

### 10.3.1. Optimiser

Four optimisers, *stochastic gradient descent (sgd)* [38], *adaptive sub-gradient (adagrad)* [38], *adam* [40] and *root mean square propagation (rmsprop)* [38] are used for the analysis to find which one achieves the highest precision. All other parameters are kept constant. From figure 38, it is concluded that the *sgd* performs worst on both the metrics, precision and loss. The absolute and compatible precision do not improve and drop in the loss curve starts very late during training. It starts off with a high value (0.65) and does not drop much within the 40 epochs of training. Out of the remaining three optimisers, *rmsprop* performs best. The performance of *adam* is comparable to *rmsprop*. The *adam* optimiser catches up with the precision measured by *rmsprop*, but slowly. Their performances converge later in the training. The plot shows that the choice of *rmsprop* as an optimiser for the baseline network is beneficial for learning. In general, *rmsprop* is a good choice for the recurrent neural network [41]. The bad performance of the *sgd* may be attributed to its non-adaptive parameter update method which does not adapt to the gradients. The adaptive optimisers (*rmsprop* and *adam*) adjust parameter update with the gradients of previous steps.

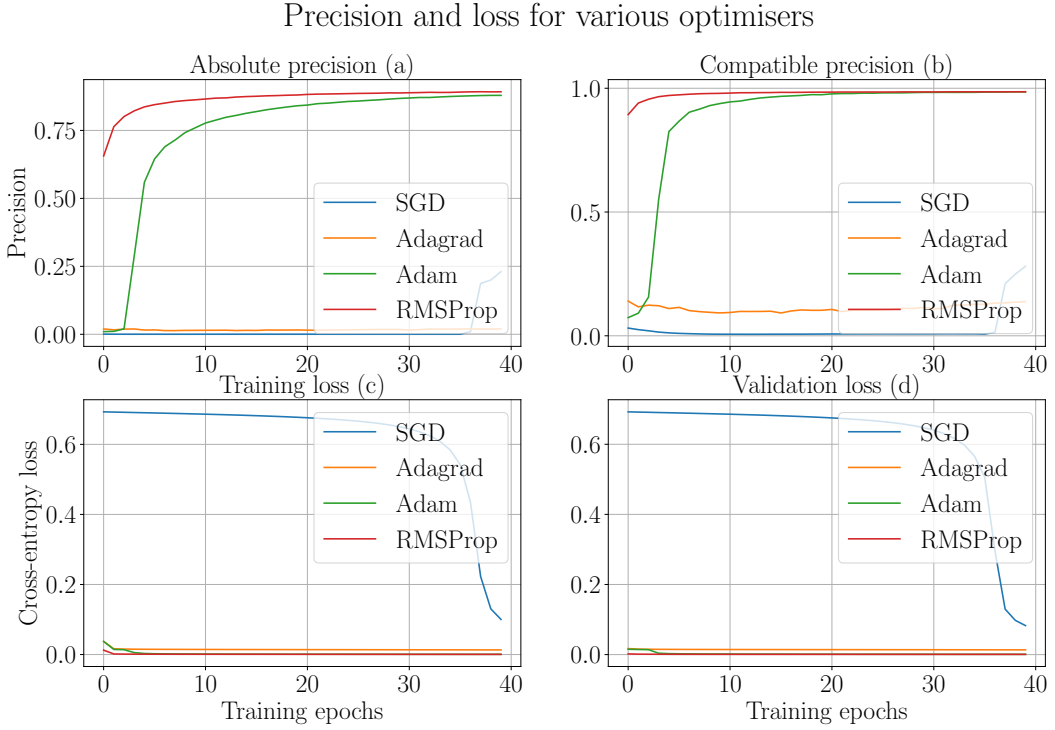


**Figure 38.: Performance of different optimisers:** The plot shows the performance of different optimisers. The subplots (a) and (b) show the absolute and compatible precision, respectively. The subplots (c) and (d) show the training and validation losses, respectively. The four optimisers are the *stochastic gradient descent (sgd)*, *adaptive sub-gradient (adagrad)*, *adam* and *root mean square propagation (rmsprop)*. All other parameters of the network are kept constant. The *rmsprop* and *adam* optimisers provide a stable learning. The baseline configuration of the recurrent neural network uses *rmsprop* as an optimiser.

### 10.3.2. Learning rate

Multiple values of learning rate from small (0.0001) to high (0.01) are used to find which one achieves the highest precision. A performance comparison of different learning rates while keeping other parameters constant is shown in figure 39. A higher learning rate (0.01) diverges the optimiser as the precision drops during training. The training loss increases and its curve has sharp edges (figure 39c). For the validation loss as well (figure 39d), there is no stable pattern (continuous drop). These situations are undesirable and they inform that the learning rate should be kept smaller. A smaller value of 0.005 works better than the previous one but not completely because the precision drops slightly towards the end of training (39a).

The smaller values 0.001 and 0.0001 help in learning as the precision improves and the loss drops during entire learning in a steady way. The value 0.0001 ensures a good learning but it is slower and would need more epochs (and more time) to converge. The value 0.001 works best out of all these values on both the metrics, precision and loss.

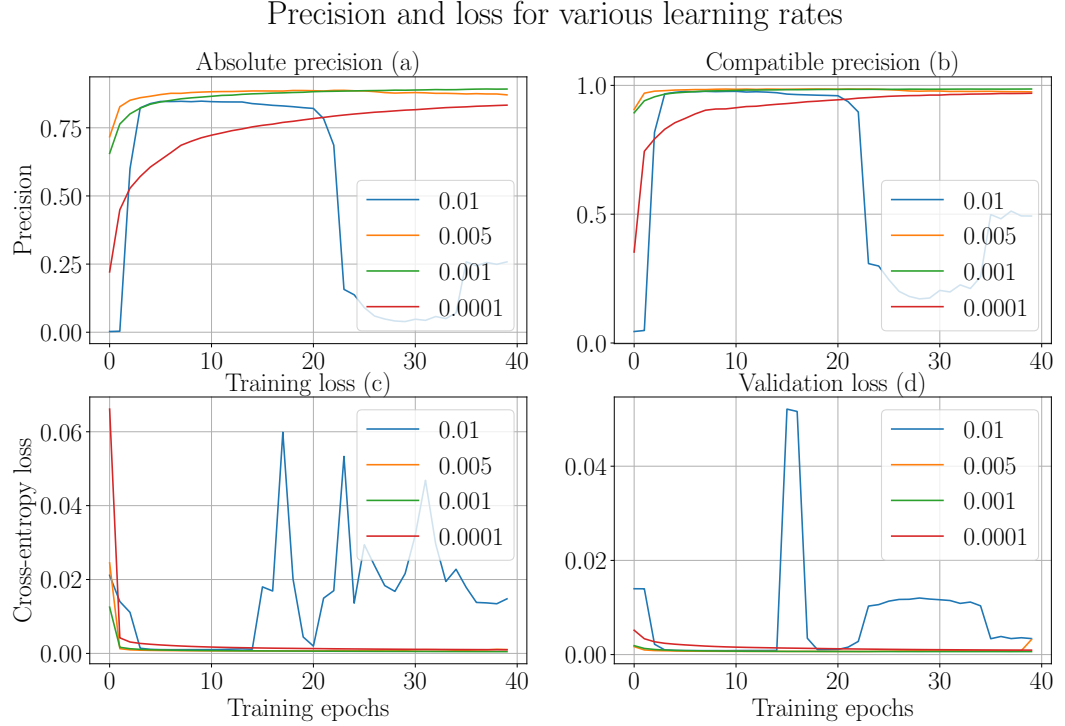


**Figure 39.: Performance of multiple learning rates:** The plot shows the performance of different values of learning rate. The subplots (a) and (b) show the absolute and compatible precision, respectively. The subplots (c) and (d) show the training and validation losses, respectively. All other parameters of the network are kept constant. A high learning rate does not provide a stable learning while a small learning rate slows down the learning. The baseline configuration of the recurrent neural network uses 0.001 as the learning rate.

### 10.3.3. Activation

Many activation functions like *tanh*, *sigmoid*, *relu* and *elu* are used to find which one achieves the highest precision. Figure 40 shows the performances of these different activation functions. The activation functions *tanh*, *relu* and *elu* perform better than *sigmoid* on both the metrics, precision and loss. The activation functions *relu* and

*elu* perform close to each other for the precision as well as loss and are better than *tanh* and *sigmoid*.

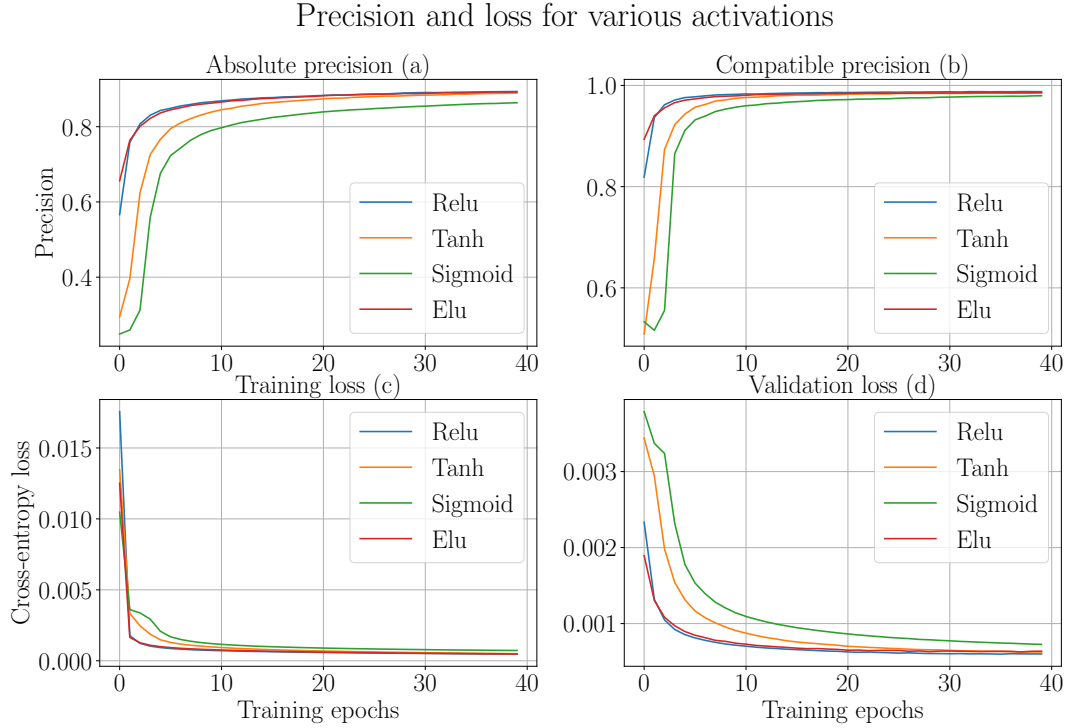


**Figure 40.: Performance of multiple activation functions:** The plot shows the performance of different activation functions. The subplots (a) and (b) show the absolute and compatible precision, respectively. The subplots (c) and (d) show the training and validation losses, respectively. All other parameters of the network are kept constant. The activations *relu* and *elu* provide better learning compared to *sigmoid* and *tanh*. The baseline configuration of the recurrent neural network uses *elu* as an activation function.

#### 10.3.4. Batch size

Different numbers like 64, 128, 256 and 512 are used as the mini-batch size to find which one achieves the highest precision. In mini-batch optimisation, a number of paths of size equal to the mini-batch size are taken and an average weight update is computed using these paths. This average update approximates update for the complete set of training paths. A smaller number adds more noise to the update as it captures less variance of the complete set. The performance of various batch sizes is shown in figure 41. It is deduced from the plot that the batch size of 64 does

not perform well. Figure 41c shows that the training loss starts increasing instead of decreasing. This proves that 64 is not the right choice of batch size. As the batch size is increased, the precision improves and the loss drops. The drop is higher for the batch size of 512 for validation loss compared to training loss. The baseline network uses 512 as the batch size. A batch size of 256 is also promising.

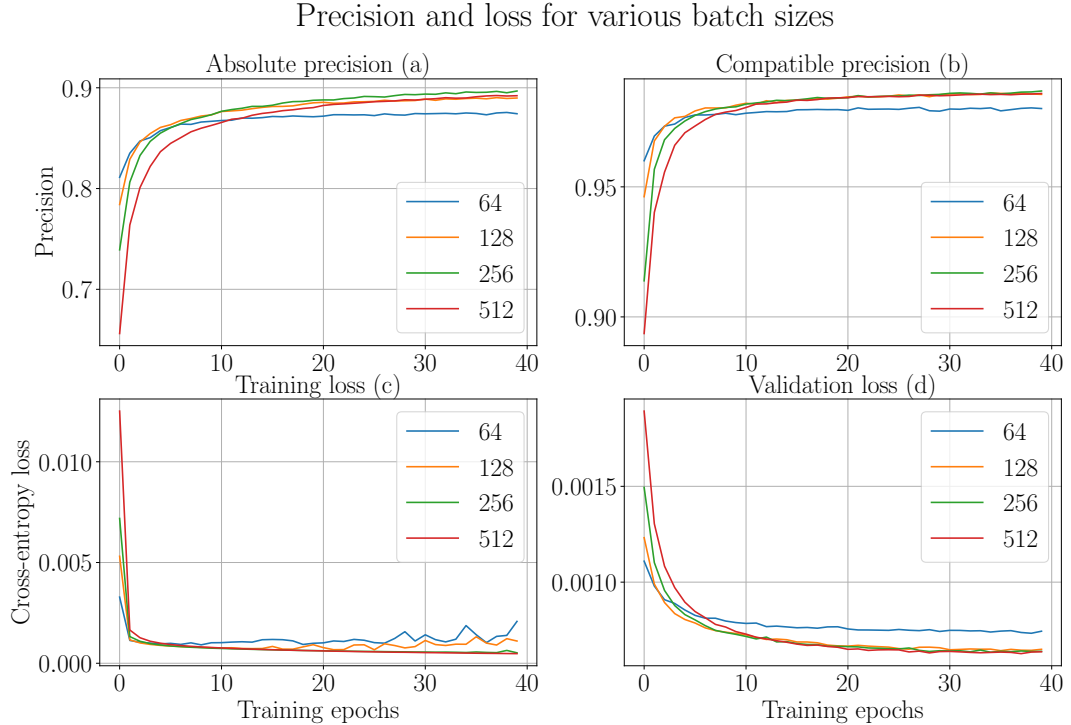


**Figure 41.: Performance of different batch sizes:** The plot shows the performance of different batch sizes. The subplots (a) and (b) show the absolute and compatible precision, respectively. The subplots (c) and (d) show the training and validation losses, respectively. All other parameters of the network are kept constant. A batch size of 64 does not perform well compared to large batch sizes (256 and 512). The baseline configuration of the recurrent neural network uses 512 as the batch size.

### 10.3.5. Number of recurrent units

Four different numbers for recurrent units are used to find which one achieves the highest precision. It specifies the dimensionality of the hidden state. The higher the number, the more expressive the network becomes. It means that the network's prediction strength or "memory" increases. This behaviour can be seen in figure 42.

As the number of units increases, the precision becomes better and the loss drop is more. 512 number of units performs the best out of the four choices of the number of recurrent units. But, the increasingly strong model tends to overfit and tries to memorise training paths. Combating overfitting is necessary when the network becomes strong. Using a higher number of memory units also increases the training time. With 64 as the number of memory units, training time for each epoch was  $\approx 6$  minutes while with 512 memory units, each epoch took  $\approx 45$  minutes.

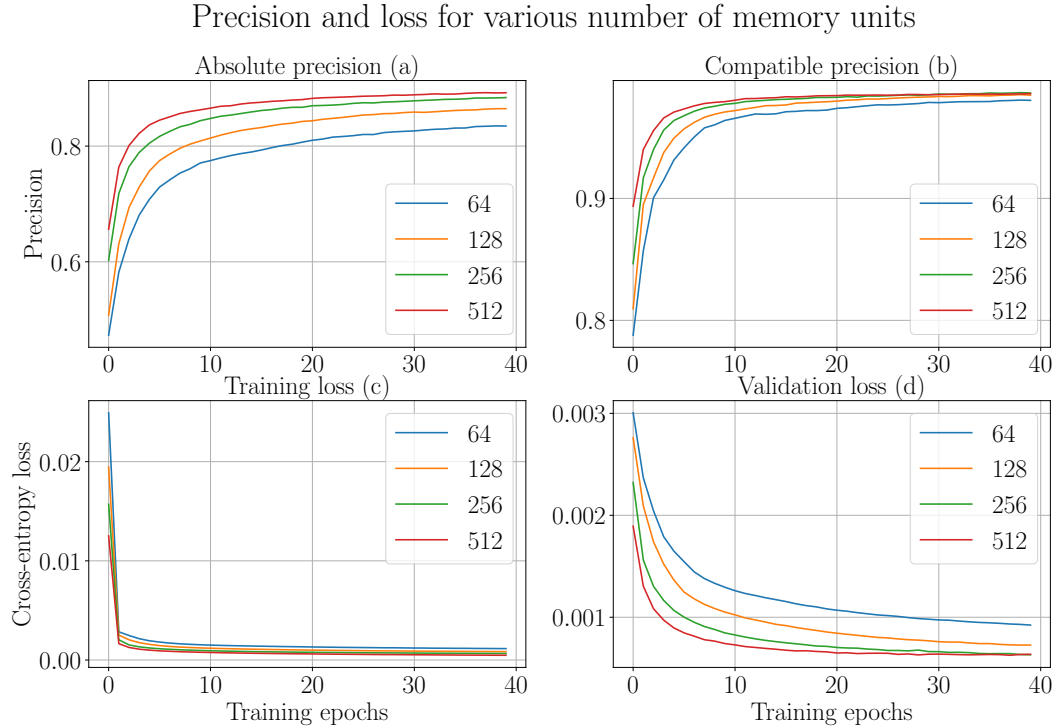


**Figure 42.: Performance of multiple values of memory units:** The plot shows the performance of different memory units. The subplots (a) and (b) show the absolute and compatible precision, respectively. The subplots (c) and (d) show the training and validation losses, respectively. All other parameters of the network are kept constant. 64 memory units for each recurrent layer do not perform well compared to a larger number like 256 or 512. The training time increases with the number of memory units. The baseline configuration of the recurrent neural network uses 512 as the number of memory units.

### **10.3.6. Dropout**

Dropout is used as a measure to overcome overfitting. To improve learning, the recurrent neural network is made stronger by adding more number of memory units and two hidden recurrent layers. Five different values of dropout are used to verify which one combats overfitting while keeping the performance high on unseen paths. Figure 43 shows the performance of different values of dropout. When no dropout (0.0) or smaller dropout (0.1) is used, the validation loss starts increasing while the training loss still decreases. The precision starts decreasing for these values of dropout. It is a clear sign of overfitting. When a higher value (0.4) is used, the recurrent neural network becomes weaker and due to this, the precision increases slowly. The numbers 0.2 and 0.3 are the better choices of dropout as they achieve better precision and the drop in the training and validation losses are more robust. The baseline network configuration uses 0.2 as a dropout. A dropout 0.3 performs close to 0.2 and can be used. The higher the value of dropout, the larger is the training time. Using no dropout took  $\approx 44$  hrs for training and evaluation while with 0.3 dropout, it took  $\approx 48$  hrs [42].

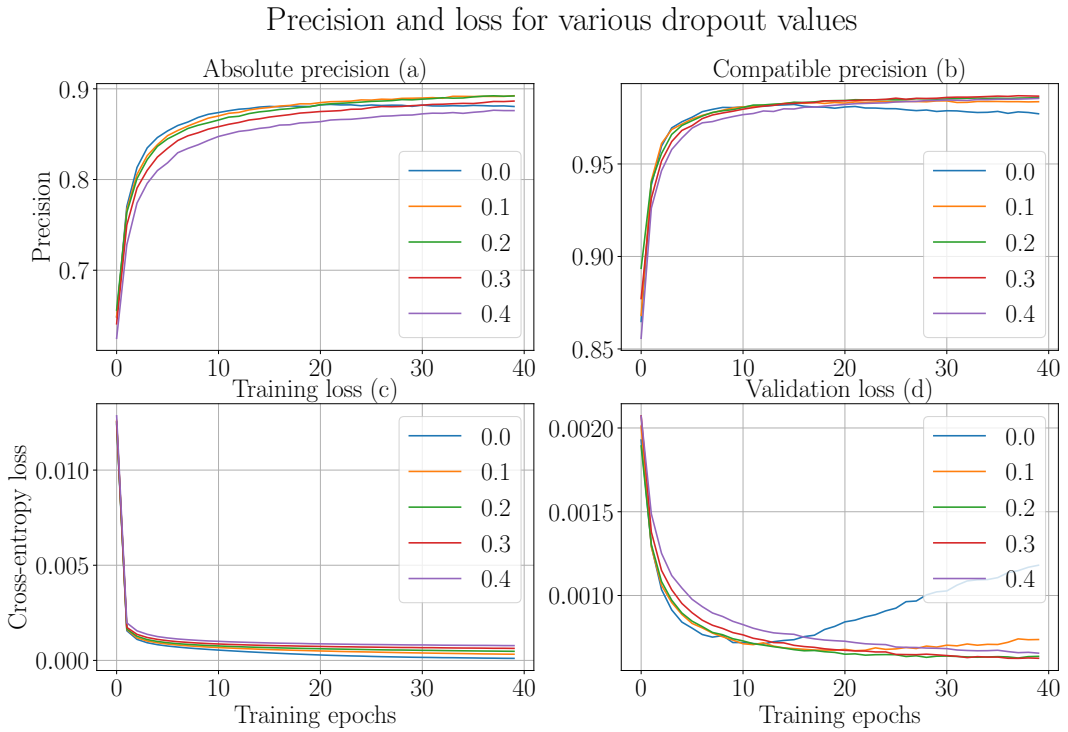


**Figure 43.: Performance of multiple values of dropout:** The plot shows the performance of different values of dropout. The subplots (a) and (b) show the absolute and compatible precision, respectively. The subplots (c) and (d) show the training and validation losses, respectively. All other parameters of the network are kept constant. No dropout shows overfitting as the validation loss increases during training (d) while a higher dropout (0.4) achieves lower precision. The baseline configuration of the recurrent neural network uses 0.2 as a dropout.

### 10.3.7. Dimension of embedding layer

Embedding layer learns a fixed-length, unique dense vector for each tool. The larger the size of this layer, the higher is its expressive power to distinguish among tools. But, with higher dimensions, there is a risk of overfitting and with a smaller dimension, underfitting can occur. Figure 44 shows the performance with different sizes of the embedding layer. All these sizes perform close to each other. A larger size performs slightly better than a smaller size. The size 1,024 performs the best while 64 also performs close especially for the training loss (figure 44c). The training time increases with the size of the embedding layer. For the size 64, it took  $\approx 30$  minutes for the training of one epoch while for 1,024, it took  $\approx 45$  minutes.

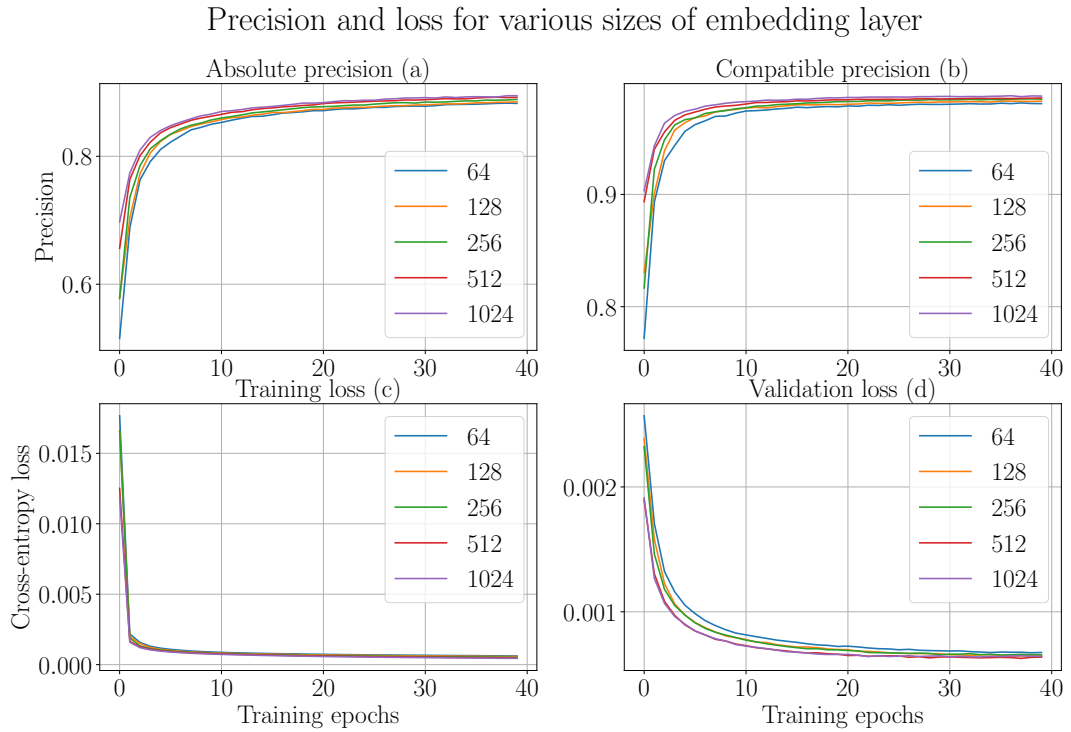


**Figure 44.: Performance of different dimensions of the embedding layer:**  
The plot shows the performance of different dimensions of embedding layer. The subplots (a) and (b) show the absolute and compatible precision, respectively. The subplots (c) and (d) show the training and validation losses, respectively. All other parameters of the network are kept constant. All the sizes perform close to each other, but a larger size performs slightly better than a smaller size. The embedding layer of 512 dimensions is used for the baseline configuration of the recurrent neural network.

### 10.3.8. Accuracy (top-1 and top-2)

Absolute and compatible top- $k$  accuracies are computed for training and test paths (figure 45).  $k$  is an integer and satisfies  $k \geq 1$ . All predicted tools are sorted in descending order of their scores and then, top- $k$  tools are extracted. For example, the absolute top- $k$  accuracy computes the number of the  $k$  predicted tools present in the set of actual next tools (section 8.1) of a path. The compatible top- $k$  accuracy computes the number of the  $k$  predicted tools present in the set of compatible tools (of the last tool) of a path (section 8.2). Top-1 (absolute and compatible) and top-2 (absolute and compatible) accuracies are computed and they are averaged for the training and test paths.

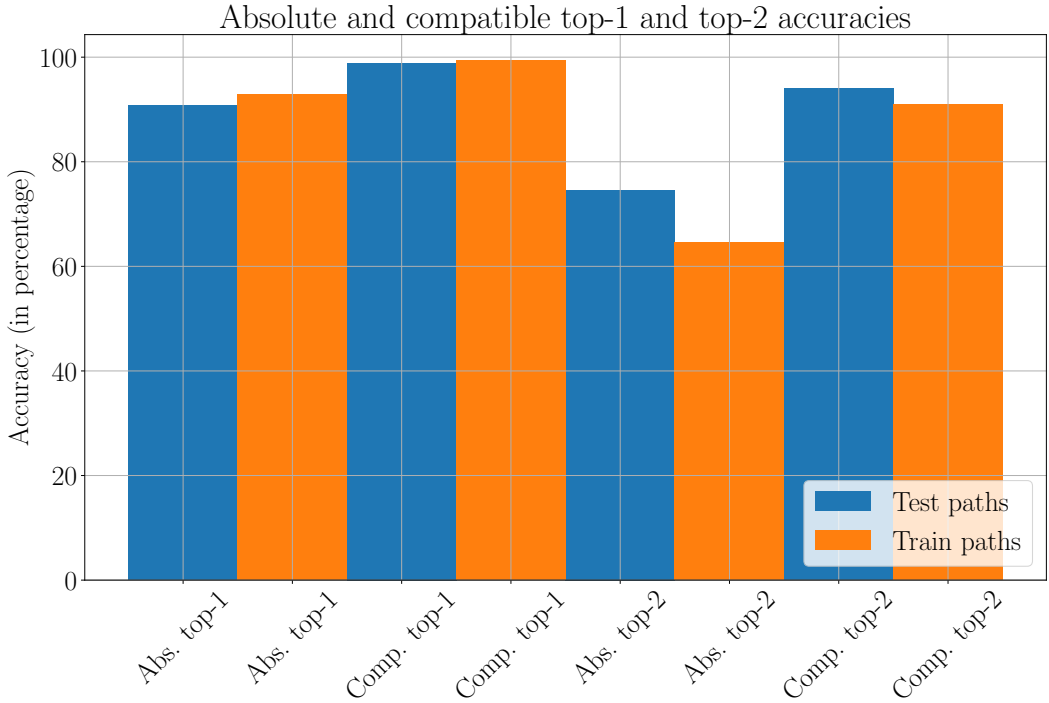


**Figure 45.: Absolute and compatible top-1 and top-2 accuracies:** The bar plot shows the absolute and compatible top-1 and top-2 accuracies. It shows that the training and test paths achieve comparable performance and the compatible accuracies remain high ( $> 90\%$ ). "Abs. top-1" refers to absolute top-1 and "comp. top-1" refers to compatible top-1 as mentioned in the plot.

Figure 45 shows that the performances of training and test paths remain similar for the absolute and compatible top-1 and top-2 accuracies. To compute absolute top-1 accuracy for a path, the tool with the highest predicted score is selected and checked whether it is present in the set of actual next tools. This accuracy is averaged for all the paths. To compute compatible top-1, the tool with the highest predicted score is checked if it is present in the set of compatible tools (of the last tool) of a path. The compatible top-1 and top-2 accuracies are higher than that of the absolute top-1 and top-2, respectively. It shows that the recurrent neural network learns tool connections from multiple paths and use them in prediction. Top-1 achieves a higher accuracy than top-2. There is a severe drop in the absolute top-2 accuracy for the training and test paths. It is because many paths have just one actual next tool in workflows. The compatible top-1 and top-2 accuracies remain high ( $\geq 90\%$ ) for the training and test paths.

### 10.3.9. Precision with the length of paths

The variation of precision (absolute and compatible) with the length of paths is shown in figure 46. The precision of predicted tools for paths containing the same number of tools is averaged for the training and test paths.

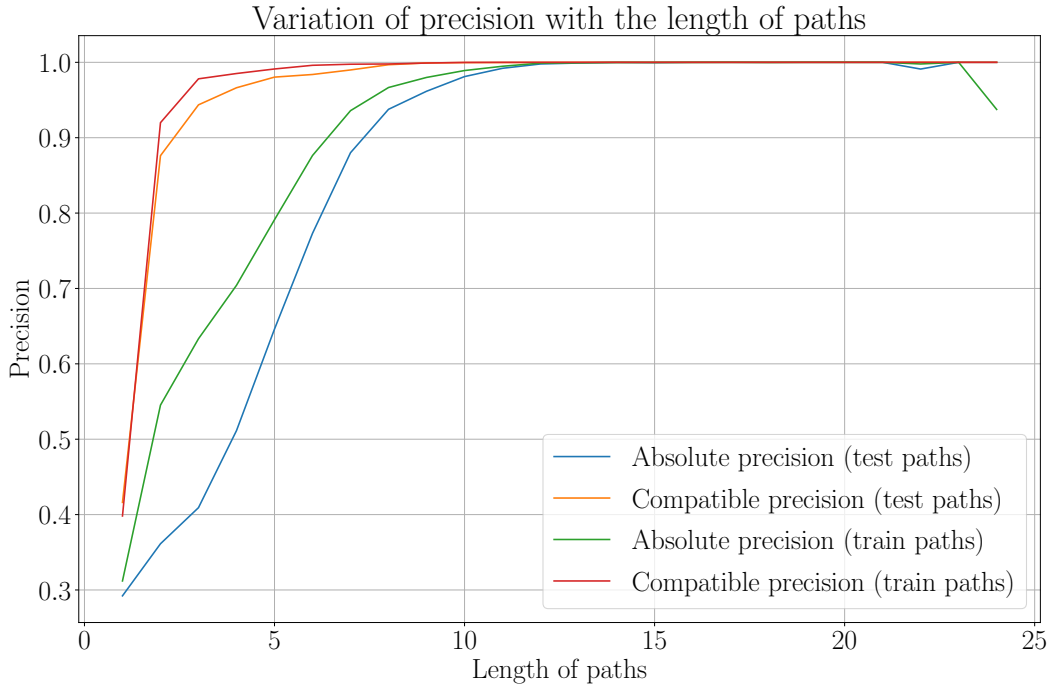


**Figure 46.: Variation of precision with the length of paths:** The plot shows how the length of paths affects precision. As the length of paths increases, the precision becomes better. This improvement is more dominant for compatible precision compared to absolute precision.

As the maximum length of a path is fixed to 25, the plot shows the maximum length as 24 and the last tool (at 25<sup>th</sup> position) is used as the next tool for each path of length 25. It is concluded from the plot (figure 46) that as the length of paths increases, the precision becomes better. This increase is more dominant for compatible precision than for absolute precision. As the length of paths increases, they have more tool connections and thereby more features. A higher number of features present in longer paths helps in predicting tools more robustly. This is achieved even though the number of paths with length  $\geq 20$  is lower compared to the number of shorter paths.

### 10.3.10. Performance with a small number of workflows

An analysis is done with a small number of workflows ( $\approx 9,000$  paths). Figure 47 shows the results. The subplots (a) and (b) show that the absolute and compatible precision are not comparable to what is achieved using a large number of workflows with  $\approx 167,000$  paths (figure 37). The absolute and compatible precision saturate around  $\approx 70\%$  and  $\approx 85\%$ , respectively. As the number of workflows is less, a weaker recurrent neural network with 256 memory units is used. A dropout of 0.2 is used to prevent overfitting. The analysis is executed for 100 epochs. After the 50<sup>th</sup> epoch, the validation loss starts increasing which proves that the network is overfitting. It is concluded that a strong recurrent neural network is required to achieve better precision, but it needs a large amount of data.

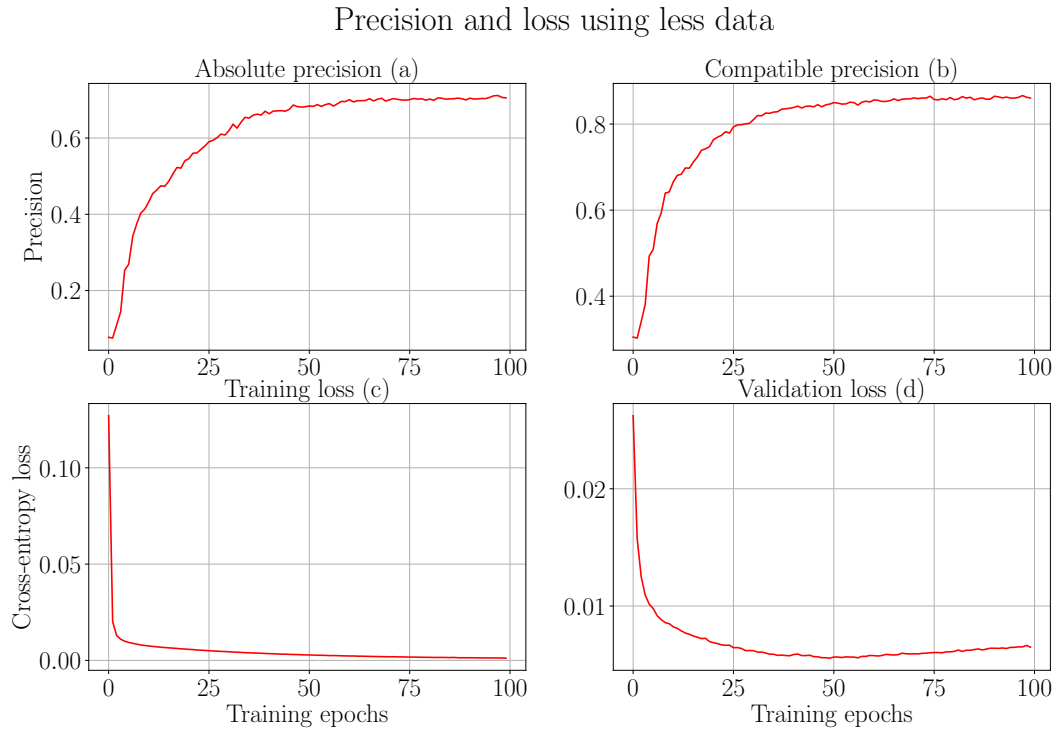


**Figure 47.: Performance with a small number of workflows:** The plot shows the performance of the recurrent neural network with a small number of workflows. The paths are decomposed keeping the first tool fixed (as described in section 10.2.3). The subplots (a) and (b) show the absolute and compatible precision, respectively. The subplots (c) and (d) show the training and validation losses, respectively. The analysis shown in the plot achieves lower precision than with a large number of workflows (figure 37) due to a weaker recurrent neural network.

### 10.3.11. Neural network with dense layers

A neural network with only dense layers is used as a classifier to compare the performance of learning on sequential data with the recurrent neural network. Two hidden layers are used with 128 neurons each. The first layer is an embedding layer and the last (output) layer is a dense layer. The dropout (0.05) is applied to combat overfitting. Rest all parameters like the optimiser, learning rate, batch size, embedding dimension, activations and loss function remain the same as for the recurrent neural network. The training and test paths are decomposed in the same way as explained in section 10.2.3. The network is trained for 40 epochs. The precision (absolute and compatible) is computed after each training epoch. The training and validation losses are also noted. Figure 48 shows the performance of this network.

Subplots 48a and 48b suggest that this network with dense layers also starts performing well (earlier in the epochs). It reaches an absolute precision of  $\approx 83\%$  and compatible precision of  $\approx 97\%$  around the 15<sup>th</sup> epoch. The learning seems to be good in the beginning, but it starts becoming worse towards the end of training. The precision starts decreasing and the training and validation losses (figure 48c and 48d) start increasing. They collectively suggest that the network is overfitting. The neural network with recurrent layers performs better (figure 37). It can be concluded that the neural network with only dense layers is not suited for learning on sequential data.

### Precision and loss using neural network with dense layers

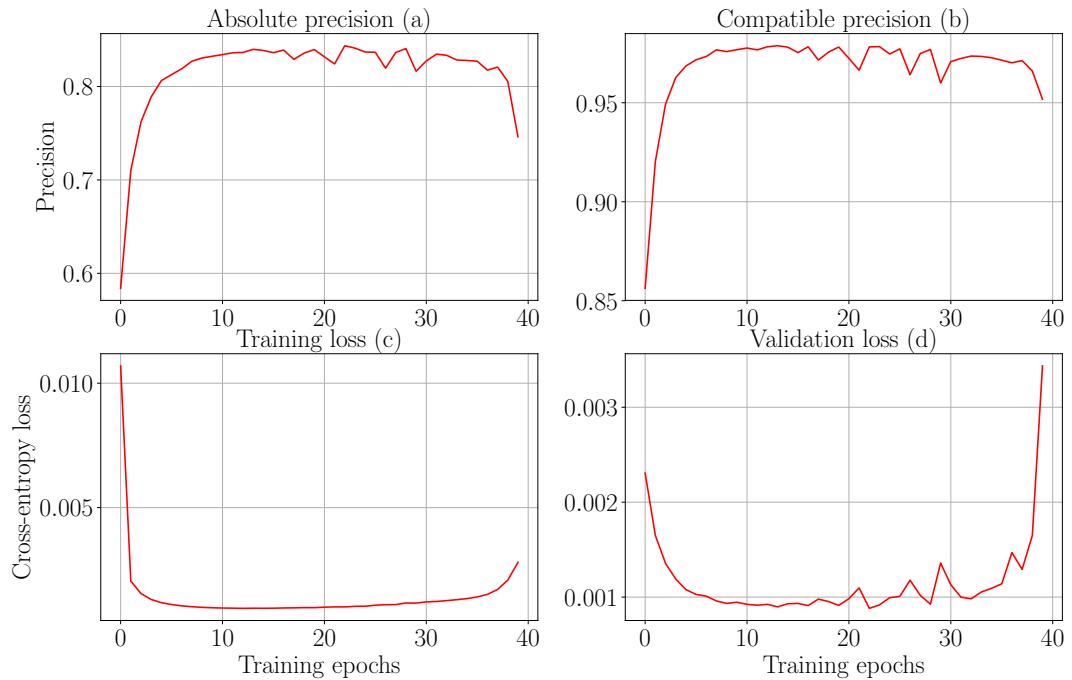


**Figure 48.: Performance of a neural network with dense layers:** The plot shows the performance of a neural network with dense layers. The paths are decomposed keeping the first tool fixed (as described in section 10.2.3). The subplots (a) and (b) show the absolute and compatible precision, respectively. The subplots (c) and (d) show the training and validation losses, respectively. The learning is not stable and the precision is lower than achieved by the recurrent neural network (figure 37). Moreover, it shows overfitting.

# 11. Conclusion

The aim of the work was to build a recommendation system which can predict tools while creating workflows. To preprocess, the workflows were first divided into paths. These paths were treated as the sequences of tools. The paths in a workflow were considered independent. The recurrent neural network was used as a classifier to learn tools connections from these paths. The absolute and compatible precision of  $\approx 89\%$  and  $\approx 99\%$ , respectively were achieved. The compatible top-1 and top-2 accuracies were  $> 90\%$ . With such high accuracies, a recommendation system can be created which predicts tools when a workflow is created. A few top (top-2 or top-3) predicted tools can be shown at each step. The similar tools (the first part of the thesis) for each predicted tool can be shown too. Using these predicted and similar tools offered by the recommendation system, workflows can be created with ease and in a shorter time. It removes the necessity to find (in the list of tools) and add a tool at each step of designing a workflow. Moreover, the workflow creation should be less error-prone as the predicted tools have compatible file types with the last tool of a workflow path. It will avoid the wastage of computing resources due to the poorly designed workflows (section 6.1.1). In addition, it can provide more options to the users for data processing using the Galaxy. The less experienced Galaxy users will benefit more from this recommendation system.

## 11.1. Network configuration

Many different configurations of the recurrent network were used to achieve a higher precision without overfitting. The baseline configuration of the recurrent neural network performed well. Applying dropout was found to be beneficial to reduce overfitting. A larger number of memory units and larger size of the embedding layer and mini-batch improved the precision too. The optimisers with adaptive strategies performed well compared to the non-adaptive ones. A comparison was made to ascertain the best learning rate and activation. The outcomes are explained with

plots in section 10.3.

## 11.2. The amount of data

A large number of workflows played a significant role to improve the precision. With a large number of workflows, it was ensured that the number of paths increased for each feature (tool connection). Moreover, a more complex network with 512 memory units and 512 dimensional embedding layer could be used without overfitting it. Collectively, they ensured a higher precision. But, with an increased number of workflows and a more complex network, the running time of the analysis also increased. The performances with a large and small number of workflows are explained in sections 10.2.3 and 10.3.10, respectively.

## 11.3. Decomposition of paths

Three different methods of decomposing the paths were used (section 8.4.1). The methods which created the training and test paths in an identical way (no decomposition of any path and decomposing all the paths) achieved a high precision (absolute precision of  $\approx 89\%$  and compatible precision of  $\approx 99\%$ ). The method of decomposing only the test paths did not work well. The performances are explained in sections 10.2.1 – 10.2.3.

## 11.4. Classification

The classification used in this work is multiclass and multilabel. It is multiclass because the workflow paths can connect to multiple different tools. It is multilabel because each path can connect to multiple tools. The compatible precision was higher than the absolute precision for all the approaches of path decomposition (section 8.4.1). It is because only the knowledge of next tools present in the training paths was used for the prediction. Therefore, the predicted tools did not match the actual next tools for some paths.

# 12. Future work

## 12.1. Train on longer and test on shorter paths

A poor performance was noted for the idea of decomposing only test paths. Detailed reasons should be found out and corrected to achieve a good precision for this approach too. Different configurations of the recurrent neural network can be used to check whether they can improve precision.

## 12.2. Restore original distribution

While taking unique paths into training and test sets, the original distribution of paths was not taken into consideration. The original distribution of paths should be restored for training paths only. Then, the recurrent neural network would assume that a path that repeats many times is more important. Moreover, the frequency of paths which are rare can be increased too [22]. It will increase the training time of the recurrent neural network.

## 12.3. Use convolution

The recurrent neural network achieved a precision of  $\approx 89\%$ . Using convolutional layers along with the recurrent layers, classification can be improved [14, 43]. The convolutional layers can be stacked above the recurrent layers to learn sub-features from the smaller parts of tool sequences. Convolution is well-suited to learn features irrespective of their positions.

## 12.4. Use other classifiers

The recurrent neural network was used as a classifier for this approach. *Bayesian network* and *markov random fields* can be used as classifiers to predict next tools.

They may provide different insights. Multiple configurations of a neural network with dense layers can be tried out to check whether they improve precision.

## 12.5. Decay prediction based on time

The tools which are not used regularly in Galaxy should be given less importance in the analysis. The prediction of the next tools should include more popular tools. For this, usage statistics of tools is required. To achieve that, the following two ideas can be used:

- Exclude those tools which are rarely used for a certain amount of time while processing the workflows.
- Assign less importance (small weights) to these tools while training the recurrent neural network.

# Bibliography

- [1] E. Afgan, D. Baker, M. Van Den Beek, D. Blankenberg, D. Bouvier, M. Cech, J. Chilton, D. Clements, N. Coraor, C. Eberhard, B. Grüning, A. Guerler, J. Hillman-Jackson, G. Von Kuster, E. Rasche, N. Soranzo, N. Turaga, J. Taylor, A. Nekrutenko, and J. Goecks, “The Galaxy platform for accessible, reproducible and collaborative biomedical analyses: 2016 update,” *Nucleic Acids Research*, vol. 44, pp. W3–W10, July 2016.
- [2] S. Robertson and H. Zaragoza, “The probabilistic relevance framework: Bm25 and beyond,” *Found. Trends Inf. Retr.*, vol. 3, pp. 333–389, Apr. 2009.
- [3] C. E. Shannon, “A mathematical theory of communication,” *SIGMOBILE Mob. Comput. Commun. Rev.*, vol. 5, pp. 3–55, Jan. 2001.
- [4] P. W. Foltz, “Latent semantic analysis for text-based research,” *Behavior Research Methods, Instruments, & Computers*, vol. 28, pp. 197–202, Jun 1996.
- [5] A. M. Shapiro and D. S. McNamara, “The use of latent semantic analysis as a tool for the quantitative assessment of understanding and knowledge,” *Journal of Educational Computing Research*, vol. 22, no. 1, pp. 1–36, 2000.
- [6] T. K. Landauer, “Learning and representing verbal meaning: The latent semantic analysis theory,” *Current Directions in Psychological Science*, vol. 7, no. 5, pp. 161–164, 1998.
- [7] J. Yang, “Notes on low-rank matrix factorization,” *CoRR*, vol. abs/1507.00333, 2015.
- [8] G. Shabat, Y. Shmueli, and A. Averbuch, “Missing entries matrix approximation and completion,” vol. abs/1302.6768, 2013.
- [9] Q. V. Le and T. Mikolov, “Distributed representations of sentences and documents,” *CoRR*, vol. abs/1405.4053, 2014.

- [10] G. I. Ivchenko and S. A. Honov, “On the jaccard similarity test,” *Journal of Mathematical Sciences*, vol. 88, pp. 789–794, Mar 1998.
- [11] S. Ruder, “An overview of gradient descent optimization algorithms,” *CoRR*, vol. abs/1609.04747, 2016.
- [12] I. Sutskever, J. Martens, G. Dahl, and G. Hinton, “On the importance of initialization and momentum in deep learning,” pp. III–1139–III–1147, 2013.
- [13] A. Botev, G. Lever, and D. Barber, “Nesterov’s accelerated gradient and momentum as approximations to regularised update descent,” pp. pp. 1899–1903., 2017.
- [14] W. Yin, K. Kann, M. Yu, and H. Schütze, “Comparative study of CNN and RNN for natural language processing,” *CoRR*, vol. abs/1702.01923, 2017.
- [15] X. Li, T. Qin, J. Yang, and T. Liu, “Lightrnn: Memory and computation-efficient recurrent neural networks,” *CoRR*, vol. abs/1610.09893, 2016.
- [16] Z. C. Lipton, D. C. Kale, C. Elkan, and R. C. Wetzel, “Learning to diagnose with LSTM recurrent neural networks,” *CoRR*, vol. abs/1511.03677, 2015.
- [17] J. Chung, Ç. Gülcühre, K. Cho, and Y. Bengio, “Empirical evaluation of gated recurrent neural networks on sequence modeling,” *CoRR*, vol. abs/1412.3555, 2014.
- [18] N. Boulanger-Lewandowski, Y. Bengio, and P. Vincent, “Modeling temporal dependencies in high-dimensional sequences: Application to polyphonic music generation and transcription,” 2012.
- [19] A. McCarthy and C. K. Williams, “Predicting patient state-of-health using sliding window and recurrent classifiers,” 2016.
- [20] H. Jia, “Investigation into the effectiveness of long short term memory networks for stock price prediction,” *CoRR*, vol. abs/1603.07893, 2016.
- [21] F. J. Ordóñez and D. Roggen, “Deep convolutional and lstm recurrent neural networks for multimodal wearable activity recognition,” *Sensors*, vol. 16, no. 1, 2016.

- [22] M. Buda, A. Maki, and M. A. Mazurowski, “A systematic study of the class imbalance problem in convolutional neural networks,” *CoRR*, vol. abs/1710.05381, 2017.
- [23] S. Karan and J. Zola, “Exact structure learning of bayesian networks by optimal path extension,” *CoRR*, vol. abs/1608.02682, 2016.
- [24] P. Spirtes, C. Glymour, R. Scheines, S. Kauffman, V. Aimale, and F. Wimberly, “Constructing bayesian network models of gene expression networks from microarray data,” 02 2002.
- [25] D. M. Chickering, D. Heckerman, C. Meek, and D. Madigan, “Learning bayesian networks is np-hard,” tech. rep., 1994.
- [26] G. F. Cooper, “The computational complexity of probabilistic inference using bayesian belief networks (research note),” *Artif. Intell.*, vol. 42, pp. 393–405, Mar. 1990.
- [27] D. M. Chickering, D. Heckerman, and C. Meek, “Large-sample learning of bayesian networks is np-hard,” *J. Mach. Learn. Res.*, vol. 5, pp. 1287–1330, Dec. 2004.
- [28] A. Sarkar and D. B. Dunson, “Bayesian nonparametric modeling of higher order markov chains,” vol. abs/1506.06268, 2015.
- [29] Z. C. Lipton, “A critical review of recurrent neural networks for sequence learning,” *CoRR*, vol. abs/1506.00019, 2015.
- [30] K. Cho, B. van Merriënboer, D. Bahdanau, and Y. Bengio, “On the properties of neural machine translation: Encoder-decoder approaches,” *CoRR*, vol. abs/1409.1259, 2014.
- [31] R. Pascanu, T. Mikolov, and Y. Bengio, “Understanding the exploding gradient problem,” *CoRR*, vol. abs/1211.5063, 2012.
- [32] S. Hochreiter and J. Schmidhuber, “Long short-term memory,” *Neural Comput.*, vol. 9, pp. 1735–1780, Nov. 1997.
- [33] M. Hermans and B. Schrauwen, “Training and analysing deep recurrent neural networks,” pp. 190–198, 2013.

- [34] D. Clevert, T. Unterthiner, and S. Hochreiter, “Fast and accurate deep network learning by exponential linear units (elus),” *CoRR*, vol. abs/1511.07289, 2015.
- [35] N. Srivastava, G. Hinton, A. Krizhevsky, I. Sutskever, and R. Salakhutdinov, “Dropout: A simple way to prevent neural networks from overfitting,” *Journal of Machine Learning Research*, vol. 15, pp. 1929–1958, 2014.
- [36] W. Zaremba, I. Sutskever, and O. Vinyals, “Recurrent neural network regularization,” *CoRR*, vol. abs/1409.2329, 2014.
- [37] Y. Gal and Z. Ghahramani, “A theoretically grounded application of dropout in recurrent neural networks,” pp. 1027–1035, 2016.
- [38] S. Ruder, “An overview of gradient descent optimization algorithms,” *CoRR*, vol. abs/1609.04747, 2016.
- [39] M. Li, T. Zhang, Y. Chen, and A. J. Smola, “Efficient mini-batch training for stochastic optimization,” in *Proceedings of the 20th ACM SIGKDD International Conference on Knowledge Discovery and Data Mining*, KDD ’14, (New York, NY, USA), pp. 661–670, ACM, 2014.
- [40] D. P. Kingma and J. Ba, “Adam: A method for stochastic optimization,” *CoRR*, vol. abs/1412.6980, 2014.
- [41] A. Graves, “Generating sequences with recurrent neural networks,” *CoRR*, vol. abs/1308.0850, 2013.
- [42] S. Wang and C. Manning, “Fast dropout training,” vol. 28, pp. 118–126, 17–19 Jun 2013.
- [43] J. Wang, Y. Yang, J. Mao, Z. Huang, C. Huang, and W. Xu, “CNN-RNN: A unified framework for multi-label image classification,” *CoRR*, vol. abs/1604.04573, 2016.

# A. Appendix

## A.1. Visualiser

Few visualisers are created to showcase the results of the first part of the thesis (find similar scientific tools). For *latent semantic analysis* approach, there are two websites and for *paragraph vectors* approach, there is one website. In addition to showing similar tools for the selected tool, visualisers also show a few plots for the error, gradient, learning rates and the selected tool's similarity scores with all other similar tools. Links to the websites are as follows:

- Full-rank document-token matrices<sup>1</sup>.
- Document-token matrices reduced to 5% of the full-rank<sup>2</sup>.
- Paragraph vectors<sup>3</sup>

## A.2. Code repository

The following sections provide the locations of the codebase (*github* repositories) used for this work. All the repositories are under MIT license.

### A.2.1. Find similar scientific tools

There are separate branches for the two approaches, (*latent semantic analysis* and *paragraph vectors*). For *latent semantic analysis* approach, there are two branches:

- Full-rank document-token matrices<sup>4</sup>.

---

<sup>1</sup>[https://rawgit.com/anuprulez/similar\\_galaxy\\_tools/lsi/viz/similarity\\_viz.html](https://rawgit.com/anuprulez/similar_galaxy_tools/lsi/viz/similarity_viz.html)

<sup>2</sup>[https://rawgit.com/anuprulez/similar\\_galaxy\\_tools/lsi\\_005/viz/similarity\\_viz.html](https://rawgit.com/anuprulez/similar_galaxy_tools/lsi_005/viz/similarity_viz.html)

<sup>3</sup>[https://rawgit.com/anuprulez/similar\\_galaxy\\_tools/doc2vec/viz/similarity\\_viz.html](https://rawgit.com/anuprulez/similar_galaxy_tools/doc2vec/viz/similarity_viz.html)

<sup>4</sup>[https://github.com/anuprulez/similar\\_galaxy\\_tools/tree/lsi](https://github.com/anuprulez/similar_galaxy_tools/tree/lsi)

- Document-token matrices reduced to 5% of the full-rank<sup>5</sup>.

Both of these branches differ only in their ranks of corresponding document-token matrices. There is a separate branch for *paragraph vectors* approach<sup>6</sup>.

### A.2.2. Predict next tools in scientific workflows

The Galaxy workflows are represented as directed acyclic graphs and they can be visualised in a website<sup>7</sup>. Workflow chosen from the drop-down is displayed as a cytoscape<sup>8</sup> graph. Separate code repositories are maintained for the ideas (decomposition of workflow paths) discussed in section 8.4.1. They are listed as follows:

- No decomposition of paths<sup>9</sup>
- Decomposition of only test paths<sup>10</sup>
- Decomposition of the training and test paths<sup>11</sup>

---

<sup>5</sup>[https://github.com/anuprulez/similar\\_galaxy\\_tools/tree/lsi\\_005](https://github.com/anuprulez/similar_galaxy_tools/tree/lsi_005)

<sup>6</sup>[https://github.com/anuprulez/similar\\_galaxy\\_tools/tree/doc2vec](https://github.com/anuprulez/similar_galaxy_tools/tree/doc2vec)

<sup>7</sup>[https://rawgit.com/anuprulez/similar\\_galaxy\\_workflow/master/viz/index.html](https://rawgit.com/anuprulez/similar_galaxy_workflow/master/viz/index.html)

<sup>8</sup><http://js.cytoscape.org>

<sup>9</sup>[https://github.com/anuprulez/similar\\_galaxy\\_workflow/tree/train\\_longer\\_paths](https://github.com/anuprulez/similar_galaxy_workflow/tree/train_longer_paths)

<sup>10</sup>[https://github.com/anuprulez/similar\\_galaxy\\_workflow/tree/train\\_long\\_test\\_decomposed](https://github.com/anuprulez/similar_galaxy_workflow/tree/train_long_test_decomposed)

<sup>11</sup>[https://github.com/anuprulez/similar\\_galaxy\\_workflow/tree/extreme\\_paths](https://github.com/anuprulez/similar_galaxy_workflow/tree/extreme_paths)

